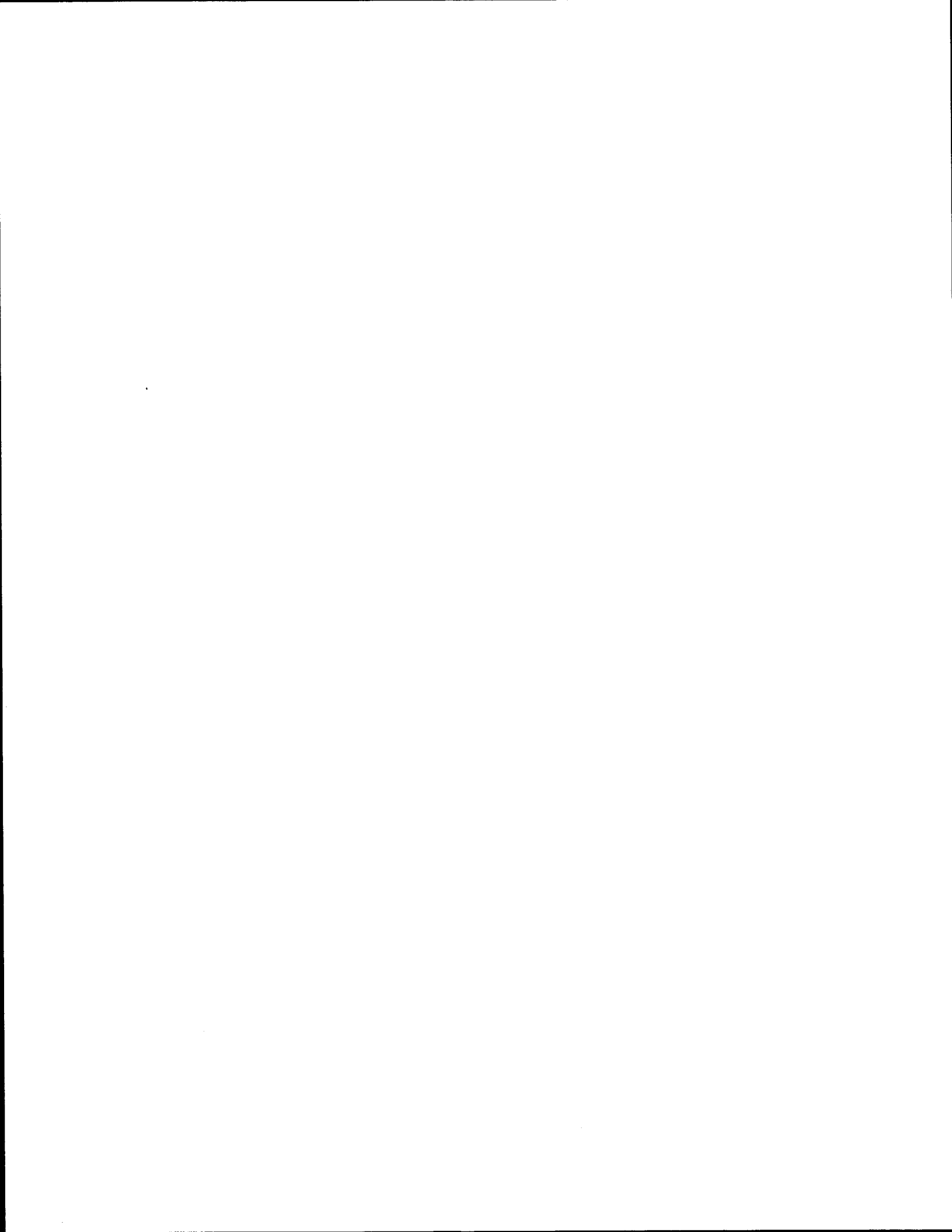| 1. Report No.<br>FHWA-01/1520-2 | 2. Government Accession No. | 3. Recipient's Catalog No. |
|---|---|---|
| 4. Title and Subtitle<br>FRP REINFORCING BARS IN BRIDGE DECKS: STATE OF THE ART REVIEW | | 5. Report Date<br>November 2000 |
| | | 6. Performing Organization Code |
| 7. Author(s)<br>David Trejo, Francisco Aguiniga, C. Eugene Buth, Robert Yuan, Ray W. James, Peter B. Keating | | 8. Performing Organization Report No.<br>Report 1520-2 |
| 9. Performing Organization Name and Address<br>Texas Transportation Institute<br>The Texas A&M University System<br>College Station, Texas 77843-3135 | | 10. Work Unit No. (TRAIS) |
| | | 11. Contract or Grant No.<br>Project No. 9-1520 |
| 12. Sponsoring Agency Name and Address<br>Texas Department of Transportation<br>Construction Division<br>Research and Technology Transfer Section<br>P. O. Box 5080<br>Austin Texas 78763-5080 | | 13. Type of Report and Period Covered<br>Research:<br>August 99 – March 2000 |
| | | 14. Sponsoring Agency Code |
| 15. Supplementary Notes<br>Research performed in cooperation with the U.S. Department of Transportation, Federal Highway Administration.<br>Research Project Title: FRP Reinforcing Bars in Bridge Decks | | |

16. Abstract

Fiber-reinforced polymers (FRP) are being increasingly used in the construction industry. One application is to use FRP bars as reinforcement in concrete. This report presents the state of the art on FRP bars, its constituent components, methods of fabrication, and the behavior of the composite materials. Mechanical properties, test methods, and factors affecting these properties are reviewed. Factors affecting the mechanical properties of the bars are addressed. Current applications and development of FRP reinforcement in Canada, Europe, Japan, and in the United States are also presented.

| 17. Key Words<br>FRP, concrete, composite, fiber, polymer, degradation | | 18. Distribution Statement<br>No restrictions. This document is available to the public through NTIS:<br>National Technical Information Service<br>5285 Port Royal Road<br>Springfield, Virginia 22161 | |
|---|---|---|---|
| 19. Security Classif.(of this report)<br>Unclassified | 20. Security Classif.(of this page)<br>Unclassified | 21. No. of Pages<br>155 | 22. Price |

Form DOT F 1700.7 (8-72)      Reproduction of completed page authorized

# FRP REINFORCING BARS IN BRIDGE DECKS:
# STATE OF THE ART REVIEW

by

David Trejo
Assistant Professor
Texas A&M University

Francisco Aguiniga
Research Assistant
Texas Transportation Institute

C. Eugene Buth
Director of Impact Test Facility
Texas Transportation Institute

Robert Yuan
Professor
University of Texas at Arlington

Ray W. James
Manager, Major Highway Structures Program
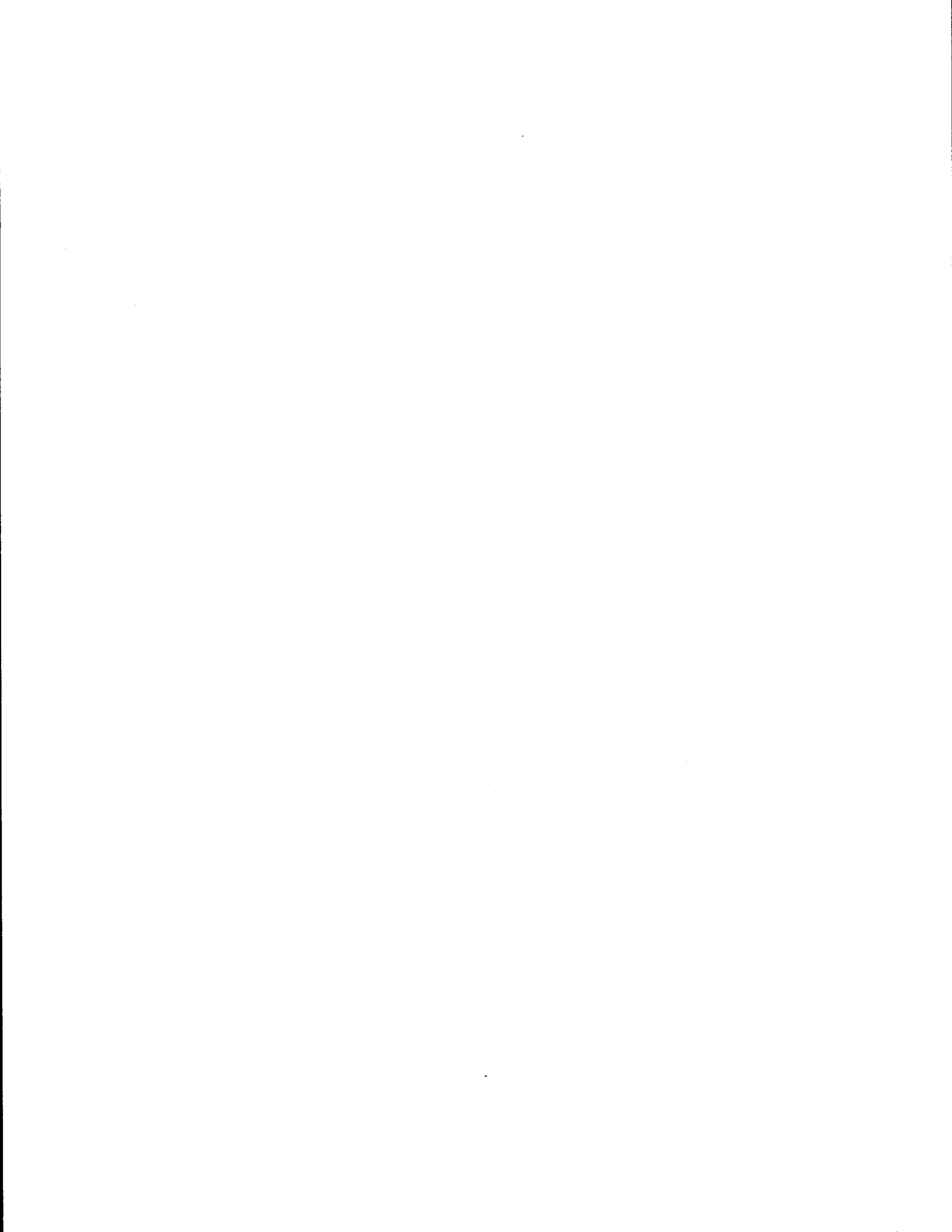Texas Transportation Institute

Peter B. Keating
Associate Professor
Texas A&M University

# DISCLAIMER

The contents of this report reflect the views of the authors who are responsible for the facts and the accuracy of the data presented herein. The contents do not necessarily reflect the official view or policies of the Texas Department of Transportation. This report does not constitute a standard, specification or regulation.

# ACKNOWLEDGEMENTS

# TABLE OF CONTENTS

# LIST OF FIGURES

# LIST OF TABLES

# I. INTRODUCTION

The development of fiber-reinforced polymer (FRP) materials began in the late 1940s [1]. The need for materials with high strength, high stiffness, and lightweight was born in the aerospace and high-performance transportation industries where the high initial costs were justified in exchange for the improved performance of the new materials. Composite materials have a number of attractive properties such as tailorability, high stiffness, high strength, corrosion resistance, low weight, magnetic permeability, low electrical conductivity, dimensional stability, etc. Nevertheless, the disadvantages of composite materials include high initial cost and unknown long-term durability. For highway infrastructure applications, challenges also include adapting the material characteristics for reliable design and performance.

The main motivation for the use of FRP-reinforcing bars in concrete structures depends on the region where they will be used [2]. In Japan, two- and three-dimensional FRP grids have been economically used in tunnel lining applications, resulting in reduced construction time and labor costs. In Canada and the U.S., the main interest is focusing on alleviating the damage and costs associated with corrosion of steel reinforcement. For concrete applications, the interests in Europe concerning FRP are a mixture of the above, including the retrofitting of valuable historic buildings.

FRP reinforcement products used in concrete structures include internal reinforcement such as reinforcing bars, tendons, 2-D grids, and 3-D fabric. External reinforcement includes tendons, fabrics, and bonded plates. This report is focused on the basic materials design, tests, and applications of FRP internal reinforcement for concrete structures.
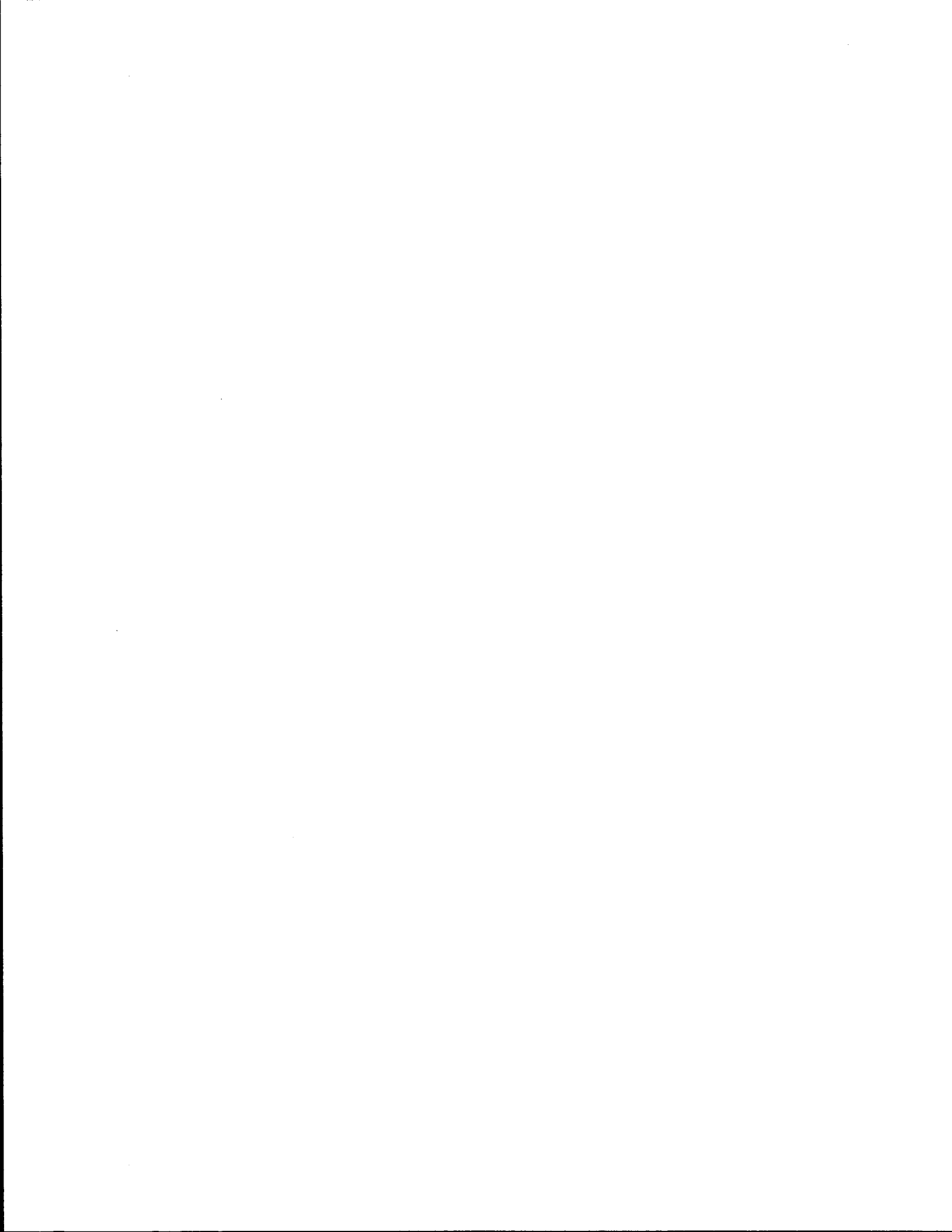
# II. DESCRIPTION OF COMPONENTS OF FIBER REINFORCED POLYMER (FRP) REBARS

FRP bars are continuous fiber composite materials. The components of the composite are fibers and resin. The properties of the composites are a combination of the properties of the fibers and the matrix. However, the fiber/matrix interface also plays an important role in defining the properties of the composite. The properties of the most commonly used composite constituents are described next.

**FIBERS**

Fibers are characterized by high specific strength and high specific stiffness [1]. Once in the composite, the fibers contribute most of the strength and stiffness to the composite. The main types of fibers used in the fabrication of FRP rebars are glass fibers, carbon fibers, and aramid fibers.

Individual glass, carbon, and aramid fiber filaments have high tensile strength and have a linear stress-strain behavior up to failure as depicted in Figure 1.
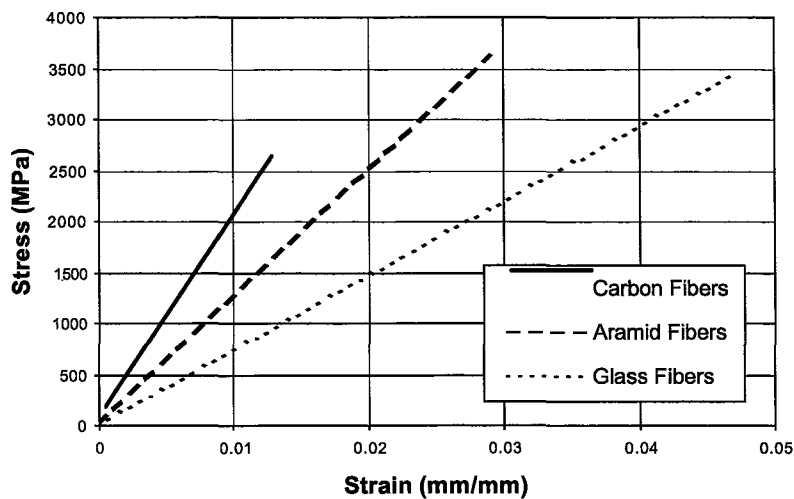
**Figure 1. Stress-Strain Curve of Glass, Carbon, and Aramid Fibers.**

Typical fiber origin and characteristics are illustrated in Table 1. Properties of typical fibers are presented in Table 2.

## Table 1. Typical Fiber Origin and Characteristics.

| Fiber Type | | Origin | Fabrication Method | Filament Size, μm (μin.) | Filaments/ Tow |
|---|---|---|---|---|---|
| Glass | S-2 glass | Molten glass | Fiber-drawing | 6-14 (230-550) | 2000 |
| | E-glass | Molten glass | Fiber-drawing | 3-20 (118-787) | 2000 |
| Organic | Kevlar 49 | Liquid crystal | Spinning | 12 (472) | 1000 |
| Carbon | AS4 | PAN | Heat and stress | 8 (315) | 12000 |
| | PS-100S | Pitch | Heat | 10 (393) | 2000 |
| | IM8 | PAN | Heat and stress | 5 (197) | 12000 |
| Ceramic | Boron | Tungsten core | CVD | 142 (5600) | 1 |
| | Nicalon (SiC) | Polymer precursor | Pyrolisis | 15 (600) | 500 |
| | SCS-6 | Carbon core | CVD | 127 (5000) | 1 |
| | Alumina | Slurry mix | Spin and heat | 20 (800) | 1 |

## Table 2. Properties of Typical Fibers.

| Material | Density $\rho$, g/cm$^3$ (lb/in.$^3$) | Modulus $E_L$, GPa (Msi) | Poisson's Ratio $\nu_L$ | Strength $\sigma_{uL}$, MPa (ksi) | Specific Stiffness $(E/\rho)/$ $(E/\rho)_{Al}$ | Specific Strength $(\sigma_u/\rho)/$ $(\sigma_u/\rho)_{Al}$ | Thermal Expansion Coefficient $\alpha_L$, $\mu/°C$ ($\mu/°F$) |
|---|---|---|---|---|---|---|---|
| METALS | | | | | | | |
| Steel | 7.8 (0.284) | 200 (29) | 0.32 | 1724 (250) | 1.0 | 1.2 | 12.87 (7.1) |
| Aluminum | 2.7 (0.097) | 69 (10) | 0.33 | 483 (70) | 1.0 | 1.0 | 23.4 (13.0) |
| Titanium | 4.5 (0.163) | 91 (13.2) | 0.36 | 758 (110) | 0.95 | 1.2 | 8.8 (4.9) |
| FIBERS (Axial Properties) | | | | | | | |
| AS4 | 1.80 (0.065) | 235 (34) | 0.20 | 3599 (522) | 5.1 | 11.1 | -0.8 (-0.44) |
| T300 | 1.76 (0.064) | 231 (33) | 0.20 | 3654 (530) | 5.1 | 11.5 | -0.5 (-0.3) |
| P100S | 2.15 (0.078) | 724 (105) | 0.20 | 2199 (319) | 13.2 | 5.5 | -1.4 (-0.78) |
| IM8 | 1.8 (0.065) | 310 (45) | 0.20 | 5171 (750) | 6.7 | 16.1 | - |
| Boron | 2.6 (0.094) | 385 (55.8) | 0.21 | 3799 (551) | 5.8 | 8.3 | 8.3 (4.6) |
| Kevlar 49 | 1.44 (0.052) | 124 (18) | 0.34 | 3620 (525) | 3.6 | 13.9 | -2.0 (-1.1) |
| SCS-6 | 3.3 (0.119) | 400 (58.0) | 0.25 | 3496 (507) | 5.1 | 6.1 | 5.0 (2.77) |
| Carbon PAN Type I | 1.95 (0.070) | 350 (50.8) | - | 2500 (363) | 7.0 | 7.2 | -0.5 (-0.3) |
| Nicalon | 2.55 (0.092) | 180 (28) | 0.25 | 2000 (290) | 2.8 | 4.4 | 4.0 (2.2) |
| Alumina | 3.95 (0.143) | 379 (55) | 0.25 | 1585 (230) | 3.7 | 1.9 | 7.5 (4.2) |
| S-2 Glass | 2.46 (0.090) | 86.8 (12.6) | 0.23 | 4585 (665) | 1.4 | 10.4 | 1.6 (0.9) |
| E-Glass | 2.58 (0.093) | 69 (10.0) | 0.22 | 3450 (550) | 1.05 | 7.5 | 5.4 (3.0) |
| Sapphire | 3.97 (0.143) | 435 (63) | 0.28 | 3600 (522) | 4.3 | 5.1 | 8.8 (4.9) |

## Glass Fibers

Sand, limestone, and alumina are used to make glass fibers. These materials are dry-mixed and melted in a furnace at approximately 1260 °C. The molten glass is then passed through an orifice as a hot, thin fiber. Thousands of these tiny fibers are then drawn to reduce their diameter further, followed by rolling on a roving for storage [1, 3]. To minimize fiber damage and increase the fibers' adhesion to the matrix, a sizing (coating) is applied to the surface of the fiber. The main advantages of glass fibers compared with other fibers are their low cost and high tensile strength [1]. The disadvantages are low tensile modulus, sensitivity to abrasion and alkaline environments, and their relatively low resistance to moisture, sustained loads, and cyclic loads.

The most common types of glass fibers used in the composite industry are E-glass (calcium aluminoborosilicate) and S-glass (magnesium aluminoborosilicate) [1]. E-glass is used in applications where strength, electrical resistance, acid resistance, and low cost are important. S-glass fibers have higher strength, stiffness, and ultimate strain than E-glass, but they have higher susceptibility in alkaline environments and cost more than E-glass fibers. C-glass fibers have a soda-lime-borosilicate composition that makes them very stable chemically and advantageous for use in acidic environments. To minimize weight and strength loss over time, alkali-resistant (AR) fibers have been developed. These fibers are not completely immune to degradation in alkaline environments, although performance is superior to conventional glass fibers. Softening points of glass fibers are approximately 800 to 1000 °C.

The standard nomenclature of glass fibers is described in Figure 2. Figure 3 shows a micrograph taken with a scanning electron microscope of a failed composite made with glass fibers [4]. The smooth-fractured surface of the glass fibers shown in Figure 3 is characteristic of brittle materials.

## GLASS
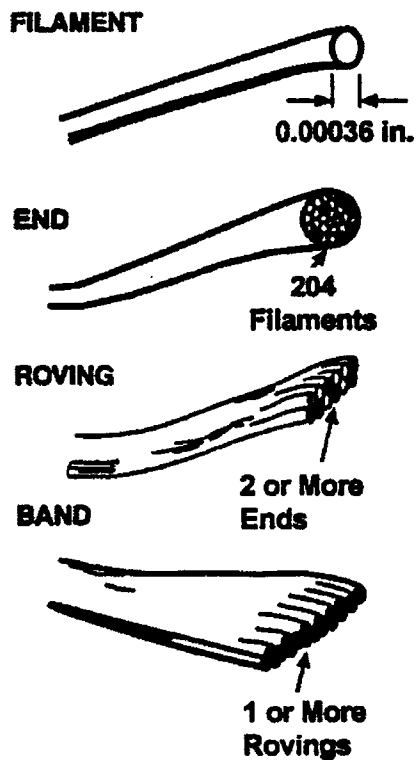


**Figure 2. Nomenclature Used for Glass Fibers.**
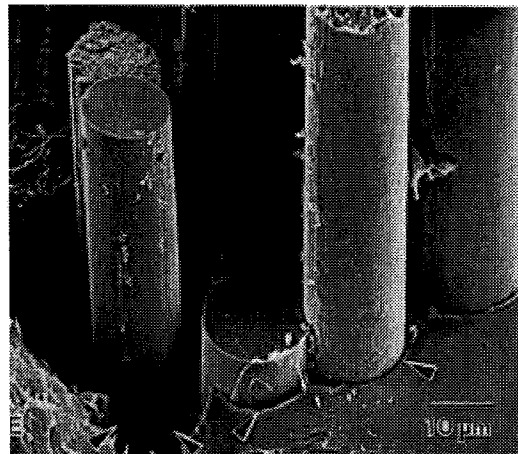


**Figure 3. SEM Photograph of a Composite with Glass Fibers [4].**

## Carbon Fibers

The majority of graphite and structural carbon fibers is based on the layered hexagonal networks present in graphite [1]. The crystal structure of graphite is shown in Figure 4, where two basel planes containing the hexagonal structure of crystals are sketched [5]. Figure 5 shows a schematic representation of the texture of the fibers, where stacks of basel planes can be flat or folded and run parallel to the axis of the fiber [5]. Figure 6 presents a micrograph of an actual carbon fiber, where the folded structure can be easily identified.
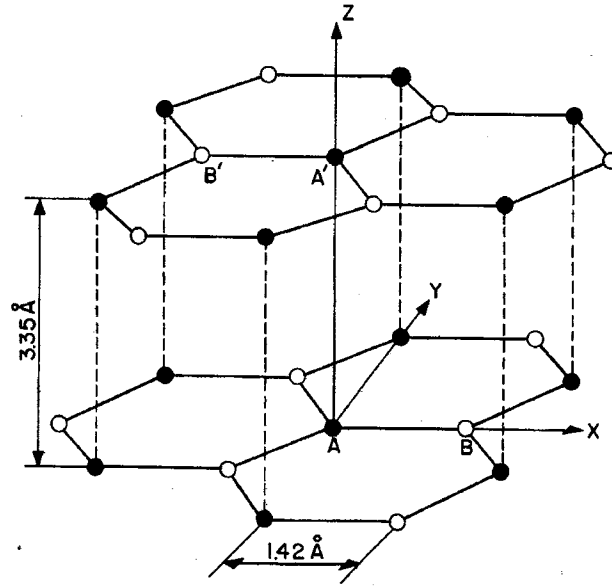
**Figure 4. Crystal Structure of Graphite [5].**
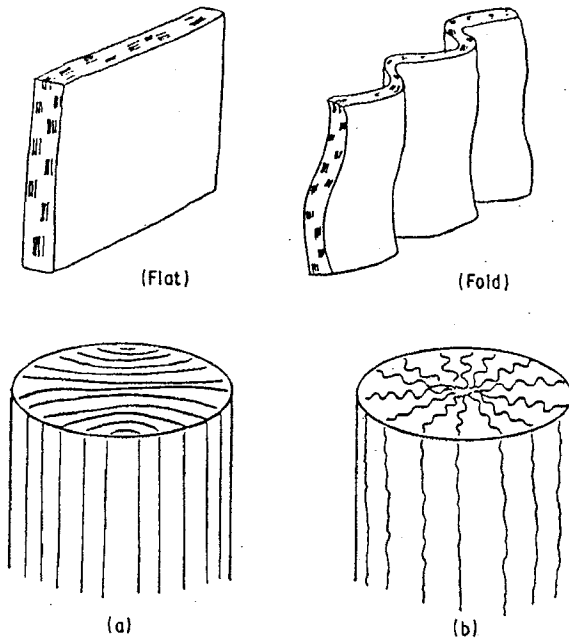


**Figure 5. Texture Models of Carbon Fibers: (a) Oriented Structure and (b) Folded Layer Structure [5].**
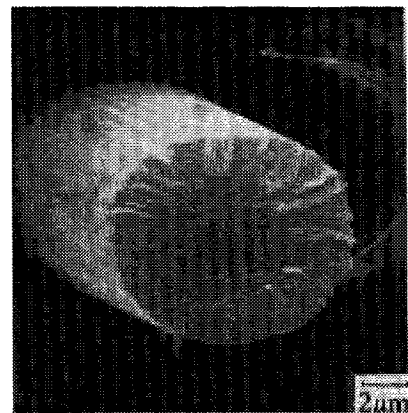


**Figure 6. SEM Photograph of Carbon Fibers [5].**

The production of commercial carbon fibers is based on organic precursors such as rayon, polyacrylonitril (PAN), and isotropic and liquid crystalline pitches (complex mixture of thousands of different species of hydrocarbon and heterocyclic molecules) [1]. The strength and stiffness of the fibers are much higher in the longitudinal direction as compared to the transverse direction because the fibers have a highly oriented microstructure. Production of carbon fibers involves: (a) heating the fibers in air to prevent melting or fusion of the precursor; (b) carbonizing the fibers in an inert atmosphere to eliminate the noncarbon elements; and (c) "graphitizing" the fibers at high temperatures (above 2500 °C). The progressive heating and stretching of the fibers generates the highly oriented structure of carbon fibers. The main advantages of carbon fibers are their high strength, high stiffness to weight ratios, low longitudinal and transverse coefficients of thermal expansion (CTEs), low sensitivity to fatigue loads, and excellent moisture and chemical resistance. The transverse and shear stiffness and the strength of carbon fibers are very low when compared to their longitudinal properties. Water, bases, solvents, and weak acids at room temperature do not affect significantly the mechanical properties of carbon fibers.

**Aramid Fibers**

The development of high-performance polymers has led to the development of highly oriented materials by modification of conventional polymers and by the design of rod-like liquid crystalline polymers (LCP) [4]. Figure 7 depicts the unit cell forming the structure of poly (p-phenylene terephthalamide), a liquid crystalline polymer. Figure 8 illustrates the supramolecular structure of Kevlar® (Kevlar is the brand name of an aramid fiber registered to DuPont).
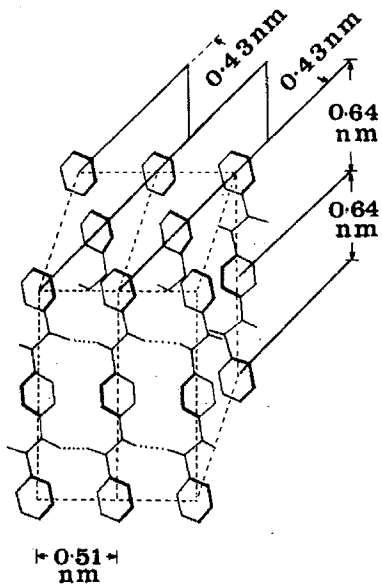
**Figure 7. Schematic Diagram of the Unit Cell of Poly (P-Phenylene Terephthalamide) Indicating the Lattice Planes Resolved in the Transmission Electron Microscope [6].**
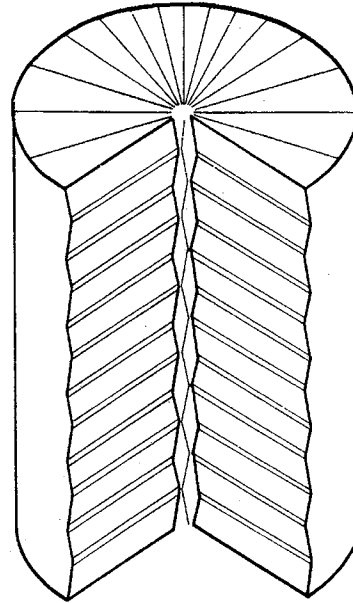
**Figure 8. Schematic Diagram of Kevlar® 49 Fibers Showing Radially Arranged Plated Sheets [6].**

A liquid crystalline polymer is one that forms a partially ordered state on heating (thermotropic LC) or in solution (lyotropic LC). Heating a thermotropic liquid crystal results in decreasing the molecular order, thus rendering the material isotropic. Aramid fibers are manufactured by extruding hot liquid crystalline polymer solution through a spinneret (a small metal cap with fine holes) [1]. This process results in the formation of a crystalline fiber with a surface skin [4]. The structure of these fibers is illustrated in Figure 9.
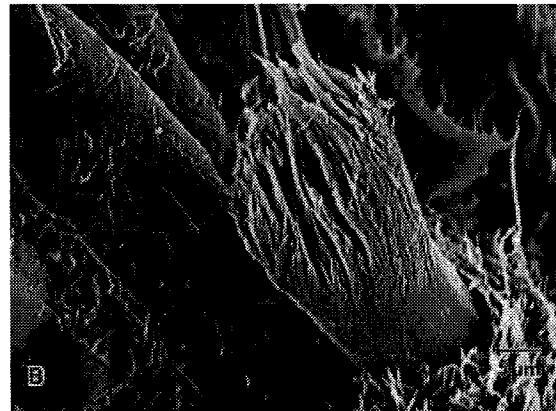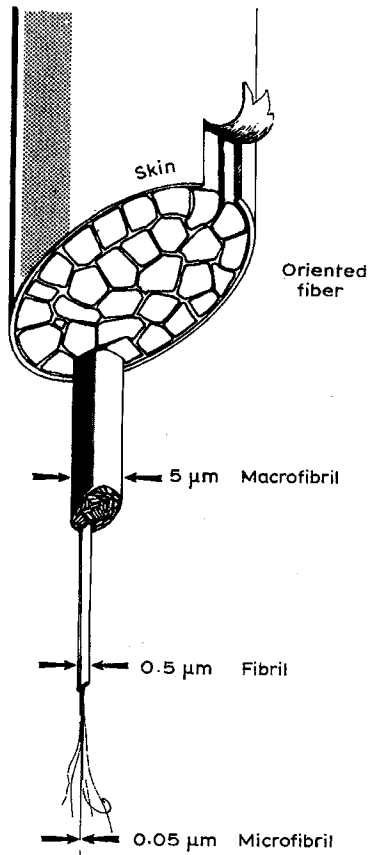
**Figure 9. Structure of Uniaxially Oriented LCP Fibers [4].**

**Figure 10. SEM of Aramid Fibers [4].**

Aramid fibers have high strength, excellent thermal stability, and high modulus due to the high orientation of the semicrystalline polymer. Aramid fibers have a negative CTE in the longitudinal direction and a positive CTE in the transverse direction. The fibrillar microstructure of aramid fibers gives it poor flexural and compressive properties. The poor flexural and compressive properties permit easy local yielding, buckling, and kinking of the fiber in compression [3]. Figure 10 shows a micrograph of a failed aramid fiber. It can be observed that the fibrils are drawn and necked, which is a characteristic failure mode of ductile materials. The application temperature range of aramid fibers is –200 to 200 °C. Moisture softens the structure of the fibers resulting in increased creep, and these fibers can degrade if exposed to ultraviolet radiation [1].

**MATRIX**

Polymers are widely used as the matrix for composite materials. A brief description of polymers follows. Polymers can be classified as thermoplastic or thermosetting according to their structure and properties.

**Thermoplastics:** Thermoplastic polymers have a structure of linear or branched-chain molecules having strong intramolecular bonds but weak intermolecular bonds. Thermoplastic polymers can reversibly melt or solidify and be reshaped upon applying heat and pressure. They are either semicrystalline or amorphous in structure. Some thermoplastics are polyethylene, polystyrene, nylons, polycarbonate, polyacetals, and polyimide-imide.

**Thermosets:** Thermosetting polymers have crosslinked structures with covalent bonds between all molecules. These polymers decompose upon heating rather than softening. After they cure (solidify by crosslinking), they cannot be reshaped. Examples of thermoset polymers are epoxides, polyesters, phenolics, ureas, melamine, silicone, polyimides, and vinyl ester.

**Polymer Structure**

Monomers are small organic molecules and are the base for the formation of polymers [7, 8]. Polymers are formed by the reaction and chemical bonding of large numbers of monomers. When a polymer has formed, it consists of long interwoven chains similar to a bowl of spaghetti [9]. In thermoplastic polymers, there are long chains with strong bonds (covalent or ionic) [7, 8]. The chains are joined to one another at variable intervals by weak molecular attraction or sharing of atoms (secondary bonding) between the molecules of the long chains. The secondary bonds are weaker than the chemical bonds that hold together the main chains. In thermosetting polymers, all of the

11

long chains are joined together by shorter chains but are connected with covalent or ionic bonds. Therefore, a thermosetting polymer is a giant molecule.

**Glass Transition Temperature**

At low temperatures, polymers are solids, and the motion of atoms is limited to small movements (usually vibrations) of a few atoms [8]. With an increase in temperature, more atoms participate in the motion, and the motions become larger. Due to the limited amount of space available in solid materials, only vibrations, rotations, and twisting of the polymer chains are the types of motions generated in the material. At this stage, since atoms need to move, they are forced apart, and the polymer experiences a minor volume expansion coupled with a small increase in temperature. The minor increase in volume is measured by the coefficient of thermal expansion. With further heat input, the translational motions become more important. These movements are accompanied by slow disentanglement, separation of the polymer chains, and an increase in space between the atoms. This increase in space results in a strength decrease in the secondary bonds. If more heat is applied to the polymer, atoms in a chain begin to move in small groups and translate similar to a jump rope. These long-range motions result in a significant increase in the flexibility of the material. When atoms begin to exhibit this behavior, an added thermal input will cause the energy to remain constant, and other polymer chains will begin long-range motions. To visualize this, imagine that the first atoms that exhibit long-range motions are the ones on the surface of the polymer piece, followed by the atoms located away from the surface. In this case, the long-range movement is called glass transition temperature ($T_g$). Figure 11 describes the behavior of a polymer at different temperatures.

| Heat Distortion Temperature HDT | Glass Transition Tg | Melting Point Tm | Decomposition Temperature Td |
|---|---|---|---|

Increasing temperature →

| • Hard<br>• Stiff<br>• Glass-like<br>• Limited atomic movement<br>• Small volume increases | • Moderately hard to stiff<br>• Creep<br>• Slightly higher atomic movement<br>• Small volume increases<br>• Limit for structural applications | • Pliable, leathery<br>• Larger, longer range and coordinated movements | • Liquid<br>• Entire polymer molecules move independently | • Degradation<br>• Chain breakage<br>• Gas release<br>• Char formation<br>• Dramatic and non-reversible change in properties<br>• Color change |

**Figure 11. Behavior of a Polymer at Different Temperatures [8].**

The glass transition temperature is important because the mechanical properties of the polymer change profoundly at this point [7]. Above $T_g$ polymers exhibit relatively low strength, high ductility, and toughness. Above $T_g$ the Young's modulus of the material decreases dramatically [8]. In some polymers it can decrease as much as 1000 times. The variation of the Young's modulus with temperature is illustrated in Figure 12.
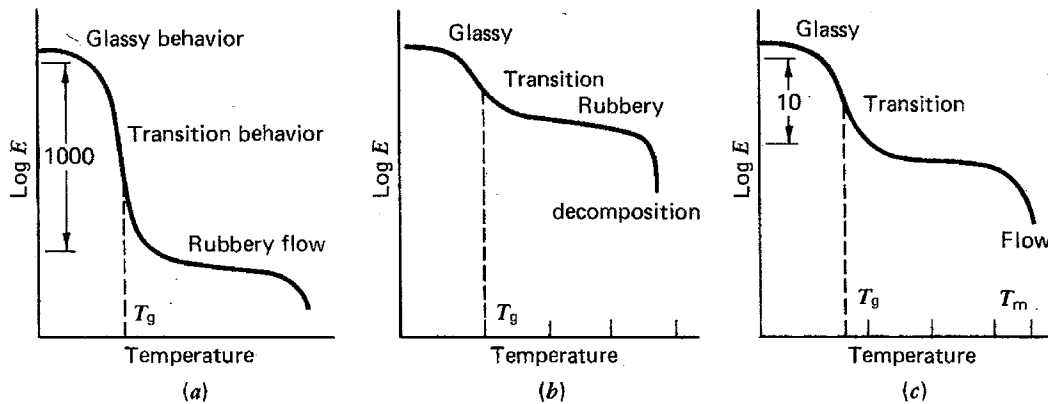


**Figure 12. Variation of Young's Modulus with Temperature: (a) Thermoplastic, Amorphous; (b) Thermoset, Highly Crosslinked; (c) Semicrystalline [3].**

13

Other properties affected in the glass transition region are:

- the coefficient of thermal expansion,
- heat capacity,
- refractive index,
- nuclear magnetic and electro spin resonance behavior,
- mechanical damping,
- electrical properties,
- tensile strength and ultimate elongation in elastomers [10].

**Stress-Strain Behavior**

The stress-strain behavior of polymers is linear at low loads [8]. With an increase in load, the behavior becomes nonlinear until yielding occurs. After yielding, the polymer relaxes (softens), and there is a reduction in stress accompanied by constant increase in strain. At some point, the polymer strain-hardens and begins to take more stress up until fracture occurs.

By increasing the temperature from well below $T_g$ to above $T_g$, the following behavior is observed [10]. At low temperatures, the ultimate elongation of the polymer ($\varepsilon_u$) is low, and there is no yield point. At higher temperatures, there is a yield point and $\varepsilon_u$ greatly increases. Finally, at high temperatures, where the material is extremely soft, $\varepsilon_u$ may again decrease. The yield stress decreases as the temperature increases. In addition, at high rates of loading the polymers behave in a brittle manner, and at low strain rates they have a ductile behavior. The effects of the rate of loading and temperature are depicted in Figure 13.
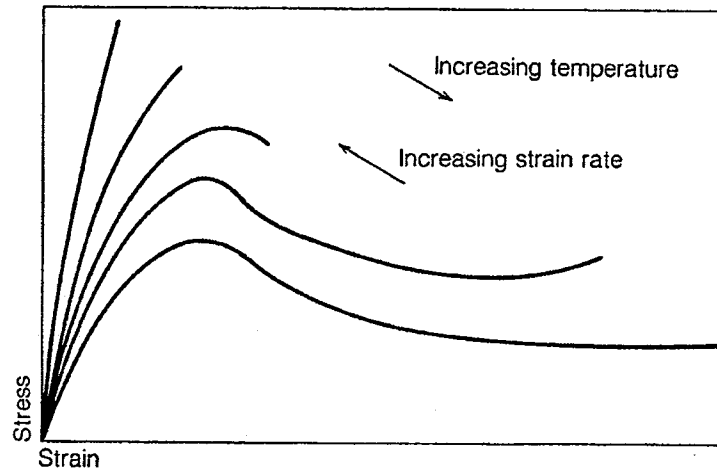
**Figure 13. Typical Tensile Stress-Strain Curves of a Thermoplastic Showing the Effects of Strain Rate and Temperature [3].**

## Creep

Viscoelastic materials experience deformations under constant loads less than the yield load over a period of time [8]. A material has viscoelastic behavior when its shear modulus changes with and depends only on time. The amount of deformation depends on the amount of load, the duration of loading, and the temperature. Polymer molecules are entangled and coiled when the polymer is formed. Upon application of constant load, there is gradual uncoiling and stretching of the molecules, and if the load is high, some molecules may even slip past each other. Similarly, rising the temperature supplies more energy that can be used to facilitate molecular movement. Typical creep behavior of a polymer under shear stress is illustrated in Figure 14. The creep behavior of a polymer subjected to tensile stress is shown in Figure 15.

The tangent modulus of elasticity of polymers decreases when creep takes place [7]. This decrease is evident by substituting values of the strain curves from Figure 15 into the following expression:

$$E(t) = \frac{\sigma}{\varepsilon(t)}$$

where,

$E(t)$    = elastic modulus as a function of time

$\sigma$    = normal stress

$\varepsilon(t)$    = normal strain

This equation is known as creep modulus, and it is smaller at larger applied loads [7].
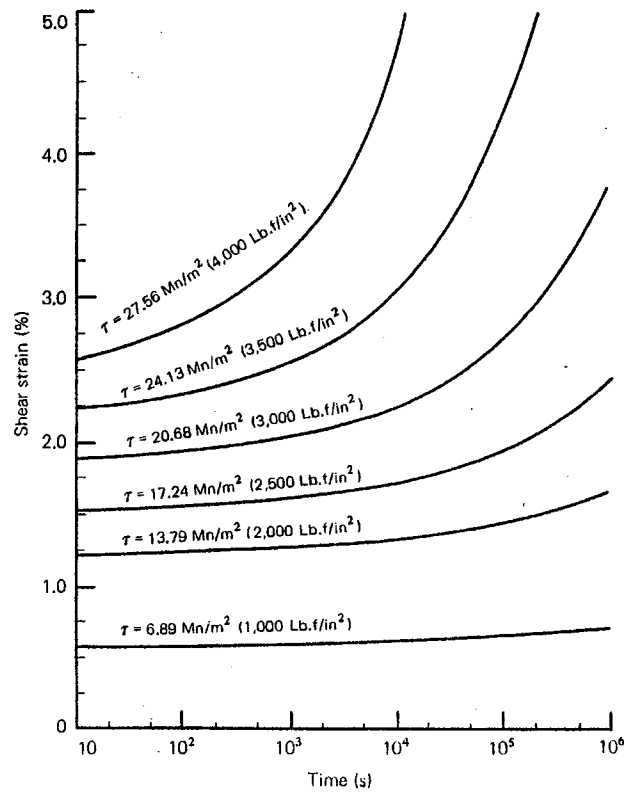


**Figure 14. Shear Strain Response of PVC to Pure Shear Stress [11].**
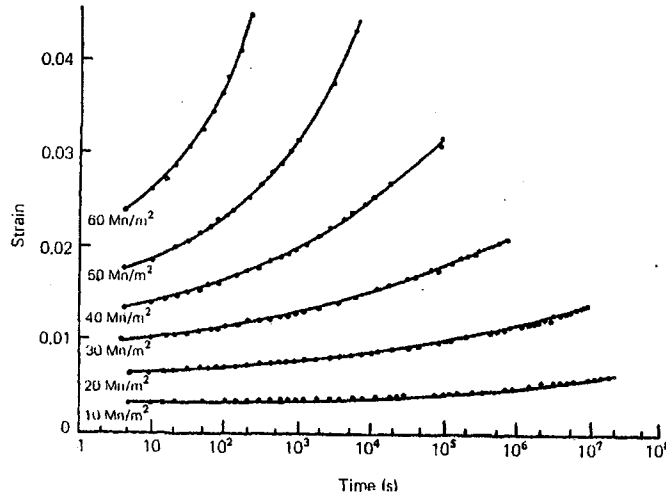
**Figure 15. Typical Tensile Creep Behavior of a Glassy Amorphous Polymer. (A Modified PMMA at 20 °C) [11].**

The matrix is usually a thermosetting polymer. Typical polymers used are polyester, vinyl ester, epoxy, and polyimide. The matrix has several functions in the composite:

- it bonds the fibers together to form a composite structure,
- it protects the fibers from physical damage and chemical attack, and
- it transfers the load to the fibers.

Factors affecting the selection of a matrix are cost, stiffness, strength, fracture toughness, upper use temperature, CTE, processing temperature, thermal shrinkage during curing, ability to wet and bond fibers, and sensitivity to moisture, chemicals, and ultraviolet radiation [1]. Large differences in the CTE between the fibers and the matrix can produce large residual stresses in the fibers and cracking of the matrix. Typical types of matrices used in FRP rebars are described next.

**Polyester Resin**

A typical polyester resin used in FRP products is an unsaturated (reactive) polyester solid dissolved in a polymerizable monomer [3]. Unsaturated polyesters are long-chain linear polymers containing a number of carbon double bonds. They are made by a condensation reaction between a glycol (ethylene, propylene, diethylene glycol) and

17

an unsaturated dibasic acid (maleic or fumaric.) The polymerizable (reactive) monomer such as styrene, which also contains carbon double bonds, acts as a crosslinking agent by bridging adjacent polyester molecules at their unsaturated points (making them capable of forming polymer products by chemical addition). The monomer also acts as a diluent, reduces viscosity, and makes it easier to process. The curing or crosslinking process is initiated by adding a small quantity of a catalyst such as organic peroxide [2, 12]. Since there is no by-product of the reaction, the curing is done at room temperature or elevated temperature with or without the application of pressure. The degree of unsaturation of the polyester resin depends on the presence of a saturated dibasic acid such as phthalic anhydride, isophthalic acid, or adipic acid [1]. A larger frequency of unsaturation results in a higher crosslinking density, which in turn improves stiffness, glass transition temperature, and thermal stability, but lowers ductility. Polyesters can be made quite resistant to fire, moisture, acids, and alkalis, although chlorinated solvents have a detrimental effect in their durability. The upper operating temperature of polyesters is in the vicinity of 120 °C.

The main advantages of polyesters for manufacturing of FRP bars are low viscosity, fast cure time, dimensional stability, excellent chemical resistance, and moderate cost [1]. The main disadvantage of unfilled polyesters is their high volumetric shrinkage during curing, which induces high residual stresses in FRPs. The manufacturing processes most used for polyesters are compression molding, filament winding, hand lay-up, mat molding, vacuum bag molding, pultrusion, and spray-up.

**Epoxy Resin**

Epoxy resins are low-molecular-weight organic liquids containing a number of epoxide groups, which are three-membered rings with one oxygen and two carbon atoms [3]. The most common process for producing epoxies is the reaction of epichlorohydrin with bisphenol-A amino or acid compounds. Crosslinking is then obtained by introducing chemicals that react with the epoxy and hydroxy groups between the adjacent chains. A curing agent is mixed into the liquid epoxy to induce polymerization. A solid network

crosslinked polymer then forms. Epoxy systems, like polyesters, can be cured at room temperature, but quite often heat is added to accelerate and improve curing.

Epoxy polymers yield excellent adhesion with a variety of fibers, moisture resistance, and chemical resistance.

**Vinyl Ester Resin**

Vinyl ester resins are produced by the reaction of a monofunctional unsaturated acid, such as methacrylic acid, and an epoxy resin [1]. As with polyesters, styrene monomers are used to decrease viscosity prior to cure and to crosslink unsaturated points in neighboring vinyl ester molecules during cure.

Vinyl esters have better chemical and high temperature resistance than polyesters [1]. Vinyl esters are easier to handle during processing than either polyester or epoxies due to their relatively low crosslinking. The hydroxyl (OH) groups occurring along the length of the vinyl ester molecule form hydrogen bonds with similar groups on the surface of glass fibers. This formation results in good wet-out (wetting of the surface of fibers) and high interfacial strength. The properties of the epoxy resins used in the process have a significant influence on the heat resistance and thermal stability of vinyl ester, although tensile strength is not appreciably influenced. A disadvantage of vinyl ester resins is their volumetric shrinkage during processing. Vinyl esters are well suited for hand lay-up and are now being used as the matrix for FRP reinforcing bars.

**Polyimide Resin**

Polyimides are polymers containing cyclic imide groups in the main molecular chain [1]. Condensation-type polyimides are made from low viscosity starting materials. Full curing of the condensation-type polyimides implies imidization (coupling of aromatic rings (imide linkages)–that is, linkages in which two carbonyl (CO) groups are attached to the same nitrogen (N) atom [13]) of the polymer at temperatures of 200 to 260 °C. Polyimides are available in both thermoplastics and thermosets [14].

19

Bismaleimide (BMI) is a typically used addition-type polyimide. BMIs are capable of epoxy-like processing in terms of cure temperature and handling characteristics [1]. It is common to post-cure this resin at 232 °C to develop full temperature capability. This resin can be used in temperatures ranging from -240 to 315 °C, which is why they are referred to as high-heat-resistant plastics [14].

The main advantages of polyimides are their excellent resistance to heat, thermal degradation, organic solvents, high-energy radiation, low coefficient of friction, and excellent resistance to wear [2, 14]. They are moderately susceptible to attack by dilute acids and are dissolved by strong mineral acids such as nitric acid or sulfuric acid, especially at high temperatures. In addition, they are hydrolyzed by alkalis [1].

**Resin Fillers and Additives**

Fillers are used to reduce the volume of polymer used without excessive detriment to the properties of the composite [1]. Fillers also help lower costs and improve the mechanical or aesthetical properties of the composite [14]. Some common fillers are peanut and walnut shells, fly ash, wood cellulose, hollow glass beads, alumina powder, calcium carbonate, cotton, jute, kaolin, mica, silica, fluorocarbon, and talc. Fillers help attain specific properties to the composite such as higher stiffness, strength, viscosity, and toughness [1]. Filler fractions can be as high as 50 percent with the viscosity of the resin setting the upper limit. Calcium carbonate ($CaCO_3$) is a filler commonly used to reduce shrinkage and cost of polyester and vinyl ester resins. Alumina silicate (clay) improves corrosion resistance, electrical properties, and surface finish.

Various available resin additives can be used to improve the resistance of matrices to smoke generation, flames, moisture, microbial degradation, oxidation, chemicals, heat, shrinkage, surface roughness, and ultraviolet radiation [1].

# III. FABRICATION OF COMPOSITES

The processes most commonly used to manufacture FRP bars are pultrusion, braiding, and filament winding. A brief description of those processes follows.

## PULTRUSION

In the pultrusion process, the fibers are pulled from the rovings, wet in a resin bath and slowly pulled through a preforming fixture where excess resin and/or air are removed, and then finally pulled through a heated die where the matrix cures [2, 3]. After passing the die, the bars are cut with an abrasive saw [1]. A schematic representation of the pultrusion process is illustrated in Figure 16. Pultruded profiles can be made solid, hollow, with foam, wood, or wire cores. The basic pultrusion machine consists of the following elements: creels, resin bath, heated dies, driver mechanism, and cut-off saw. A creel is a metallic shelf that holds roving packages.

A good resin for pultruded FRPs must be able to gel and cure rapidly to properly release from the die wall [1]. High chemical shrinkage such as in the case of polyester is a favorable property for pultrusion manufacturing. Epoxies are not suited for pultrusion because of slow reaction times, short pot lives, higher scrap losses, and a tendency to stick to the wall of the die.
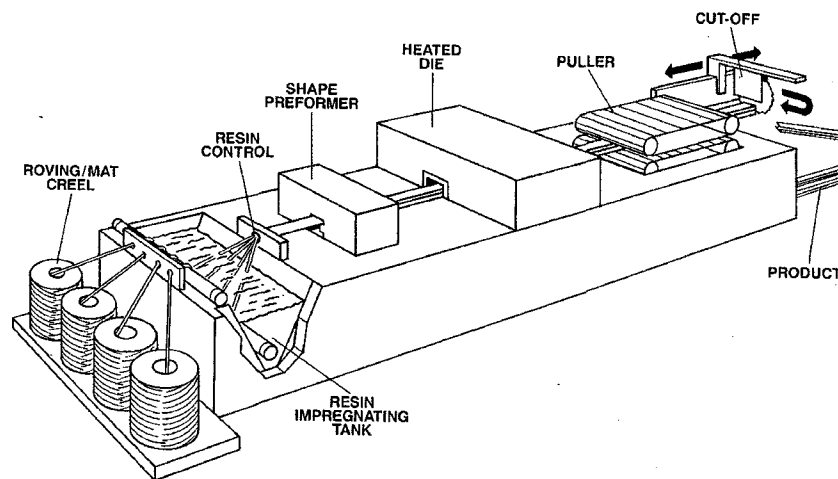


Figure 16. Pultrusion Process [3].

21

In the construction industry, bars are commonly fabricated with deformed surfaces to aid bonding of the rebar to the concrete [1]. Bar deformations can be made by braiding or wrapping the bar with additional resin-soaked fibers in a helical pattern just before curing, or lugs can be made on the surface of bars by forming sections of the bar one at a time in a heated die.

## BRAIDING

This process consists of interlacing two or more yarns to form an integrated structure [1]. When compared to unidirectional FRP composites, braided FRPs have better resistance to impact and delamination because of the interlaced yarns. However, they have lower in-plane stiffness owing to fiber curvature and lower fiber content. After the braided fiber has been manufactured, resin is typically injected using the resin transfer molding technique. Therefore, resin viscosity and pot life are important factors to consider when selecting resins for braided FRPs. A schematic diagram of the principle used in braiding is presented in Figure 17.
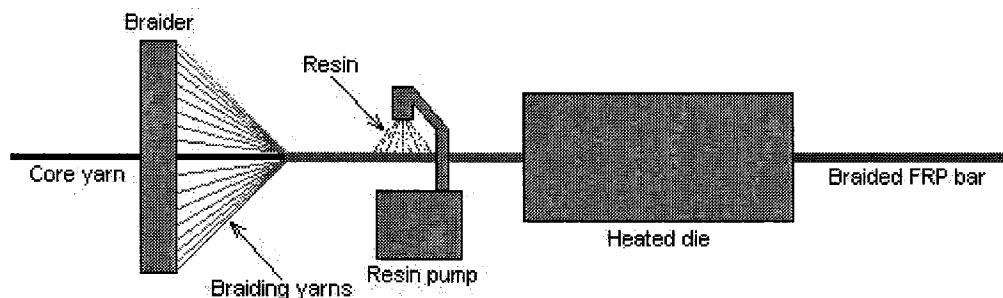


**Figure 17. Schematic Representation of the Braidtrusion Process.**

# FILAMENT WINDING

Filament winding is a process used to manufacture cylindrical products. Filament winding is attained by wrapping a narrow band of resin-impregnated tow around a convex, rotating mandrel, resulting in a hollow structure that can be subsequently cured in an oven [2, 3]. The fiber tows can be impregnated either previously or just prior to winding by passing them through a spreader and a resin bath. Machines that control the traversing speeds synchronized with the mandrel rotation set the winding angles and place the fibers [3]. Figure 18 depicts the filament winding process.
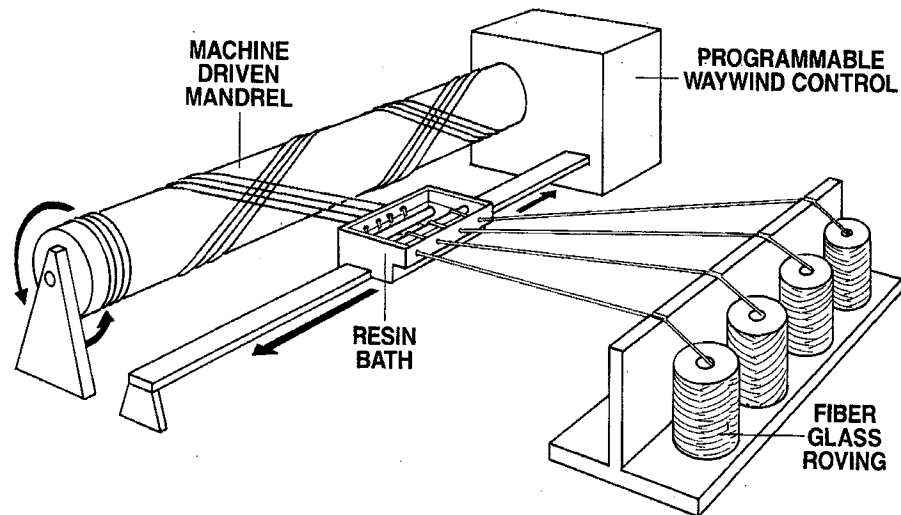


**Figure 18. Filament Winding Process [3].**
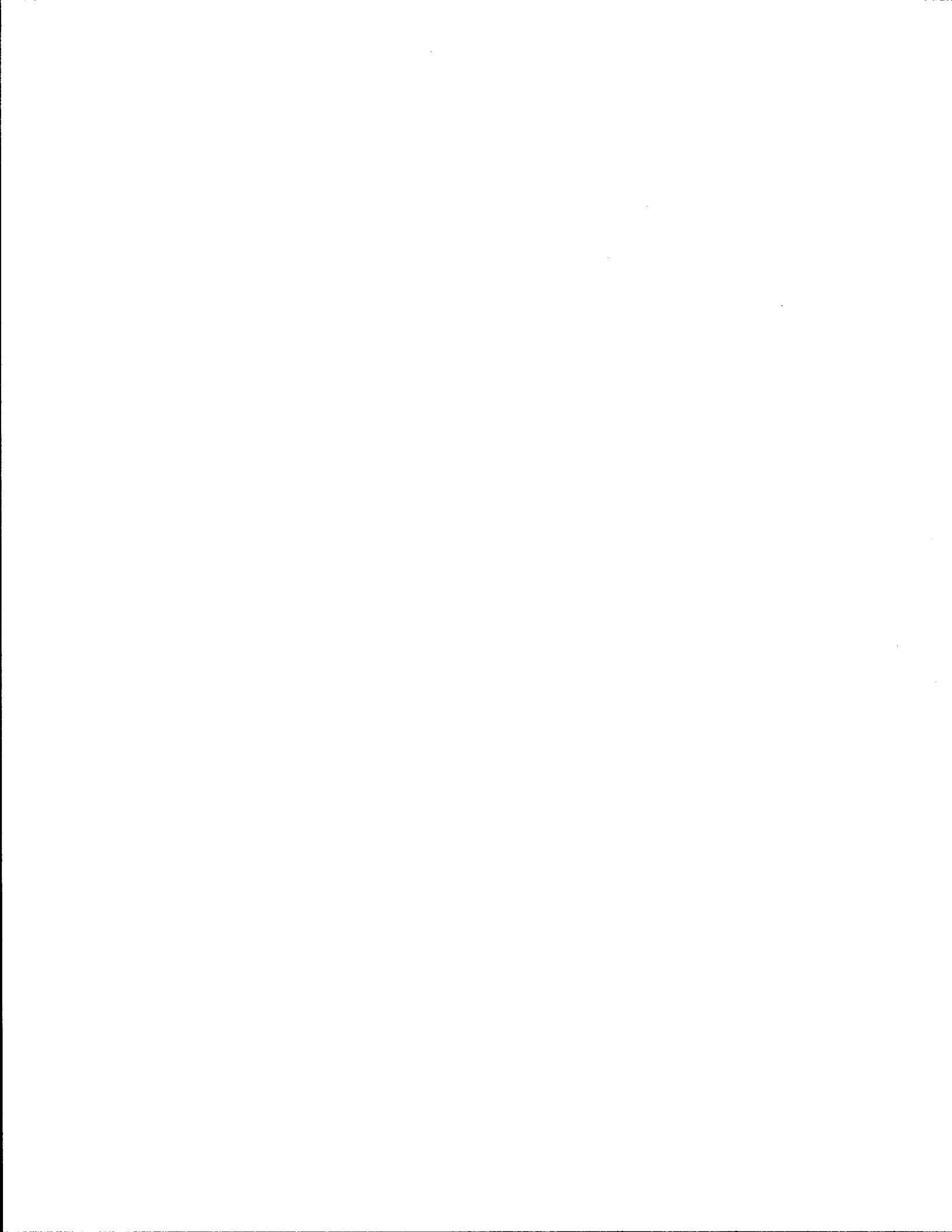
# IV. COMPOSITE BEHAVIOR

Most FRP bars can be modeled as unidirectional composites. However, some FRP reinforcement such as tendons and braided bars require a different model [3].

## LONGITUDINAL STRENGTH AND STIFFNESS

The properties of the composite material depend on the properties of the constituent materials and their chemical interactions and distribution [3]. Although theoretical and semi-empirical models to predict the properties of composites exist, they may not be reliable for design purposes. Experimental measurements of the properties of composites are preferable over theoretical models, although the theoretical models can be useful to judge whether spurious experimental data has been obtained.

The following expression predicts with reasonable accuracy, the elastic modulus of a unidirectional composite:

$$E_c = E_f V_f + E_m V_m$$

where,
$E_c, E_f, E_m$ = Young's modulus of the composite, fiber, and matrix, respectively, in the longitudinal direction.
*volume of the composite = volume of fibers + volume of matrix*
$V_f$ = volume fraction of the fibers [= *volume of the fibers/volume of the composite*]
$V_m$ = volume fraction of the matrix [= *volume of the matrix/volume of the composite*]

The above equation shows that fibers are very effective in increasing the modulus of the composite in the longitudinal direction.

## INITIAL STRESS-STRAIN BEHAVIOR

Unidirectional composites may be modeled assuming that fibers are uniform in property, diameter, and are continuous and parallel throughout the composite. If it is assumed that perfect bonding exists between the fibers and the matrix such that slippage does not take place at the interface, the strains experienced by the fiber, matrix, and composite are equal. With these assumptions, the stress in the composite can be determined using:

$$\sigma_c = \sigma_f V_f + \sigma_m V_m$$

where,

$\sigma_c$, $\sigma_f$, $\sigma_m$ = stress in the composite, fibers, and matrix, respectively

$V_f$ and $V_m$ are as defined above

The above expression can be used to predict the initial mechanical behavior of the composite when the stress-strain diagrams of the fibers and matrix are known [3]. Most fibers have a linear stress-strain diagram up to rupture, while polymers have a nonlinear stress-strain diagram. The stress-strain diagram of the composite can be constructed using the stress-strain diagrams of the constituents. At a given strain level, the stress in the fibers and the matrix can be obtained from their corresponding stress-strain diagrams. Since polymeric matrices are nonlinear, the composite stress-strain behavior will be nonlinear. However, for typical fiber volume fractions and elastic properties of the fibers and matrix used in composite bars, the composite behavior is nearly linear.

## BEHAVIOR BEYOND INITIAL DEFORMATION

In general, the deformation of a composite may proceed in four stages [3]:

(1) Both the fibers and the matrix deform in a linear elastic manner.

(2) The fibers continue to deform elastically, but the matrix now deforms nonlinearly.

(3) The fibers and the matrix deform nonlinearly.

(4) The fibers fracture followed by the overall composite fracture.

A hypothetical stress-strain behavior of composites with brittle and ductile fibers, and a matrix with a nonlinear behavior are shown in Figure 19 [3].
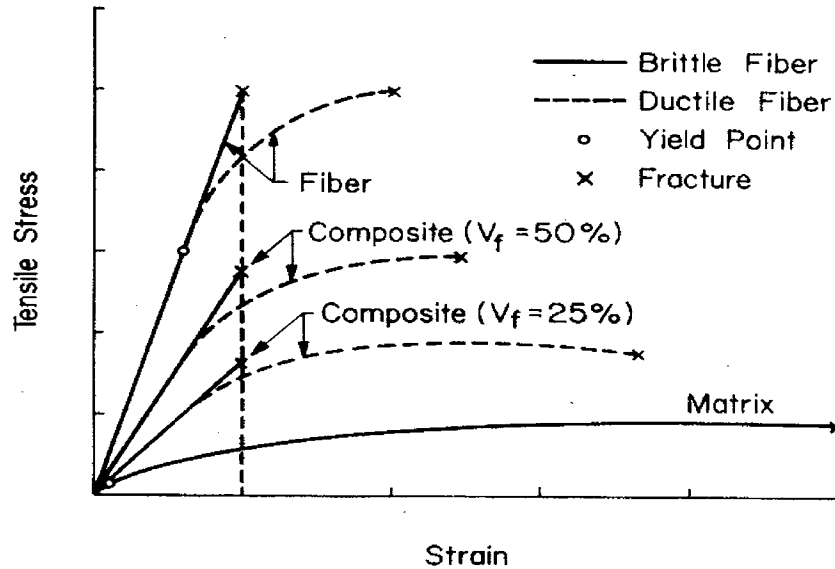


**Figure 19. Stress-Strain Curves for Hypothetical Composite Materials with Ductile and Brittle Fibers and Typical Ductile Matrix [3].**

For typical fiber volume fractions used in composite FRP bars, the ultimate strength of the composite can be estimated with the following expression (assuming there are no voids) [3]:

$$\sigma_{cu} = \sigma_{fu} V_f + (\sigma_m)_{\varepsilon fu} V_m$$

where,

$\sigma_{cu}$, $\sigma_{fu}$ = stress in the composite and fibers, respectively, at failure

$(\sigma_m)_{\varepsilon fu}$ = stress in the matrix at the strain level at which the fibers rupture

$V_f$ and $V_m$ are as defined above

27

**CREEP**

Creep is the increase in strain with time for a material subjected to a constant load. As discussed above, the longitudinal strength of composites is dominated by the strength of the fibers themselves [15]. Therefore, composites exhibit creep rupture behavior when the fibers exhibit creep rupture. Creep rupture (or stress rupture) is the failure with time of a material under constant stress in air. Creep rupture of a composite may occur as a result of a combination of the statistical strength of brittle fibers coupled with time-dependent properties of a viscoelastic matrix (a material has viscoelastic behavior when its shear modulus changes with and depends only on time) [15]. This combination may result in a continually changing state of stress inside the composite even when subjected only to constant load. These changes ensure a delayed fracture of the composite. Thus, the properties of both the matrix and the fibers have an important influence in the stress rupture of composites. Matrices that have a small effect on the short-term longitudinal strength of composites play a very important role in their long-term strength.

The strength of glass fibers is reduced with time and at high temperatures [15]. At room temperature, fibers lose nearly 3 percent of their short-term strength for every tenfold increase in load duration [15]. The endurance time is a function of the stress level, the microenvironment surrounding the element, and the temperature [15]. Stress rupture tests for virgin E-glass at various temperatures and 50 percent relative humidity are shown in Figure 20.
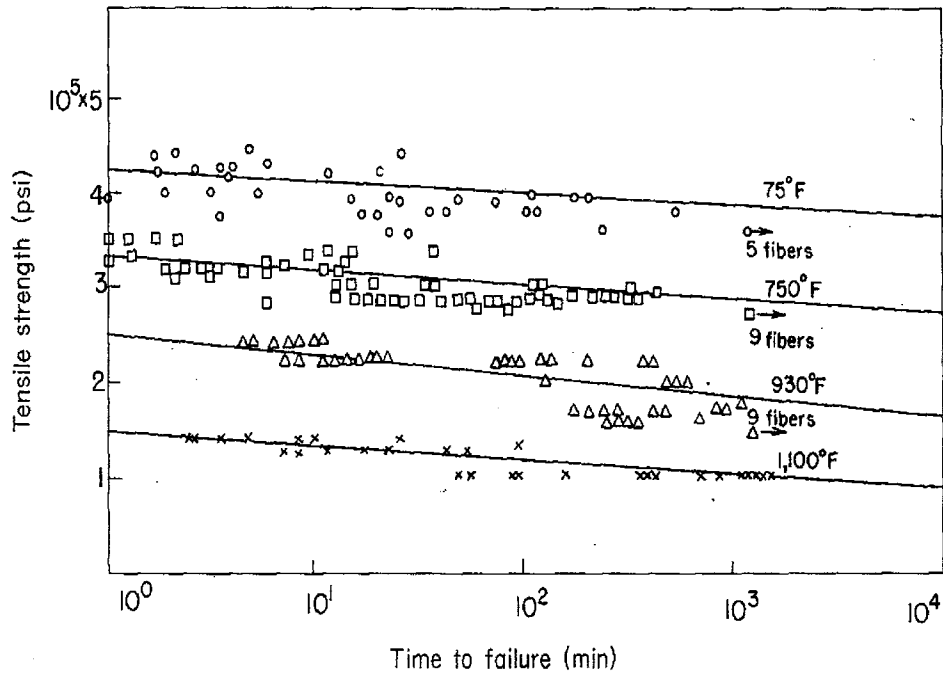
**Figure 20. Static-Fatigue Test for Virgin 0.004-in. Diameter E-Glass at Various Temperatures and 50 Percent Relative Humidity [15].**

Since the strength of glass is time dependent, many researchers believe that the delayed failure mechanism of glass-reinforced polymers is caused by the stress rupture properties of the glass only [15]. However, other authors have shown that the stress rupture of composites can take place even when the strength of the fibers is not time dependent [15]. Tests on carbon-reinforced epoxy have evidenced stress rupture, even though carbon fibers appear not to suffer from static fatigue.

Rosen [15] has treated the fibers as having a statistical distribution of defects resulting in rupture of the fibers prior to composite failure. According to his model, the accumulation of those breaks coupled with stress concentrations results in composite failure. The distribution of breaks in the fibers leads to the development of local shear stresses in the matrix, which is expected to relax. As a consequence, larger portions of fibers near broken ends become ineffective to carry load, and portions of the fiber away from the fiber end become stressed to higher levels. This sequence of events suggests the likelihood of time-dependent failure of fiber composites. The probability lines for stress-rupture of S-glass epoxy strands are illustrated in Figure 21.

29
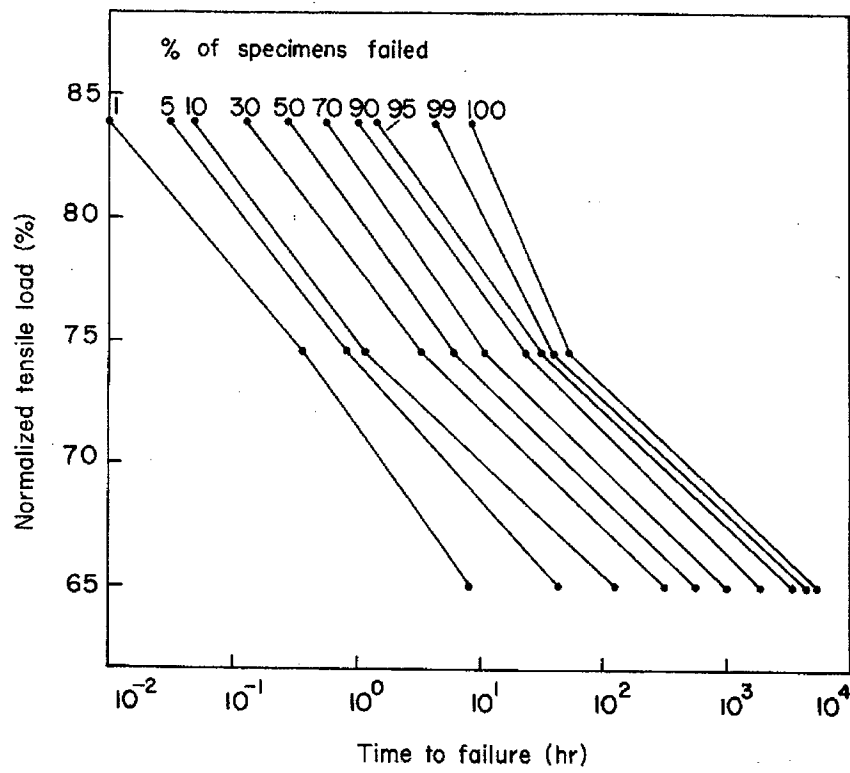
**Figure 21. Probability Lines for Stress-Rupture of S-Glass Epoxy Strands [15].**

# V. MECHANICAL PROPERTIES AND TEST METHODS OF FRP BARS

For comparison, typical properties of common FRP bars, FRP tendons, and steel bars are illustrated in Table 3. This table shows that almost all the FRP bars have a higher tensile strength than steel bars. The tensile modulus of all FRP bars is lower than the tensile modulus of steel bars, especially for GFRP bars. The shear strength of all FRP bars is lower than the shear strength of steel bars. The ultimate elongation is lowest for carbon FRP tendons and highest for steel bars. The coefficient of thermal expansion of all types of FRP bars is lower than that of the steel bars. The transverse coefficient of thermal expansion of FRP bars is nearly four times that of steel bars. Finally, the specific gravity of FRP bars is one fourth or less than that of steel bars.

## PHYSICAL AND MECHANICAL PROPERTIES

FRP bars are anisotropic materials and, unlike steel reinforcement, the properties of FRP rebars vary depending on the manufacturer. No standard tests have been established in the United States to determine the properties of the bars although ACI committee 440 K has prepared a draft of a set of proposed test standards. The only standard test methods for FRP reinforcement currently available were developed by the Japanese and are included in *Recommendation for Design and Construction of Concrete Structures Using Continuous Fiber Reinforcing Materials* [16].

The ACI state-of-the-art report [17] recommends that designers verify the properties of the actual FRP bars being specified. Some researchers recommend taking the maximum strength as the average reported strength minus three standard deviations [18]. The Canadian Highway Bridge Design Code (CHBDC) recommends that the specified tensile strength $f_{pu}$ of a FRP bar used in design should be its fifth percentile tensile strength. The CHBDC indicates that the above material property is obtained from the manufacturer [19].

## Table 3. Properties of Common FRP Bars and Tendons.

| Bar Type | Tensile Strength MPa (ksi) | Tensile Modulus GPa (ksi) | Direct Shear Strength MPa (ksi) | Ultimate Elongation mm/mm | Longitudinal Coefficient of Thermal Expansion $(10^{-6}/^{\circ}C)$ | Transverse Coefficient of Thermal Expansion $(10^{-6}/^{\circ}C)$ | Specific gravity |
|---|---|---|---|---|---|---|---|
| GFRP Bar | 517-1207 (75-175) (a) | 41-55 (6000-8000) (a) | 151 (22) (c) | 0.035-0.05 (a)(1) | 7.5 (b) | 44 (b), (d) | 1.5-2.0 (a) |
| AFRP Tendon | 1200-2068 (170-300) (a) | 50-74 (7000-11000) (a) (2) | 219 (32) (c) (Bar) | 0.02-0.026 (a) | -1.0 (a) | N/A (d) | 1.25 (a) |
| CFRP Tendon | 1650-2410 (240-350) (a) | 152-165 (22000-24000) (a) | 236 (34) (c) | 0.01-0.015 (a) | 0 (a) | N/A (d) | 1.5-1.6 (a) |
| Steel Bar | 483-690 (70-100) (a) | 200 (29000) (a) | 523 (76) (c) | >0.10 (a) | 11.7 (a) | 11.7 | 7.9 (a) |

(a)  Source [17], (b) Source [20], (c) Source [21]
(d)  The transverse coefficient of thermal expansion depends heavily on the properties of the matrix.
(1)  These reported values seem high when compared with values of 0.029 obtained in tests performed by the authors.
(2)  The actual reported lower bound value is 70,000 ksi, which we believe has a typographical error.

Figure 22 shows some typical FRP bars currently available in Japan.
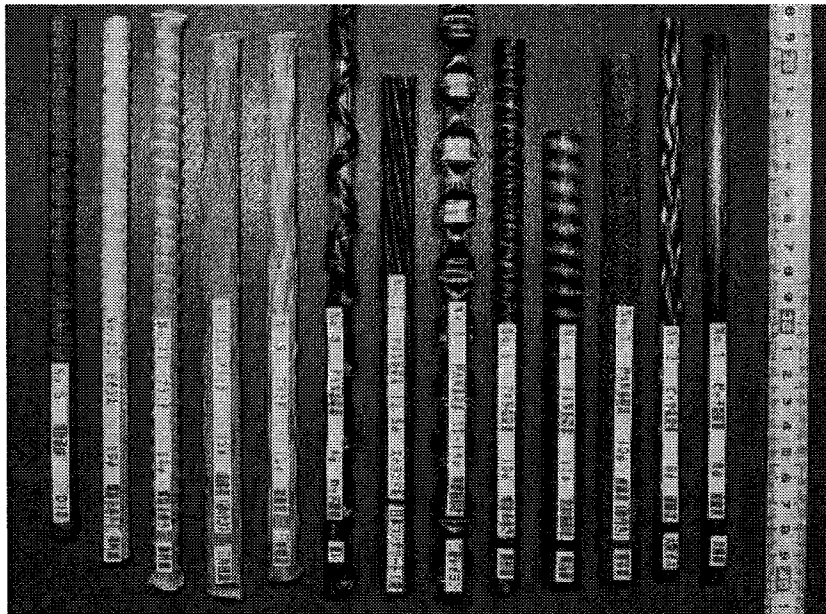


**Figure 22. Typical FRP Bars Available in Japan [22].**

The following sections describe some material properties of FRP bars.

## Specific Gravity

The specific gravity of bars is the ratio of the weight of a piece of bar to the weight of water with the same volume as the piece of bar [14]. The specific gravity of FRP bars varies between 1.25 and 2.0 [17]. This light weight property saves time and costs during handling, transportation, and installation.

## Thermal Expansion

The coefficient of thermal expansion (CTE) of concrete varies from 6 to 11 x $10^{-6}/°C$ [17]. The longitudinal CTE of FRP rebar is similar to that of concrete. However, the transverse CTE of FRP rebar is about four times that of the concrete. This difference in thermal expansion coefficients can lead to cracking of the surface of bridge decks due to thermal incompatibility. Gentry and Husain [20] studied the thermal effects of bars embedded in cylindrical concrete specimens and found that a stress of 6 MPa (870 psi) could be developed on the concrete surrounding a 19 mm diameter FRP bar, for a specimen with a concrete cover of 50 mm and a 40 °C temperature change. It is not unusual to register high temperatures on the surface of concrete bridge decks in the summer. Hoffman et al. [23] recorded 47 °C on July 7, 1979, on the surface of the deck of a prestressed concrete segmental box-girder bridge located in Pennsylvania. Instrumentation and monitoring of the Kishwaukee River Bridge, located in Illinois, over a period of more than 2000 days revealed maximum air temperature change of 33 °C near the bridge site [24]. Monitoring for 1500 days of the Denny Creek Bridge, located in Washington, evidenced maximum air temperature changes of approximately 25 °F near the bridge site [24].

## Tensile Strength

FRP rebars have a linear elastic stress-strain behavior up to failure when tested in tension [25]. The tensile strength of GFRP rebars is dependent on the diameter of the bars [26]. The larger the bar diameter, the lower the tensile strength. This ratio is believed to

be the result of shear lag. Shear lag occurs when stresses are transferred to the bar through bond, and excessive shear stresses concentrate on the surface of the bar causing progressive failure of individual fibers [26]. Tamuzs and Tepfers [27] manufactured hybrid FRP bars with carbon and aramid fibers to obtain bars with a nonlinear stress-strain curve when fibers break progressively. The fibers that can sustain the least ultimate tensile strain break first, followed by the fibers that can stand more strain before rupture, until all of the fibers fail. As already noted, the tensile strength of the bar is controlled by the properties of the fibers. Typical stress-strain curves of FRP bars and an A-615 grade 60 steel bar are illustrated in Figure 23.
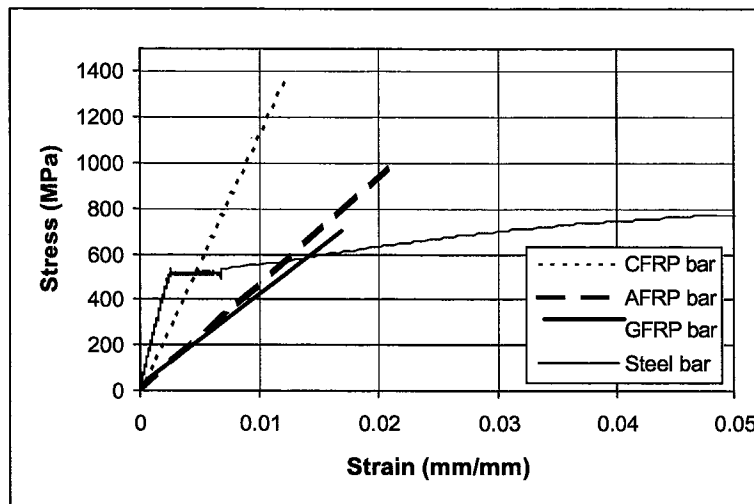


**Figure 23. Stress-Strain Curves for Glass, Carbon, and Aramid FRP Bars or Tendons and Steel Bar [16].**

**Tensile Modulus**

The longitudinal modulus of elasticity of composite FRP reinforcement is dominated by the properties of the fibers as described in the section of composite behavior. The longitudinal modulus of elasticity of GFRP rebar is approximately 25 percent of that of steel [17]. Typical values of the bar's longitudinal modulus are shown in Table 3.

34

**Ultimate Tensile Strain**

The ultimate tensile strain of FRP bars depends heavily on the ultimate strain of the fibers [3]. Typical ultimate strain values of composite FRP bars are given in Table 3 [17]. Uomoto and Hodhod [28] reported higher strains for aramid FRP bars and lower ultimate strains for glass FRP bars. Marshall Industries reported ultimate strains of nearly 1.8 percent for glass FRP bars [29]. Deitz [25] found ultimate strains of GFRP bars to be approximately 1.3 percent.

**Compressive Strength**

The compressive strength of FRP rebars is lower than the tensile strength [3]. The compressive strength of FRP bars depends on whether the surface is smooth or ribbed, on the buckling strength of fibers, on fiber volume fraction, on stiffness of the matrix, on provision of confinement, etc. [17]. Fibers and matrix both have an important influence in the longitudinal compressive strength of the composite bar [3]. The transverse compressive strength is governed by the properties of the matrix. Deitz [25] carried out a series of compression tests on 15 mm diameter glass–fiber–reinforced polymer (GFRP) bars with different specimen lengths, with both ends fixed, and found that specimens with lengths under 110 mm failed by crushing of the bar; specimens with lengths greater than 210 mm failed in buckling mode; and specimens with intermediate lengths failed in a combined mode (bucking followed by crushing). Wide scatter was reported in the results of the specimens that failed in crushing, little scatter in the specimens that failed in buckling, and intermediate scatter in the results of specimens with intermediate lengths. Based on the above observations the author proposed the following design equations for the bars used in the experiments:

Crushing Failure ($0 \leq L \leq 110$ mm)

$\sigma = 325$ *MPa*

Combined Buckling and Crushing Failure (110 mm ≤ L ≤ 210 mm)

$$\sigma(MPa) = 325 - \frac{1}{2}(L - 110)$$

Buckling Failure (L > 210 mm)

$$\sigma = \frac{\pi^2 E}{\left(\dfrac{KL}{r}\right)^2}$$

A plot of compressive strength versus unbraced length, including the proposed design equations is presented in Figure 24. The radius of gyration of 3.6 mm reported by the author seems low. Calculations performed by the research team yield a value of 14.1 mm. Using this radius of gyration and a theoretical value of K = 0.5 for columns fixed at both ends, a factor of (KL/r = 3.91) is obtained for L = 110 mm and (KL/r = 7.47) for L = 210 mm.
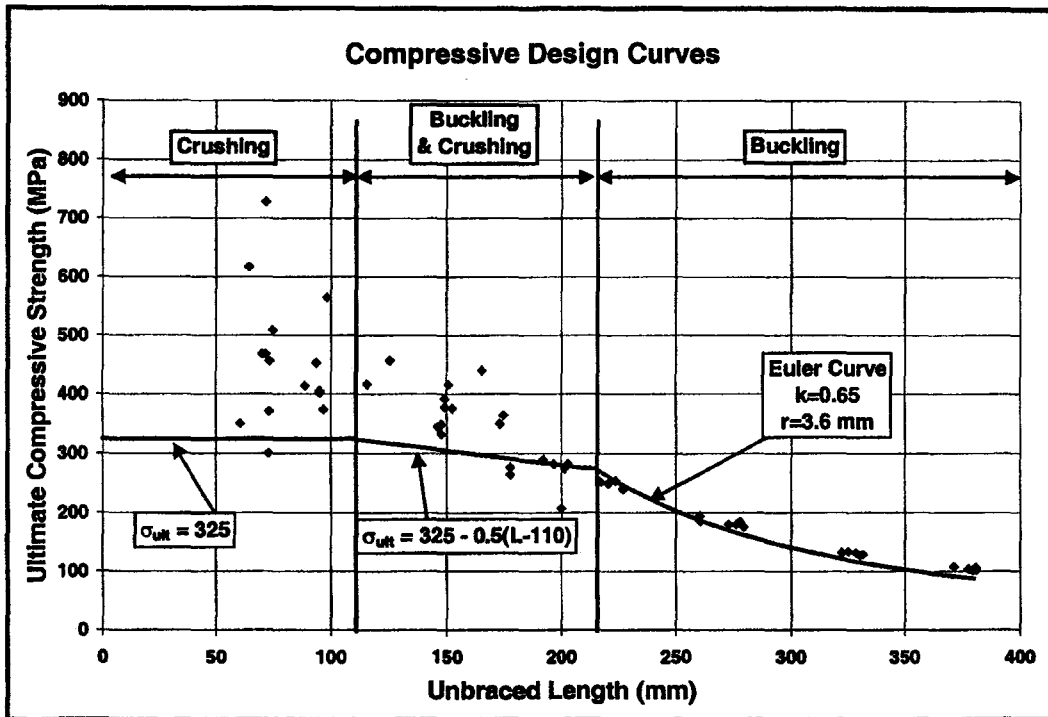


**Figure 24. Ultimate Compressive Strength Versus Unbraced Length [25].**

## Compressive Modulus

The longitudinal compressive modulus is governed by the properties of the fibers [3]. Compressive modulus depends on the type of FRP bar, bar size, quality control during manufacturing, and length-to-diameter ratio of the specimens [17]. Tests on specimens with 55 to 60 percent volume fraction of E-glass fibers in a vinyl ester matrix resulted in a modulus of 34 to 48 GPa [30]. Deitz [25] found the elastic moduli of 15 mm diameter GFRP bars in compression to be 41.7 GPa for specimens 80 mm long, 44.6 GPa for specimens 200 mm long, and 41.2 GPa for specimens 300 mm long. A plot of the stress-strain behavior of GFRP bars tested in compression is presented in Figure 25.
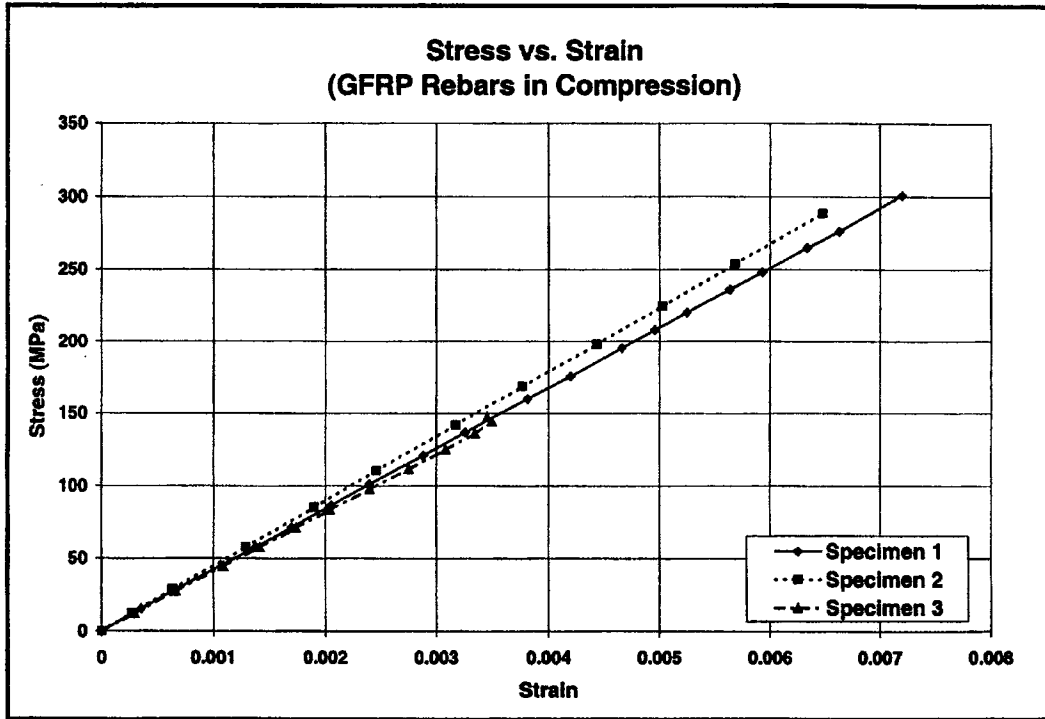


**Figure 25. Stress-Strain Curves for Glass FRP Bars in Compression [25].**

## Shear Strength

The shear modulus of composites is governed by the properties of the matrix, while the shear strength is governed by the properties of the matrix and interface [3]. Shear tests have been performed on FRP bars using the Isopescu shear procedure [31].

37

Ueda et al. [32] carried out tests on aramid FRP stirrups subjected to simultaneous tensile and shear forces and determined that the shear strength of the stirrups is reduced significantly by the presence of tensile stresses. The strength of FRP stirrups is significantly reduced at bent sections and can be as low as 40 percent of the reduction in strength experienced at the midsection of the stirrup. Finite element analyses based on the maximum strain criterion carried out by the authors were in excellent agreement with experimental results. Accurate estimation of the shear modulus of FRP bars, depth of the concrete conical failure around the FRP bar, and the bond stress-slip relationship of the FRP bar are sufficient for predicting the strength of FRP bars at the intersection of cracks and at the bent portions of stirrups. The authors developed the interaction failure envelopes shown in Figure 26, which account for the simultaneous action of tensile and shear forces. The plots demonstrate that the specimens failed in shear for a crack width of 1 mm, while they failed in tension for crack widths of 3 and 4.2 mm.
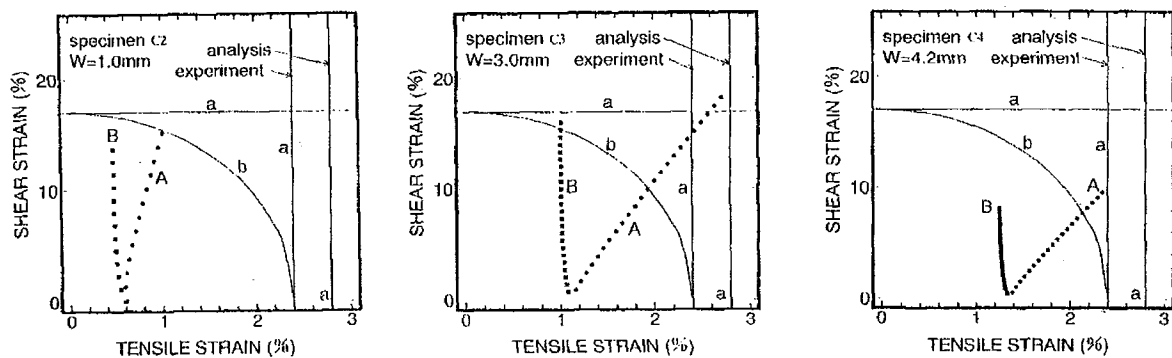


**Figure 26. Interaction Diagrams for Normal and Shear Strains in FRP Bars [32].**

## Creep

As mentioned in the section of composite behavior, FRP bars subjected to the action of a constant load may suddenly fail. For steel reinforcement and prestressing strands, the usual range of 75 percent of the characteristic static tensile strength can be endured indefinitely without fracture or strength loss [17].

Studies by Budelmann and Rostasy [33] show that stress rupture does not occur if the sustained stress is limited to 60 percent of the short-term strength of FRP bars. Although the reinforcement in concrete structures is usually subjected to sustained stresses below 60 percent, material degradation due to environmental factors may reduce the endurance time of FRP bars. Therefore, stress rupture may be a concern, especially for prestressed concrete structures. As the ratio of the sustained stress to the short-term strength increases, creep rupture time decreases. Creep test results for FiBRA® bars made with carbon fibers are illustrated in Figure 27.



**Figure 27. Creep Test Results for FiBRA® Bars [17].**

In a model presented by Budelmann and Rostasy [33], GFRP bars stressed at 65 percent of their initial strength were predicted to fail at $5 \times 10^5$ hours (57 years).

Since the tensile strength of FRP reinforcement is time dependent, the ACI state-of-the-art report [17] recommends limiting the sustained load in FRP reinforcement to 50 to 60 percent of the static tensile strength. However, results of stress rupture tests on S-glass epoxy composites conducted over a 10-year period at the Lawrence Livermore Laboratory, California, showed that 2 percent of the test specimens failed at a sustained stress of 40 percent of the short-term tensile strength, while none failed at stresses of 35 percent of the short-term tensile strength [21].

**Fatigue Strength**

GFRP bars typically have good fatigue resistance, although the fatigue resistance of glass composites is lower than that of steel at low stress ratios [34]. Investigators found that dowel bars in shear had good fatigue resistance when tested to 10 million cycles. Other tests on GFRP bars to be used in prestressing applications were subjected to repeated cyclic loading with a maximum stress of 496 MPa (72 ksi) and a stress range of 345 MPa (50 ksi). The bars withstood more that 4 million cycles of loading prior to the appearance of signs of failure at the anchorage. Fatigue test results for FiBRA bars tested in tension-tension are presented in Figure 28.

*New Fiber* Composite *Ma*terial for Reinforced *C*oncrete (NEFMAC®) is a grid of FRP bars interwoven at right angles. NEFMAC specimens endured 4 million cycles of tension fatigue tests for loads between 10 and 30 percent of the ultimate tensile strength at a frequency of 5 Hz, according to Rahman et al. [35]. After enduring the 4 million cycles, the Type-CG NEFMAC specimens retained 92 percent of its initial static tensile strength, while Type-C retained 93 percent.
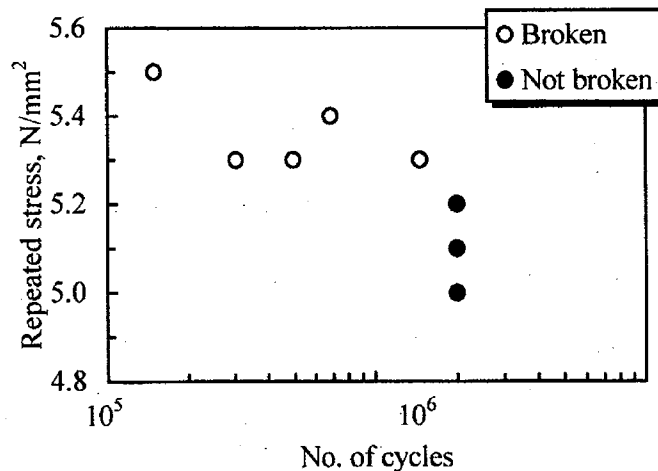


**Figure 28. Fatigue Test Results for FiBRA® Bars [16].**

Fatigue tests conducted on concrete beams with aramid fiber bars by Iwamoto et al. [21] showed that the fatigue strength of concrete beams subjected to 2 million cycles

40

was not less than 65 percent of the static ultimate strength of the FRP-reinforced concrete beams. The researchers concluded that the fatigue strength of beams with aramid fiber tendons cannot be predicted by fatigue tests on isolated aramid fiber bars.

CFRP tendons exhibited good fatigue resistance under a tension-tension fatigue test for two million cycles [36]. The maximum stress was 64 percent of the ultimate strength and the minimum was 55 percent. The elastic modulus of the tendons did not change after the fatigue test.

**Flexural Strength**

In a study by Kaski and Dolan [37], tendons were given a curvature and tested in tension. It was found that bent tendons for use in prestressing fail at the bent portion at a load lower than the tensile strength of straight tendons. The researchers recommended carrying out creep-rupture tests in curvature. It was determined that spooling of tendons in spools of typical radius causes microbuckling of fibers in the tendon. Bending stresses due to spooling, as low as 20 percent of the tensile strength of tendons, cause microbuckling of fibers.

**FACTORS AFFECTING MECHANICAL PROPERTIES**

There are many environmental factors that affect the properties of FRP bars. Their effects have been explored separately although all act simultaneously. It should be pointed out that some of the conditions under which FRP bars have been tested by different researchers are not necessarily representative of conditions experienced by the FRP bars in actual concrete structures.

**Moisture**

Water absorbed by polymers softens the polymers' structure and leads to loss of strength and stiffness of the composite [17]. Moisture also promotes growth of pre-

existing flaws [15]. According to Tannous and Saadatmanesh [38], exposure of GFRP rebars to water reduced the tensile strength by approximately 7 percent in six months. The investigators also found that the diffusivity coefficient and the saturation moisture content were higher for rebars made with polyester resin as compared to those made with vinyl ester resin, and the polyester bars degraded more than vinyl ester bars.

**Temperature**

Low temperatures cause embrittlement of polymers and make these polymers more susceptible to cracking [39]. Crazing and polymer microcracking cause irreversible damage to thermoset polymer properties.

A 35 °C temperature increase and exposure over six months reduced the strength of GFRP bars made with vinyl ester resin by nearly 23 percent. GFRP bars made with polyester resin exhibited a 28 percent reduction in strength [38]. It appears that the bars were unstressed while being exposed in the previous study.

Okamoto et al. [40] tested full-scale partially prestressed concrete beams. One beam was prestressed with carbon fiber tendons and another with braided aramid tendons. The beams were tested on a simply supported span of 6.9 m, under two loads of 65.7 kN located 2.3 m apart and simultaneously heated at temperatures up to 1000 °C. The beams were heated following the standard heating curve of JIS A 1304. Both beams endured the fire test for two hours. Note that the beams were loaded during the fire test. The time-displacement curves for both beam types are depicted in Figure 29. Specimen FAA was reinforced with aramid tendons and bars, while specimen FAC was reinforced with aramid tendons and carbon fiber bars. The heat-time curve for the beam with aramid tendons is presented in Figure 30, and the curve for the beam with carbon bars is shown in Figure 31.
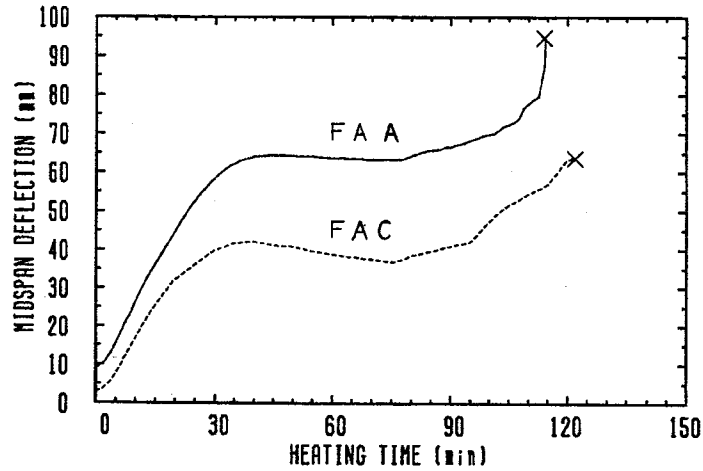
**Figure 29. Deflection Versus Heating Time [40].**
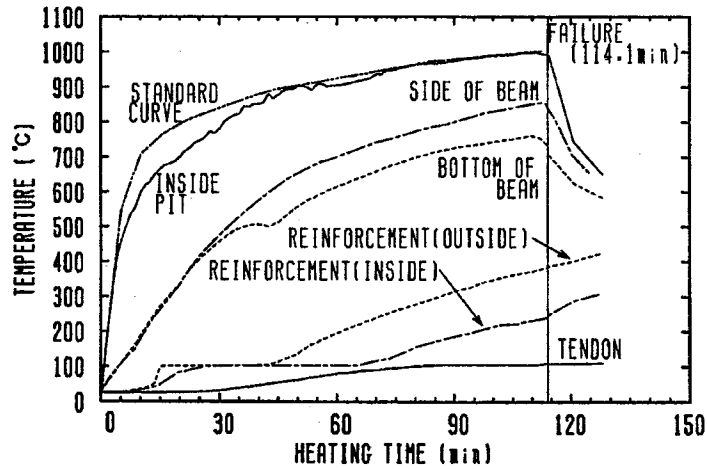


**Figure 30. Heating Curve for Specimen with Braided
Aramid FRP Bars and Tendons [40].**
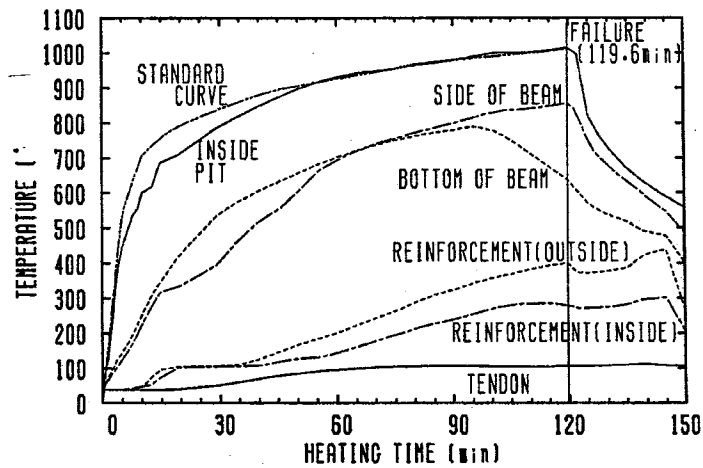


**Figure 31. Heating Curve for Specimen with Braided
Aramid FRP Tendons and Carbon FRP Bars [40].**

## Ultraviolet Rays

Prolonged exposure to ultraviolet rays causes polymer embrittlement [39], which can result in a reduction of tensile strength. The tensile strength of rebars can be reduced 5 percent over a six-month period due to ultraviolet ray exposure [38]. If the reinforcement is properly stored before placement in the concrete, ultraviolet ray degradation should not be a concern.

## Corrosion

GFRP rebars are mostly corrosion resistant [17]. However, FRP bars can fail by stress corrosion mechanisms, which result in failure of the bar under sustained stress in an aggressive chemical environment [41].

## Environmental Effects on Bars or Fibers

Most polymers that are stable in an acidic environment are also stable in an alkaline media [39]. Polymer embrittlement can result from exposure to chemicals.

GFRP bars are highly resistant to acids, but are susceptible to alkali degradation of the glass fibers [38]. Tests conducted by Tannous and Saadatmanesh [38] on GFRP bars with alkali–resistant glass fibers showed reductions in tensile strength from 23 to 28 percent, when exposed to an environment with a pH of 12 and a temperature of 60 °C for six months. Environmental degradation effects are more pronounced in the small diameter bars.

Uomoto and Nishimura [42] studied the degradation of aramid, glass, and carbon fibers, directly exposed to alkaline solution, hydrochloric acid aqueous solution, and water. Other investigators noted that acidic attack could occur in highly polluted cities where acid rain is present [19]. From the study of Uomoto and Nishimura [42], it was found that carbon fibers immersed in water for 120 days showed strength reductions of 5

to 8 percent at 20 °C. No significant reduction in strength was observed after 120 days of exposure to alkaline solution. Carbon fibers lost 20 percent of their original tensile strength when immersed in hydrochloric acid aqueous solution for 120 days at 80 °C.

In the same study by Uomoto and Nishimura [42] it was determined that glass fibers lost considerable strength when immersed in any solution at 80 °C. When exposed to an alkaline solution, glass fibers lost 54 percent of their strength at the age of 60 days in 20 °C solution, 62 percent of their strength at seven days in 40 °C solution, and 96 percent of their strength at nine hours in 80 °C solution.

Uomoto and Nishimura [42] also found that Technora® (aramid) fibers showed no signs of degradation at any temperature or exposure time when immersed in distilled water. When subjected to HCl, the strength of Technora fibers was reduced to 80 percent of the original strength. When immersed in sodium hydroxide for 90 days at 80 °C the strength was reduced to 45 percent of the original strength. The average strength of Kevlar (aramid) fibers was reduced as the temperature increased. Kevlar fibers showed degradation when exposed to any of the three solutions described above. Uomoto and Nishimura [42] determined that the strength reduction of aramid fibers immersed in acid, alkali, and distilled water can be estimated by using Weibull's weakest link theory.

Glass composition, homogeneity, temperature, stress, surrounding degradation media, resin type, and composition influence the changes in the mechanical, thermal, and chemical properties of glass [43]. Degradation of glass is mainly of two types: etching and leaching. Etching is produced by alkali attack. As the silica network is attacked, other components of the glass are released. If there is no further accumulation of reaction products on the remaining glass surface and no change in the activity of the surrounding solution, the reaction will continue at a constant rate. However, accumulation of the reaction products in solution slows the reaction rate to the extent that saturated silica at the surface will stop the reaction.

In the leaching process produced by an acid attack, hydrogen or hydronium ions are exchanged for alkali and other positive mobile ions in the glass [43]. The remaining glass network, mainly silica, remains without damage. Glass may become hydrated if the network is relatively unstable, or it may become more dense and stable than the original glass. Unless the leached layer is altered or removed, the reaction rate will eventually stop. Acid reacts slowly with glass as compared to alkali. There tends to be little difference in the effect of acidic and neutral environments.

Vijay and GangaRao [43] used a conditioned chamber to expose GFRP bars to two solutions: one with salt and another with high alkalinity. Specimens were exposed in the chamber at varying temperatures for different periods of time. In order to correlate the accelerated testing with natural weathering, a weighted chamber temperature was calculated. The bars were subjected to stresses (measured after losses) of 15 and 42 percent of the bars' ultimate tensile strength. Alkali conditioning was the most detrimental environment for the GFRP bars. Freeze-thaw conditioning degraded bars somewhat more than room temperature. The test results are described further in the following section.

**Salt and Alkaline Conditioning without Stress:** For sand-coated bars, the maximum strength reductions under salt and alkaline conditioning at room temperature were 18.5 and 32.2 percent, respectively, over 15 months duration. Likewise, maximum strength reductions in salt and alkaline conditioning under freeze-thaw environments were 21.9 and 37.5 percent, respectively, over 15 months duration. The maximum strength reductions in salt and alkaline conditioning at room temperature were 24.5 and 30 percent, respectively, over 30 months duration. Likewise, maximum strength reductions in salt and alkali conditioning under freeze-thaw environments were 51.5 and 55 percent, respectively, over 30 months duration.

**Salt and Alkaline Conditioning with Stress:** For sand-coated bars under room temperature with sustained stress, maximum strength reductions in salt and alkaline environments were 22.9 percent (8 months of 27 percent applied stress) and 49.2 percent (6 months of 37 percent applied stress), respectively. For sand-coated bars under freeze-thaw conditioning with sustained stress, maximum strength reductions in salt and alkaline

solutions were 26.5 percent (12 months of 35 percent applied stress) and 82.1 percent (12 months of 40 percent applied stress), respectively. For the GFRP reinforcing bars under sustained stress, maximum strength reductions in salt and alkaline conditioning at room temperature were 25.2 percent (10 months of 32 percent applied stress) and 14.2 percent (8 months of 25 percent applied stress), respectively.

**Stress Corrosion at High Temperature:** A temperature of 150 °C coupled with sustained stress and alkaline conditioning caused a stress reduction of 84.7 percent within four months for 40 percent stress application.

**Tensile Stiffness:** Many of the conditioned bars showed increases in the tensile stiffness.

Vijai and GangaRao [43] estimated that chamber weathering for 30 months under alkaline conditioning and freeze-thaw temperatures is conservatively equivalent to natural weathering for 60 years with 20 percent sustained stress. Furthermore, the researchers estimated a service life of up to 120 years for bars embedded in concrete.

Katsuki and Uomoto [44] conducted accelerated tests on aramid-fiber-reinforced polymer (AFRP), carbon-fiber-reinforced polymer (CFRP), and GFRP bars to investigate the penetration of alkali into the FRP bars. The authors proposed a method based on Fick's first law to predict the residual strength of the bars tested. The investigators obtained an average thickness of the damaged zone of the bars tested, then assumed the area of the intact core of the bar to have the same strength as the original strength of the bar. Finally, the authors assumed the strength of the outer ring-like damaged surface of the bar to have no residual strength. Thus it was proposed that the average ring thickness could be estimated with the following equation:

$$x = \sqrt{2kCt}$$

where,

$x$  = average ring thickness of the outer ring-like damaged surface of the bar *(cm)*

$k$  = diffusion coefficient *(mm²/hr)*

$C$  = alkaline concentration *(mol/l)*

$t$  = exposure time *(hr)*

47

Substituting the above equation in the expression to compute the strength of the bar, the following equation was obtained:

$$\sigma_t = \left(1 - \frac{\sqrt{2kCt}}{r_o}\right)^2 \sigma_o$$

where $k$, $C$, and $t$ are as defined before and,

$\sigma_t$ = residual strength of the bar at time $t$

$r_o$ = radius of the bar *(cm)*

Katsuki and Uomoto [44] reached the following conclusions:

(a) Alkali can penetrate into GFRP bars made with vinyl ester resin. Alkali penetration takes place because the resin protecting the fibers is only a thin film, and because of the poor alkali resistance of the glass fibers. It is recommended to use a thicker layer of resin to improve protection of the fibers.

(b) The alkali penetration on the GFRP bars was successfully simulated with a model based on Fick's first law. Decrease in the tensile strength of GFRP bars can be successfully predicted using the model proposed.

**Environmental Effects on Concrete Elements**

The environmental effects on GFRP bars and fibers described so far give an idea of the performance and durability of FRP bars exposed to aggressive environments. However, the situation may be different when the bars are embedded in concrete and needs to be investigated.

Concrete beams reinforced with 9.5 mm diameter GFRP bars were exposed for one and two years to deicing salts at room temperature and then tested in flexure [38]. Two of the beams were kept "dry" and tested in flexure at one and two years, respectively. All beams failed by rupture of the tension reinforcement. Reduction of beam bending strength, stiffness, and ultimate strain resulted in all exposed specimens. The

beams were divided in two groups, namely beams with polyester resin bars and beams with vinyl ester resin bars. Each of these groups had a control beam kept "dry" with no exposure to chlorides. In each group, there were also beams exposed to a 7 percent deicing salt [NaCl+CaCl$_2$ (2:1)] solution for one and two year periods. The results are described next.

**Beams with glass-fiber/polyester matrix bars:** Glass-fiber/polyester matrix bars used in the "dry" concrete beams experienced a tensile strength reduction of 7.3 percent over a year without any exposure other than the concrete environment itself. This reduction seems low when compared to the 20.8 percent strength loss found in tests carried out in the same bar type under accelerated tests after six months of direct exposure to an alkaline solution [Ca(OH)$_2$:pH=12]. The bars from the beams exposed to a 7 percent deicing salt [NaCl+CaCl$_2$ (2:1)] solution experienced a strength loss of 21.5 percent and 29.5 percent when exposed for one year and two years, respectively. A decrease in the rate of strength reduction occurs from the first to the second year.

**Beams with glass-fiber/vinyl ester matrix bars:** Glass-fiber/vinyl ester matrix bars used in the "dry" concrete beams experienced a tensile strength reduction of 14.2 percent over a year without any exposure other than the concrete environment itself. This reduction seems rather high when compared to the 12.7 percent strength loss found in tests carried out by Tannous and Saadatmanesh [38] with the same bar type under accelerated tests after six months of direct exposure to an alkaline solution [Ca(OH)$_2$:pH=12]. The results presented by Tannous and Saadatmanesh [38] are puzzling since it is first concluded from the tension tests carried out on directly exposed bars described in the previous section, that the vinyl ester resin provides better protection to the fibers, while the beam tests seem to indicate the opposite.

Sekijima et al. [45] conducted tests on concrete beams prestressed with GFRP grids. The beams were prestressed from 0 to 52.5 percent of the tensile capacity of the grid reinforcement and left outdoors for seven to eight years. After the exposure period, the concrete samples were demolished and the GFRP reinforcement was removed. The residual tensile capacity of the GFRP grid reinforcement was between 80 and 90 percent of the initial strength. The ratio of the residual tensile rigidity was between 95.6 and 107

49

percent. The load-strain relationship of the grid GFRP reinforcement was linear until rupture, and the cross section of the glass fibers of the grid GFRP reinforcement remained unattacked by the alkaline concrete pore solution and remained circular. The grid was made with vinyl ester resin and E-glass fibers with a fiber volume fraction of 40 percent.

Sen et al. [41] performed tests on beams prestressed with GFRP tendons, exposed to wet and dry cycles in 15 percent salt solution for 20 months. The following conclusions were stated:

(a) The primary cause of deterioration of S-2 glass/epoxy strands was diffusion of alkaline pore solution through the Shell Epon 9310 resin.

(b) The conclusion that alkalinity was the cause of fiber deterioration was corroborated by scanning electron micrographs. The micrographs showed little damage to the fibers in the dry segment but much greater damage in the wet or wet/dry segments. Damage to the glass fibers was higher on the fibers close to the surface of the tendon than on the fibers away from it.

**TEST METHODS FOR FRP BARS**

Testing of FRP bars and their constituents is essential to obtain design parameters and to verify assumed materials behavior. Due to the wide differences in the mechanical properties of FRP bars currently available in the market and the high variability in the properties of composite materials, it is necessary to test the FRP bars before using them. Some of the tests currently carried out on rebars include tensile strength, flexural strength, horizontal shear strength, creep test, long-term bar relaxation, tensile fatigue, coefficient of thermal expansion, performance of anchorages in prestressed elements, alkali resistance, and bond strength. A brief description of some standard tests is presented next.

**Tensile Strength**

ASTM D 3916-94 [46] can be used to carry out tension tests of 3.2 to 25.4 mm (0.12 to 1 in) diameter pultruded bars made with continuous glass fibers. In this test protocol, aluminum grips with sandblasted circular surfaces are specified to grip the bar ends. Test results from this standard include: tensile strength, elastic modulus, percent elongation, ultimate strain, and Poisson's ratio.

Researchers and manufacturers have experienced significant problems associated with the gripping systems used for evaluating the tensile strength of FRP bars. When grips are used, these grips apply large stress concentrations on the surface of the bar and lead to rupture of the bar close to the grip. Casting the FRP bars in metallic pipes filled with an epoxy resin and sand has provided better results, but the resin is expensive and the bond between the FRP bars and the resin is lower than that between the FRP bar and cementituous materials. As a result of the poor bonding between the FRP bars and the resin, the end pipes turn out to be too long to fit the testing machine fixtures. Thus the current trend is to insert the FRP bar in black pipe and cast it with expansive grout. This technique seems to yield good results and appears to be less expensive and faster than casting the bar in epoxy.

The tensile strength of FRP elements can also be determined following the Japanese standard JSCE-E 531-1995 "Test Method for Tensile Properties of Continuous Fiber Reinforcing Materials" [16].

**Flexural Strength**

ASTM D 4476-97 [47] can be used to determine the flexural strength of beams reinforced with pultruded FRP bars. The reported test results are modulus of rupture and modulus of elasticity in bending. In addition, the flexural strength of FRP bars can be determined following the Japanese standard JSCE-E 532-1995 "Test Method for Flexural Tensile Properties of Continuous Fiber Reinforcing Materials" [16].

**Shear Strength**

ASTM D 4475-96 "Apparent Horizontal Shear Strength of Pultruded Reinforced Plastic Rods By the Short-Beam Method" [48] is a short beam test method that can be used to measure the horizontal shear strength of pultruded FRP bars.

ASTM D 3914-96 "Standard Test Method for In-Plane Shear Strength of Pultruded Glass-Reinforced Plastic Rod" [49] is another method to test the shear strength of FRP bars.

The shear strength of FRP elements can be determined following the Japanese standard JSCE-E 540-1995 "Test Method for Shear Properties of Continuous Fiber Reinforcing Materials by Double Plane Shear" [16].

**Creep Test**

The steel jigs and aluminum grips of ASTM D 3916 test can be set up to provide a self-restraining frame condition to apply a constant load. The extension of the specimen can be determined with an ordinary dial gage or a strain gage to monitor the increase in strain with time under the sustained load.

The creep of FRP elements can be determined following the Japanese standard JSCE-E 533-1995 "Test Method for Creep Failure of Continuous Fiber Reinforcing Materials" [16].

**Nondestructive Testing**

Visual inspection of FRP bars should be a valuable method to determine the damage of FRP bars in the field. However, limited data is available in the literature on visual inspection.

Acoustic emissions have been used to track the behavior of GFRP rebars under tension [50, 51]. Optical fibers embedded in FRP bars during manufacture can be used to monitor the behavior of bars under tension tests and of bars embedded in concrete beams [52]. As mentioned in the section of applications and developments of FRP reinforcement, bridges have been constructed with FRP–reinforcing tendons that include optical fibers and copper wire. The optical fiber sensors allow for the monitoring of the full length of the prestressing cables, while the copper wire sensors detect when a bar or tendon ruptures and the location of the rupture [53].

**Other Tests**

Other tests to determine useful properties of FRP bars or cables can be found in Japanese standards. They are:

JSCE-E 534-1995 [16] "Test Method for Long-Term Relaxation of Continuous Fiber Reinforcing Materials."

JSCE-E 535-1995 [16] "Test Method for Tensile Fatigue of Continuous Fiber Reinforcing Materials."

JSCE-E 536-1995 [16] "Test Method for Coefficient of Thermal Expansion of Continuous Fiber Reinforcing Materials by Thermo-Mechanical Analysis."

JSCE-E 537-1995 [16] "Test Method for Performance of Anchorages and Couplers in Prestressed Concrete Using Continuous Fiber Reinforcing Materials."

JSCE-E 538-1995 [16] "Test Method for Alkali Resistance of Continuous Fiber Reinforcing Materials."

JSCE-E 539-1995 [16] "Test Method for Bond Strength of Continuous Fiber Reinforcing Materials by Pull-Out Testing."

In a state-of-the-art report by Tanano et al. [54], the authors point out that current Japanese laws have limits for adequate structural performance of fire resistant structures in the post-flashover stage. These standards are applicable to concrete elements reinforced with bar-type continuous fiber reinforcement. The International Organization for Standardization (ISO) defines fire resistance in terms of load bearing, flame resisting,

and heat-insulating capabilities of structural components. Some standard fire resistance test methods for evaluating these capabilities are mentioned in the Japanese standards. In these test methods, scale specimens are heated according to standard temperature-time curves to evaluate their fire resistance based on the deformation, rate of deformation, backside temperature, and reinforcement temperature, among other measurements. It is also required by the standards to evaluate the flammability and smoke- and gas-generating properties of continuous fiber bars when they come into contact with fire penetrating through cracks of concrete members. The same paper lists the following fire performance standards:

(a) JIS A 1304 (Method of fire resistance test for structural parts of buildings, same as MOC Notification No. 2999)

(b) ASTM E 119 (Standard fire test method for fire test of building construction and materials)

(c) BS 476, Part 20 (Method for determining fire resistance of structural members)

(d) DIN 4102, Part 20 (Fire properties of construction materials and structures – Building structures, definitions, requirements, and tests)

(e) ISO 834 (Fire tests for building structural members)

# VI. RESEARCH AND DESIGN/KNOWLEDGE OF FRP-REINFORCED CONCRETE MEMBERS

This section begins with a description of the design alternatives available for reinforced concrete members. Then an introduction to the ACI design philosophy is given, followed by a description of the ductility of concrete members reinforced with FRP reinforcement. The flexural behavior of concrete members reinforced with FRP bars is presented later, followed by the flexural cracking, deflections, fatigue performance, and shear strength of FRP-reinforced concrete members. The section closes with a review of the bond of FRP bars to concrete and the thermal effects on FRP-reinforced concrete elements.

## DESIGN PHILOSOPHIES FOR FRP-REINFORCED CONCRETE MEMBERS

It was noted by Dolan [55] that there are three alternatives for the design of FRP-reinforced concrete members. They are: 1) the working stress design method, 2) the ultimate strength design, and 3) the limit state (or performance-based) design.

Before reviewing the design philosophies, it is important to review the fundamental assumptions of reinforced concrete behavior [56]:

(1) Equilibrium between internal and external forces always exists in any section.
(2) There is perfect bonding between the concrete and the reinforcement (no slip).
(3) The distribution of strains across the depth of the member is linear.
(4) The tensile strength of the concrete is neglected.

### Working Stress Design Method

Following the above assumptions, the transformed area of the section after cracking can be obtained [57]. Equating the moments produced by the compressive force

and the tensile force about the neutral axis yields an expression for the depth of the neutral axis.

$$kd = \left( \sqrt{(\rho n)^2 + 2\rho n} - \rho n \right) d$$

where,

$kd$ = distance from the extreme compression fiber to the neutral axis

$\rho$ = FRP reinforcement ratio [$= A_{FRP}/bd$]

$A_{FRP}$ = area of FRP reinforcement

$b$ = width of the section

$d$ = distance from extreme compression fiber to centroid of reinforcement

$n$ = modular ratio [$= E_{FRP}/E_{concrete}$]

$E_{FRP}$ = longitudinal modulus of elasticity of FRP reinforcement

$E_{concrete}$ = modulus of elasticity of concrete

Thus the external moment acting on the section can be computed with the expression:

$$M = Tjd = Cjd$$

where,

$M$ = external bending moment acting on the section

$T$ = tensile force in the FRP reinforcement

$C$ = compressive force in the concrete

$jd$ = distance from centroid of compressive force to tensile force [$= d \ (1-k/3)$]

and the stresses in the FRP reinforcement and extreme concrete compression fiber are:

$$f_{FRP} = \frac{M}{A_{FRP} \, jd}$$

$$f_c = \frac{M}{\frac{1}{2}bd^2kj}$$

As long as $f_{FRP}$ remains less than $\alpha f_{fu}$, and $f_c$ less than 0.45 $f_c'$, the allowable stresses of FRP reinforcement and concrete, respectively, these expressions can be used to estimate the stresses in the concrete and in the FRP reinforcement.

Dolan [55] shows that because of the low modulus of elasticity of the FRP reinforcement, limiting the tensile stresses present in the reinforcement will control both the cracking and the deformations. Because service level stresses are associated with cracked sections, a working stress approach is not suitable for prestressed concrete elements.

At the present time there is not a coherent design methodology for shear design at allowable stress levels [55]. The larger cracks resulting from the lower modulus of elasticity of the reinforcement lead to a reduction in the concrete contribution to shear resistance, and premature shear failure may occur.

**Ultimate Strength Design Method**

Strength design assumes that failure takes place when either the tensile strength, $f_{fu}$, of the FRP bar is reached, or when a compressive strain of 0.003 is reached in the concrete. The moment capacity of the section can be computed using the Whitney rectangular stress block [56]. Based on the assumptions listed before, Dolan [55] proposed that there is a reinforcement ratio that yields simultaneous crushing of the concrete and rupture of the reinforcement:

$$\rho_{br} = 0.85\beta_1 \frac{f_c'}{f_{fu}} \frac{\varepsilon_{cu}}{\varepsilon_{cu} + \varepsilon_{fu} - \varepsilon_{pi}}$$

where,

$\rho_{br}$      = balanced reinforcement ratio

$\varepsilon_{cu}$      = ultimate concrete strain

$\varepsilon_{fu}$      = ultimate strain of the tendon

$\varepsilon_{pi}$      = strain due to prestress including losses

$f_{fu}$      = tensile strength of the tendon

$f_c'$      = compressive strength of concrete

$\beta_1$      = material property to determine the location of the depth of the compression block from the neutral axis

If the reinforcement ratio $\rho$ is less than $\rho_{br}$, failure will occur by rupture of the reinforcement [17]. If the reinforcement ratio $\rho$ is greater than $\rho_{br}$, crushing of the concrete will be the failure mode.

Faza and GangaRao [26] have modified the ACI equation and proposed the following expression to determine the bending strength of a concrete section reinforced with FRP bars:

$$M_n = A_r f_{yf} d \left( 1 - 0.585 \rho \frac{f_{yf}}{f_c'} \right)$$

where,

$M_n$      = moment capacity of the section

$A_r$      = area of FRP reinforcement

$f_{yf}$      = pseudo yield stress of FRP reinforcement [= $0.8f_u$]

$f_c'$      = compressive strength of concrete

$\rho$      = FRP reinforcement ratio [= $A_r/bd$]

$b$      = width of the section

$d$      = distance from extreme compression fiber to centroid of reinforcement

The equation presented by Faza and GangaRao [26] is applicable only to underreinforced sections ($\rho < \rho_{br}$). The use of high-strength concrete helps in attaining the underreinforced condition. Beam shear behavior is described next.

The shear strength of FRP-reinforced concrete beams depends on the stiffness and strength of stirrups [55]. As a result of the low elastic modulus of the FRP stirrups, larger crack widths will develop accompanied by a reduction in the concrete and dowel action contributions to shear strength. Design provisions for shear strength are not yet developed. One method for shear design is to proportion a member following the regular concrete code provisions for steel reinforcement, and then provide the equivalent stiffness of steel reinforcement with FRP shear reinforcement. Nevertheless, this approach may still lead to unconservative results, owing to the strength reduction at the bend portion of stirrups [58].

According to Faza and GangaRao [59] both the ultimate strength design method and the working stress (elastic) design method for flexural design of concrete beams reinforced with FRP bars are acceptable.

**Limit State Design Method**

In a limit state design the designers limit the strength and service level conditions [55]. Some suggested limit states for concrete elements are flexural strength, shear strength, deflection, ductility, and bond.

**Flexural and Shear Strength:** These are the same as discussed in the ultimate strength design section.

**Deflection:** Allowable deflections are specified by building codes [55]. In the case of FRP-reinforced concrete sections, there is more cracking and deflection due to the low modulus of elasticity of the FRP reinforcement. Thus, the equations recommended by the codes to estimate the deflection of steel-reinforced concrete members are not applicable to the computation of deflections of FRP-reinforced concrete members.

59

**Ductility:** FRP reinforcement does not yield [55]. Therefore, when FRP reinforcement is placed at different levels, failure of the most highly stressed bars may precipitate sudden failure of the concrete member. The conventional method used to define ductility, developed for steel-reinforced concrete members as described below, is not suitable for FRP-reinforced concrete sections.

**Bond and Development:** Research results described in the bond section show that the bond strength of FRP bars in concrete depends on the surface characteristics of the bar, the quality of the concrete, the amount of concrete cover, and the embedment length, among other factors.

In summary, there are three design philosophies applicable to FRP-reinforced concrete members: working stress design, ultimate strength design, and limit state design.

## ACI DESIGN PHILOSOPHY

This section describes a proposed ACI approach to the design of FRP-reinforced concrete members [17].

Reinforced concrete members must be designed to satisfy strength and serviceability requirements. The basic strength requirements for flexural members are flexure and shear. Other requirements applicable to particular loading conditions may be ductility (especially important in seismic areas) and fatigue. The serviceability requirements of flexural members are limited deflections and crack width.

Flexural design should be based on first principles such as equilibrium of the cross section, compatibility of strains, and constitutive behavior [17]. The rectangular stress block at ultimate strength conditions proposed by Whitney as explained by Nilson [56] is adopted as the constitutive behavior of concrete. For FRP reinforcement, linear elastic behavior up to failure is assumed. Whitney's rectangular stress block and the linear elastic behavior models tend to fit test data well for the reinforcement in tension but not for FRP reinforcement in compression [17].

60

There are no suggestions regarding FRP shear reinforcement due to limited data available [17].

To guarantee a ductile failure, steel-reinforced concrete beams are designed to be underreinforced ($\rho_{actual} < 0.75 \, \rho_{bal}$) [17]. This requirement causes the stress in the steel to reach yield prior to the crushing of the concrete. FRP reinforcement, on the other hand, has a linear stress-strain behavior up to rupture. Thus, the failure of concrete members reinforced with FRP bars may be due to shear, flexural compression, or flexural tension, with all failures likely to be brittle in nature.

Summarizing, the flexural design of FRP concrete elements can be executed based on fundamental engineering principles, and no recommendations are given for the design of shear reinforcement.

## DUCTILITY

This section reviews the definition of ductility, a review of the traditional definition of ductility for steel-reinforced concrete members, and a proposed new definition for FRP-reinforced concrete members. This section also reviews the ACI provision for failure of flexural members at large tensile strains and the pseudo-ductile behavior of hybrid FRP materials.

Ductility is defined as the capacity of a load-resisting material to undergo large permanent deformation while resisting a load [60]. Beer and Johnston [61] define ductility as the ability of a material to yield at normal temperatures. Nadai [62] points out that materials should not be described as being brittle or ductile, but rather as being in the ductile or in the brittle state, because all brittle materials, under suitable mechanical conditions, "can be brought into the plastic state." Nadai also implies that a plastic state is that in which a material can undergo permanent deformation. Based on these concepts it

can be concluded that a ductile material is that in which yielding and considerable permanent deformation occur prior to fracture.

In steel-reinforced concrete members, ductility is defined as the ratio of the ultimate deformation to the deformation at yield as indicated on the right of Figure 32. The same concept can be expressed in terms of the total energy input to the specimen, and the elastic energy recovered after failure. For an elastic-perfectly plastic member, the above definition of ductility index is shown at the bottom of Figure 32. This ductility is a measure of the ability of a concrete member to dissipate energy when tested to failure. Naaman and Jeong [63] used the quotient of the energies equivalent definition of ductility to evaluate the "pseudo-ductility" of FRP-reinforced concrete members. The research team calls the FRP-reinforced concrete members "pseudo-ductile" because no yielding takes place when they are tested to failure. This definition of pseudo-ductility allows for the comparison of the ability of concrete members to dissipate energy when they are reinforced with FRP or steel bars. The pseudo-ductility of FRP-reinforced concrete members can be evaluated with the expression presented in Figure 33.



$$\frac{E_{tot}}{E_{el}} = 2\frac{\Delta_u}{\Delta_y} - 1$$

$$\mu = \frac{\Delta_u}{\Delta_y}$$
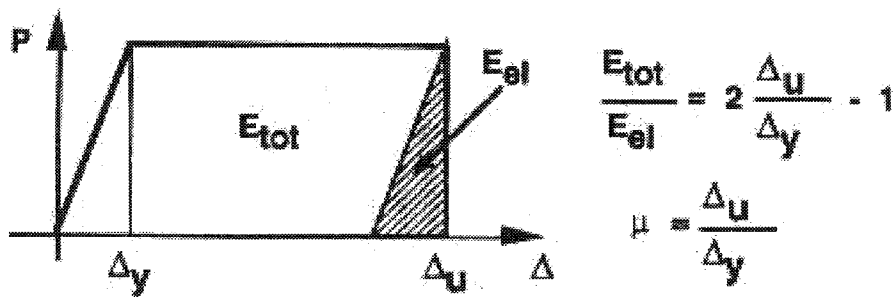
TO COMPARE OLD DEFINITION WITH NEW ONE :

$$\mu = \frac{1}{2} \left( \frac{E_{tot}}{E_{el}} + 1 \right)$$

**Figure 32. Conventional Definition of Ductility Index [63].**
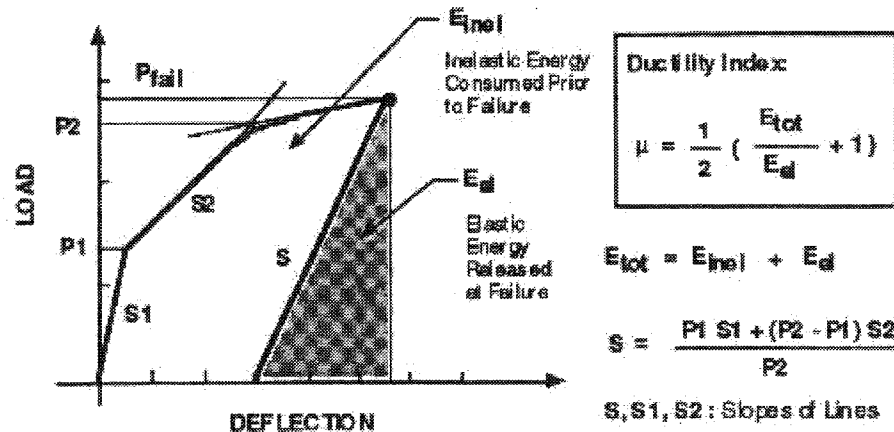
**Figure 33. New Definition of Ductility Index [63].**

Using their definition of ductility index, Naaman and Jeong [63] found the ductility of prestressed beams with GFRP bars to vary between 1.8 and 3.0, beams with AFRP bars between 1.6 and 3.2, beams with CFRP bars between 1.86 and 4.5, and beams with steel tendons between 3.7 and 4.5. Naaman and Jeong [63] also noted that although the beams reinforced with FRP bars may deform considerably before failure, they store elastically most of the energy imposed on them during loading, rather than dissipating it by yielding.

The ACI 318 1995 provisions allow the use of a maximum reinforcing ratio, defined as that which produces a net tensile strain of not less than 0.005 at nominal strength of a tension-controlled section [64]. The ACI state-of-the-art report [17] states that this provision can be applied to FRP bars since they have ultimate strains in the range of 3 percent. This statement implies using a pseudo-elastic model where the member recovery will be essentially elastic with little or no energy dissipation. The recommendation should be taken with caution when applying the provision to FRP-reinforced concrete elements, since reported ultimate strains of FRP bars are lower than 3 percent. On the other hand the provision may not be applicable if the beam is overreinforced, since in that case failure is compression-controlled.

Tamuzs and Tepfers [27] developed "ductile" bars to reinforce concrete by combining carbon and aramid fibers, and carbon, aramid, and polypropylene fibers. The

63

resulting bars exhibited a drop in stiffness after the fibers with the smallest ultimate strain failed, thus the composite bar has a step failure mode. When fibers with high modulus failed, the dynamic failure of the fibers tore off the neighboring low modulus fibers. To mitigate that effect, a resin with lower shear strength was successfully used to cushion the dynamic failure, and a hybrid pseudo-ductile behavior was observed.

Summarizing, the traditional definition of ductility inherently implies that there is yielding of the material. Since FRP reinforcement is not ductile, a new definition for the ability of FRP-reinforced concrete members to dissipate energy is proposed. The same researchers noted that most of the energy transmitted during loading to beams reinforced with FRP bars is stored elastically by the beams before failure. Some researchers have developed hybrid FRP bars with a nonlinear stress-strain behavior.

## FLEXURAL BEHAVIOR

The balanced reinforcement ratio for FRP members is revisited in this section. The effects of reinforcement ratio in the flexural behavior of concrete members are also described.

Design of FRP members follows from basic equilibrium of the cross section and constitutive behavior of the concrete and the FRP reinforcement [17]. Unlike steel reinforcement design, no constant tensile force may be assumed after yield is attained since there is no yielding. The stress in the reinforcement increases continuously until failure occurs.

The design guidelines of the ACI state-of-the-art report adopt the balanced condition of failure proposed by Dolan [55]. The balanced condition is attained at the balanced reinforcement ratio:

$$\rho_{br} = 0.85 \beta_1 \frac{f_c'}{f_{fu}} \frac{\varepsilon_{cu}}{\varepsilon_{cu} + \varepsilon_{fu} - \varepsilon_{pi}}$$

where all the terms have been previously defined.

64

If the reinforcement ratio, $\rho$, is less than $\rho_{br}$, failure will occur by rupture of the reinforcement [17]. For this condition a reduction factor ($\phi$ factor) of 0.85 is believed to be reasonable, since failure would be sudden as in the case of shear failure [17]. Nevertheless, beams with those reinforcement ratios have shown to develop large deformations prior to failure. Recently ACI committee 440 recommended using $\phi = 0.50$ when $\rho < \rho_{br}$.

According to the ACI state-of-the-art report [17], if the reinforcement ratio, $\rho$, is greater than $\rho_{br}$, compression failure of the concrete will initiate failure. For the case $\rho > \rho_{br}$ it is estimated that a reduction factor ($\phi$ factor) of 0.70 is adequate, since failure is produced by crushing of the concrete [17]. Finally, a minimum amount of reinforcement should be provided in any design to prevent brittle failure at first cracking.

It has been reported that ACI 318 Code strength equations conservatively predict the strength of FRP-reinforced concrete members [64]. That tends to be the case if the reinforcement ratio is near $\rho_{br}$ [17]. However, ACI equations are not valid for $\rho < \rho_{br}$ [17].

Nakano et al. [65] carried out an experimental investigation to evaluate the performance of concrete beams reinforced with continuous fiber reinforcing bars and prestressing tendons. The variables studied were fiber material, reinforcement ratio, concrete compressive strength, and bond of prestressing tendons. The reported moment-curvature plots of beams reinforced with aramid FRP bars for different tensile reinforcement ratio are illustrated in Figure 34. The conclusions were as follows:

(a) It is possible to evaluate the flexural performance of concrete beams reinforced with continuous fiber bars by means of using conventional methods used in concrete beams reinforced with steel bars.

(b) Although the fiber-reinforced rebars fail in a brittle manner when tested in tension, the compressive failure of concrete reinforced with those bars causes concrete beams to behave in a ductile manner.

(c) Increasing the reinforcement ratio increases the moment capacity and the post-cracking stiffness of beams reinforced with FRP bars. Nevertheless, the ultimate

strain reached by the beam is reduced for increasing values of reinforcement ratio. Using bars with higher tensile moduli increases the post-cracking stiffness of concrete beams.

(d) Prestressing can be used to control the initial cracking load as well as crack widths of concrete beams.

(e) The ultimate strain capacity of prestressed beams is reduced when tendons are not fully bonded as compared to beams reinforced with tendons bonded over the full length.

(f) Prestressing increases the ultimate strain reached by concrete beams reinforced with FRP tendons, although the increment is limited by the compressive failure of the concrete. Obviously, increasing the prestressing force increases the cracking moment.
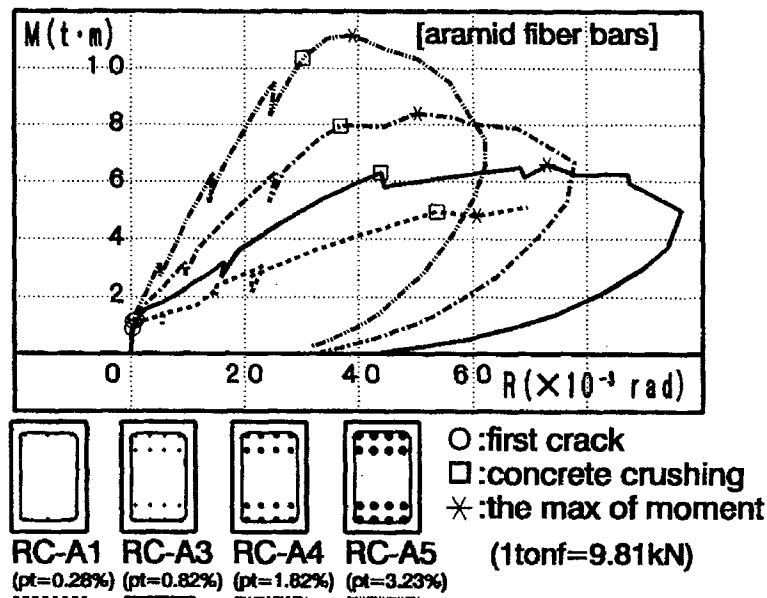


**Figure 34. Moment-Curvature Plots of Beams Reinforced with Aramid Tendons with Different Reinforcement Ratios [65].**

Beam RC-A1 in Figure 34 is underreinforced since it has a reinforcement ratio slightly lower than the balanced reinforcement ratio of 0.30 percent. Beams RC-A3, RC-A4, and RC-A5 are all overreinforced. Although the unloading curve of the underreinforced section is not shown in Figure 34, results of Benmokrane et al. [66] show that underreinforced sections have a sudden drop in the applied moment at failure.

66

Increasing the reinforcement ratio in overreinforced beams increases the post-cracking stiffness of the beam as well as the moment capacity. However, the ultimate curvatures attained seem to be progressively reduced at higher reinforcement ratios. As explained in the section about ductility, beams reinforced with FRP bars elastically store most of the energy transmitted to them during loading. When the beams are underreinforced there is no crushing of the concrete, and therefore no energy dissipation, until the FRP bars break, thus abruptly releasing the large amount of elastic energy stored. For this reason, underreinforced beams fail in a brittle manner. Overreinforced sections, on the other hand, begin to dissipate energy little by little as the cracks propagate through the concrete when it begins to crush. Since the neutral axis typically lies far enough from the compression fiber, a portion of the concrete in compression is confined by stirrups, thus keeping the concrete from exploding. Instead, the concrete fails by progressive cracking. In the process, some of the elastic energy stored is released gradually, leading to a progressive failure.

Prestressing increases the ultimate strain reached by concrete beams reinforced with FRP tendons, although the increment is limited by the compressive failure of the concrete. Obviously, increasing the prestressing force increases the cracking moment.

In summary, the balanced condition of simultaneously reaching the ultimate strain in the FRP reinforcement and the ultimate strain in the concrete is described. The beam behavior at reinforcement ratios below the balanced condition and above the balanced condition is described. It is observed that underreinforced beams have a brittle failure, and that overreinforced beams can have a progressive failure.

## FLEXURAL STRENGTH

Results of investigations regarding the flexural strength of FRP-reinforced concrete elements are presented in this section.

Nawy and Newerth [67] state that in a series of FRP-reinforced concrete beams where $\rho > \rho_{br}$, no increase in strength was observed for increasing reinforcement ratios because the beams failed by compression of the concrete. However, Figure 34 shows a clear increase in moment capacity for increasing reinforcement ratios.

As a result of the low elastic modulus of FRP rebars relative to that of concrete, limited tensile stress can be transmitted from the concrete to the FRP reinforcement [67].

Bank et al. [68] tested full-scale concrete slabs, some reinforced with FRP grating and others reinforced with steel. The ratio of failure load to service load for FRP-reinforced concrete slabs was 4.26, 3.89, 4.17, and 4.16. The ratio for steel-reinforced slabs was 3.34.

A study by Faza and GangaRao [69] concentrated on concrete beams of 152 mm (6 in.) by 305 mm (12 in.) rectangular cross section reinforced with GFRP bars. The tensile strength of the GFRP bars was 551 MPa (80 ksi) and 895 MPa (130 ksi) for 25.4 mm and 9.53 mm diameter bars, respectively. The bars studied were smooth and sand coated. The concrete compressive strength varied from 29 MPa (4.2 ksi) to 69 MPa (10 ksi). The results of 27 beam tests lead to the following conclusions:

(a) High-strength concrete needs to be used if full advantage of the FRP bars is to be achieved. A 90 percent increase in ultimate moment capacity of high-strength concrete beams (69 MPa) was observed when FRP bars with ultimate tensile strength of 895 MPa were used instead of an equal area of mild steel bars (tensile strength of 413 MPa = 60 ksi). The ultimate moment capacity of the beams reinforced with sand-coated bars was 70 percent higher than that of beams with the same area of steel bars.

(b) Using sand-coated bars increased the cracking moment, reduced the crack widths, and eliminated the sudden propagation of cracks to the compression zone. This improvement was due to better bond transfer when compared to the smooth bars. The crack pattern was very similar to that expected from beams reinforced with steel bars.

(c) Beams reinforced with two 25.4 mm FRP reinforcing bars showed a 50 percent increase in moment capacity when using high-strength concrete (51.7 MPa = 7.5 ksi), relative to beams where normal-strength concrete was used (29 MPa = 4.2 ksi).

A study by Nanni [70] found that the flexural behavior of beams reinforced with FRP rebars is bilinear, namely uncracked sections have a linear behavior, and cracked sections are linearly elastic to failure. In this study, beams with sand-coated bars exhibited 25 percent more flexural capacity than beams with smooth bars. Sand-coated bars were found to promote smaller crack widths and higher post-cracking stiffness.

Bemokrane et al. [66] tested eight concrete beams reinforced with Type 1, Grade B, C-Bar® reinforcing bars in flexure under static load. Crack widths and crack spacing were measured, as well as midspan deflections, strains, and loading. The following conclusions were reached:

(a) Average crack spacing in beams reinforced with FRP rebars is similar to corresponding beams reinforced with steel bars at low loads (25 percent $M_u$). Nevertheless, at moderate (50 percent $M_u$) and high (90 percent $M_u$) loads, the average crack spacing was about half that of beams reinforced with steel rebars.

(b) The effect of the reinforcement ratio on crack spacing is negligible. Average crack spacing for C-Bar reinforcing bars is about 139, 104, and 97 mm, respectively, at low, moderate, and high loads.

(c) Maximum crack width of the beams reinforced with FRP bars was three to five times that of identical beams reinforced with steel rebars.

(d) Perfect bond was observed between the FRP bars and concrete.

(e) Crack width in concrete beams reinforced with FRP C-Bar bars can be predicted adequately using a modified Gergely-Lutz equation, where the coefficient $K_g$ equals 41 for the C-Bar reinforcing bars.

(f) Two models of deflection prediction were compared with experimental data and showed excellent agreement. One equation to predict beam deflections was

originally proposed by Benmokrane et al. [66] and the other by Faza and GangaRao [71].

(g) As the reinforcement ratio increases, the moment capacity increases, but this increase is limited by the concrete compressive failure strain for the C-Bar-reinforced concrete beams.

Summarizing, sand-coated bars have better bonding to concrete than do smooth bars. Using sand-coated bars results in an increased cracking moment, a reduction of crack widths, and elimination of the sudden propagation of cracks to the compression zone. Tests showed that beams reinforced with FRP bars fail at loads not less than 3.8 times the service load. Maximum crack width of beams with FRP bars is three to five times the crack width of beams with steel reinforcement. A modified Gergely-Lutz equation can be used to predict crack width.

## FLEXURAL CRACKING

This section reviews the motives for the control of crack width in FRP-reinforced concrete elements. Additionally, several expressions for the computation of crack widths in FRP-reinforced concrete elements are reviewed.

It is the experience of designers that the design of FRP-bar-reinforced bridge decks is controlled by the need to limit crack widths to some reasonable value.

Due to the lower elastic modulus of the composite reinforcement, design must consider allowable crack widths. For both durability (corrosion) and aesthetic reasons, ACI recommendations limit the crack width for steel-reinforced concrete structures [64]. Because the corrosion mechanism afflicting steel is not an issue with FRP reinforcement, crack width limits intended to reduce this type of corrosion may seem overly restrictive for structures reinforced with FRP bars. Crack width limits for FRP-bar-reinforced concrete might seem more appropriately based on such considerations as aesthetics, freeze-thaw effects, moisture penetration, chemical degradation, and thermal effects.

However, factors such as tensile force and shear force interaction could cause large strains, and possibly failure, in FRP reinforcement if crack widths are large in concrete beam elements [32]. Therefore, it appears that maximum crack widths should not only be limited for degradation and aesthetics reasons, but also for structural reasons such as strength and stiffness.

Tests by Nawy and Newerth [67] evidenced that beams reinforced with steel rebars had fewer cracks than beams reinforced with FRP bars because of the lower modulus of the FRP bars. The uniform distribution of cracks in the specimens reinforced with FRP bars was an indication of adequate bond.

Faza and GangaRao [69] found that concrete beams reinforced with spiral FRP reinforcing bars using concrete with compressive strengths of 28 MPa (4000 psi), developed sudden crack formation that propagated to the compression zone after the concrete reached its tensile strength. It was found that crack spacing was closely related to the stirrup spacing. Using sand-coated bars and higher strength concrete (52 MPa (7.5 ksi) to 69 MPa (10 ksi)) resulted in a decrease in the sudden propagation of cracks, in a decrease of crack widths, and a decrease of crack spacing.

If it is assumed that the maximum crack width can be approximated by the strain in the FRP-reinforcing bar multiplied by the expected crack spacing, an equation for maximum crack width is governed by the following parameters [69]:
(a) bond strength of FRP bar,
(b) splitting tensile strength of concrete,
(c) cross-sectional area of concrete in tension,
(d) number of reinforcing bars in tension,
(e) size of reinforcing bar, and
(f) effective yield strength or working stress of FRP-reinforcing bar.

This results in the following expression for maximum crack width:

$$W_{max} = \frac{\left(\dfrac{f_f}{E_f}\right) 2 f_t' A}{\mu_m \pi D}$$

where,

$W_{max}$  = crack width *(in.)*

$f_t'$    = 75 $(f_c')^{1/2}$ (the constant recommended by the ACI design code to compute the

modulus of rupture of concrete is 7.5 instead of 75 [64])

$f_c'$    = concrete compressive strength *(psi)*

$f_f$    = maximum stress in FRP reinforcement at service load level with 0.5 $f_y$ to be

used if no computations are available *(ksi)*

$A$     = effective tension area of concrete surrounding the principal reinforcement

divided by the number of reinforcing bars. It is defined as having the same

centroid as the reinforcement *(in.$^2$)*

$\mu_m$   = maximum bond stress *(psi)*

$D$     = diameter of reinforcement *(in.)*

$E_f$    = elastic modulus of FRP reinforcement *(psi)*


A study by Benmokrane et al. [66] showed that at 25 percent of $M_u$ the crack
pattern and spacing of FRP-reinforced concrete beams were similar to those in steel-
reinforced beams. At service (50 percent) and ultimate (90 percent) loads, there were
more and wider cracks than in the steel-reinforced beams.


Benmokrane et al. [72] evidenced that crack width increases under cyclic loading.
The tests showed crack widths in slabs to be 0.42 mm after four million cycles of loading.
A description of the specimens, reinforcement, and loading is given in the fatigue section.


Crack spacing decreases as the applied load and reinforcement ratio increases
[73]. In a study by Toutanji and Saafi [73], the authors suggest that crack width depends
primarily on average crack spacing and on average reinforcement stress, which are

related to the mechanical properties of the concrete, the reinforcement, and the bond between them. They proposed the following equation for crack width prediction:

$$w_m = \frac{2f_o}{E_{FRP}} \left[ d + A \tanh \left( \cosh^{-1} \sqrt{\frac{f_o}{f_o - \frac{f_t'}{\rho_{FRP}}}} \right) \right]$$

where,

$w_m$     = crack width ($mm$)

$f_o$     = stress in the FRP reinforcement at a specified load ($MPa$)

$d$     = parameter function of the concrete strength and load levels obtained from pull-out tests ($mm$)

$f_t'$     = tensile strength of concrete ($MPa$)

$\rho_{FRP}$     = FRP reinforcement ratio calculated based on the effective tension area of concrete surrounding the main tension reinforcement and having the same centroid as the reinforcement

$E_{FRP}$     = elastic modulus of FRP reinforcement ($MPa$)

Figure 35 displays a comparison of the predicted versus measured crack widths using the above expression [73].
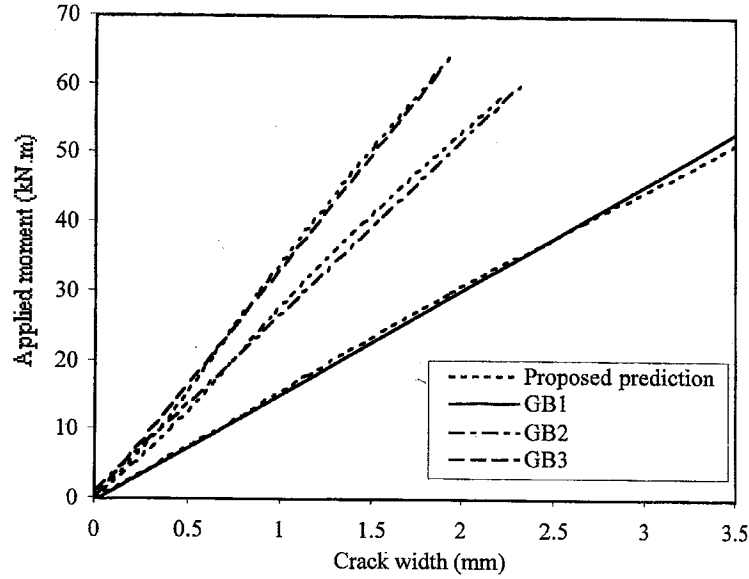
**Figure 35. Comparison Between Theoretical and Measured
Crack Widths in GFRP Beams [73].**

According to Nakano et al. [65] and Sonobe et al. [74], current Japanese
provisions predict crack widths with reasonable accuracy. The following expressions
have been proposed:

$$W_{av} = L_{av}\varepsilon_{av}$$

$$W_{max} = 1.5W_{av}$$

$$L_{av} = 2\left(c + \frac{s'}{10}\right) + \frac{kd_b}{P_e}$$

$$\varepsilon_{av} = \frac{1}{E_f}\left[\sigma_t - \frac{f_t'}{\left(2x10^3\varepsilon_{av} + 0.8\right)p_e}\right]$$

where,

$W_{av}$ = average crack width *(cm)*

$W_{max}$ = maximum crack width *(cm)*

74

$L_{av}$ = average crack spacing *(cm)*

$\varepsilon_{av}$ = average longitudinal reinforcement strain

$c$ = average concrete cover [= *(c_s+c_b)/2* (for slabs: $c = c_b$)] *(cm)*

$c_s$, $c_b$ = concrete cover on side and bottom faces *(cm)*

$s'$ = interval between centers of longitudinal reinforcement *(cm)*

$k$ = coefficient [= *0.1* (for beams), = *0.0025t* (for slabs, $k <= 0.01$)]

$t$ = slab thickness *(cm)*

$p_e$ = effective tensile reinforcement ratio [= *A_ft/A_ce*]

$A_{ce}$ = cross-sectional area of tensile concrete where its center of gravity of longitudinal tensile reinforcements overlap [= *(2c_b+d_b) b_w*] *(cm²)*

$d_b$ = bar diameter *(cm)*

$b_w$ = width of concrete specimen *(cm)*

$s_t$ = longitudinal reinforcement stress at crack cross section *(kgf/cm²)*

$f_t'$ = tensile strength of concrete *(kgf/cm²)*


A comparison of predicted and measured crack widths is illustrated in Figure 36.
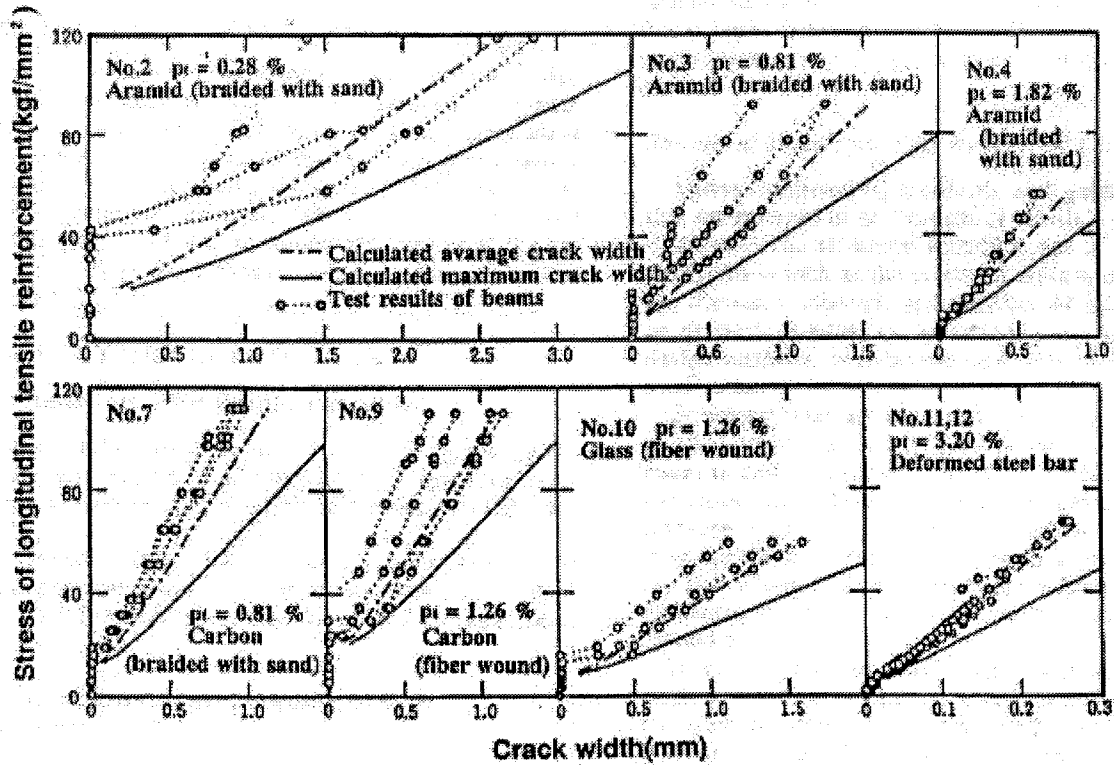
**Figure 36. Comparison Between Crack Widths Predicted by the Japanese Code and Measured Crack Widths [73].**

Makizumi et al. [75] tested concrete slabs 2 m long, 500 mm wide, and 80 mm thick. Slabs S1C, S2C, and S3C were prestressed with six symmetrically placed steel SWPR7A 9.3 mm diameter wires and reinforced with a Carbon Fiber Net (CFN) grid. Specimen S1C was additionally reinforced with four D13 steel bars, while specimen S2C was additionally reinforced with four D6 steel bars. The investigators made a comparison of the crack width predicted by the Comite Euro-International du Beton (CEB), Japan Society of Civil Engineers (JSCE), and American Concrete Institute (ACI) equations. A plot of the comparison including the experimental results of specimens S1C, S2C, and S3C is presented in Figure 37. In general, the European code appears to predict smaller crack widths than measured, the ACI code predictions appear to be conservative, and the Japanese predictions appear to fit the experimental data better.
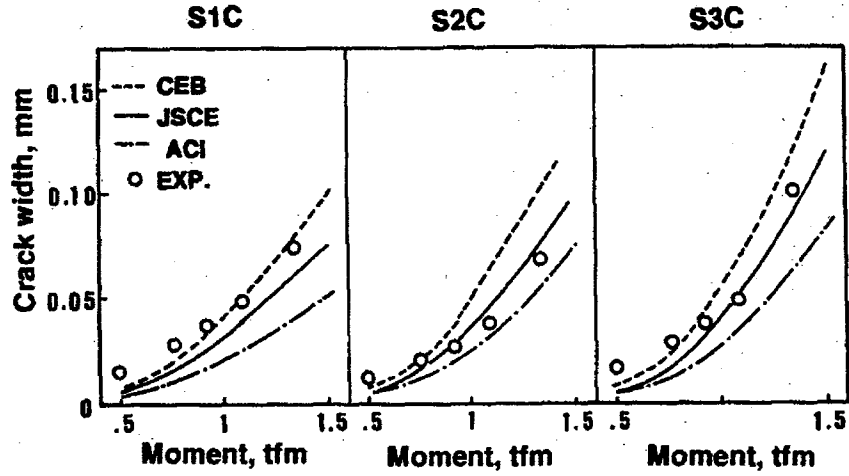
**Figure 37. Comparison Between Crack Widths Predicted by
CEB, JSCE, and ACI, with Measured Crack Widths [75].**

Makizumi et al. [75] proposed an alternative equation to predict crack width. The equation proposed can be used to estimate the crack width at different locations along the mesh shown in Figure 38. The proposed equation is:

$$W = 2L\sum_{i=0}^{n}\left[\varepsilon_{f,i}\left(1+\frac{E_f A_f}{E_c A_c}\right)-\frac{T}{E_c A_c}+Sh\right]$$

where,

$$\varepsilon_{f,1} = \frac{T-K\delta_1}{E_f A_f}$$

$$\varepsilon_{f,2} = \frac{(1+\beta)\cdot T-(2+\beta)\cdot K\delta_1}{E_f A_f}$$

$$\varepsilon_{f,3} = \frac{(1+3\beta+\beta^2)\cdot T-(3+4\beta+\beta^2)\cdot K\delta_1}{E_f A_f}$$

$$\varepsilon_{f,4} = \frac{(1+6\beta+5\beta^2+\beta^3)\cdot T-(4+10\beta+6\beta^2+\beta^3)\cdot K\delta_1}{E_f A_f}$$

$$\beta = Km$$

$$m = \frac{L}{E_f A_f}$$

The value $n$ depends on the mesh location as indicated in Figure 38.
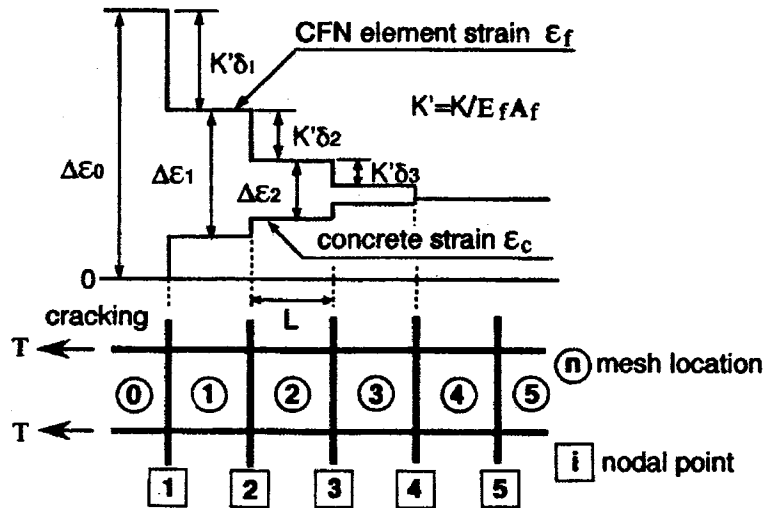


**Figure 38. Schematic Distribution of Longitudinal Strain in the CFN Element and in the Concrete [75].**

and $\delta_l$ is varied with the mesh location, $n$, as follows:

$$\text{at } n=2, \ \delta_1 = \frac{1}{1+\beta} mT$$

$$\text{at } n=3, \ \delta_1 = \frac{2+\beta}{1+3\beta+\beta^2} mT$$

$$\text{at } n=4, \ \delta_1 = \frac{3+4\beta+\beta^2}{1+6\beta+5\beta^2+\beta^3} mT$$

where,

$\sigma_{pe}$    = effective prestressing stress in PC wire $(kgf/mm^2)$

$A_c$    = cross-sectional area of concrete symmetric with reinforcement divided by number of longitudinal strands of Carbon Fiber Net (CFN) $(mm^2)$

78

$A_f$ = area of longitudinal element of CFN $(mm^2)$

$E_f$ = Young's modulus of CFN $(tonf/mm^2)$

$E_c$ = Young's modulus of concrete $(tonf/mm^2)$

$L$ = spacing of a mesh $(mm)$

$Sh$ = drying shrinkage of concrete $[= 150 \times 10^{-6}]$

A comparison between the predicted crack width of the equation described above and experimental results is illustrated in Figure 39.
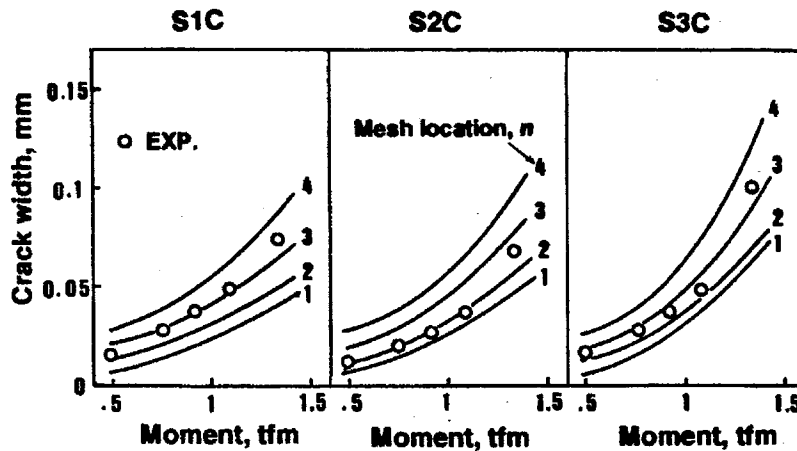


**Figure 39. Comparison Between Crack Widths Predicted by Makuzami et al. with Measured Crack Widths [75].**

It appears that crack width limitations should not be based on aesthetics or durability factors alone, but crack width limits should be based on strength and stiffness considerations as well. Several expressions for crack width prediction were reviewed in this section. Of particular interest is the comparison made between the crack widths predicted by the CEB, Japanese, and the ACI codes.

## DEFLECTIONS

Limiting the deflections of reinforced concrete elements is necessary to keep the structure functional, to give the users confidence in the structure, to limit damage to nonstructural elements, and to prevent the structural behavior from being different from that assumed [76]. Examples of undesirable effects due to excessive deformations of

79

concrete structures are: a sagging roof structure that "runs" water, the presence of vibrations uncomfortable to the users, cracking of nonstructural elements, excessive deflections that cause instability in arches, shells, and long columns, and excessive rotation of the ends of a beam that causes stress concentrations at the support.

This section describes the low flexural stiffness of FRP-reinforced concrete elements after cracking. The long-term effects on the deflections are considered, and several proposed expressions to estimate the post-cracking deflections of FRP-reinforced concrete elements are reviewed.

FRP-reinforced concrete members will generally deform more than steel-reinforced concrete members [17]. Figure 40 shows a concrete element reinforced with FRP bars deforming considerably before failure. This deformation indicates that FRP-reinforced concrete flexural members, even with limited ductility, may provide ample signs of warning before collapse.
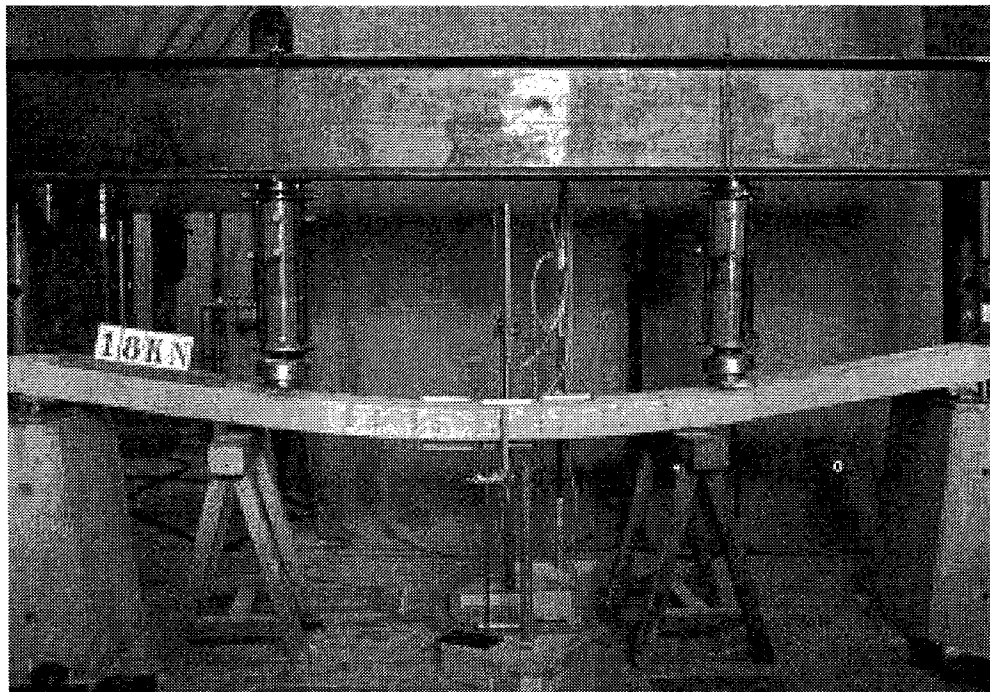


**Figure 40. Concrete Slab Prestressed with Aramid FRP Bars [77].**

ACI 318 deflection limitations are independent of reinforcement type and may be applicable to members reinforced with FRP reinforcement. There are several alternatives to determine deflections of FRP-reinforced concrete elements. One alternative is to use the ACI 318 equation originally proposed by Branson:

$$I_e = \left(\frac{M_{cr}}{M_a}\right)^3 I_g + \left[1 - \left(\frac{M_{cr}}{M_a}\right)^3\right] I_{cr} \leq I_g$$

where,

$I_e$ = effective moment of inertia of the section

$I_{cr}$ = cracked moment of inertia of the section

$I_g$ = gross moment of inertia of the section

$M_{cr}$ = cracking moment

$M_a$ = maximum moment in the member at stage deflection is computed

Another approach is to use the following equation, proposed by Benmokrane et al. [78]:

$$I_e = \left(\frac{M_{cr}}{M_a}\right)^3 \beta I_g + \left[1 - \left(\frac{M_{cr}}{M_a}\right)^3\right] I_{cr} \leq I_g$$

where $\beta$ is a reduction coefficient estimated as:

$$\beta = \alpha\left(\frac{E_{FRP}}{E_s} + 1\right)$$

and

$E_{FRP}$ = longitudinal elastic modulus of FRP bar

$E_s$ = longitudinal elastic modulus of steel bar

$\alpha$ = bond-dependent coefficient

The rest of the terms are as defined before.

81

Another method is to integrate the moment-curvature diagram. For example, a method for determining deflections of fiber-reinforced polymer-reinforced concrete beams proposed by Razaqpur et al. [79] assumed that:

(a) The moment-curvature relation of FRP sections is linear in the precracked and postcracked stages. The effect of cracking is a reduction in the flexural rigidity of the member.

(b) Unlike steel-reinforced concrete, the tension-stiffening effect can be ignored in computing the deflection of flexural members.

(c) In FRP-reinforced concrete members, the movement of the neutral axis after cracking is relatively small and has negligible effect on the curvature of the member under service loads.

In the paper by Razaqpur et al. [79] flexural deflections were calculated using the method of virtual work. The predicted deflections agree within 5 percent with deflections obtained in a number of flexure tests on reinforced concrete beams and slabs measured at service load (50 to 60 percent of ultimate). The method presented did not account for shear deformations.

A study by Benmokrane et al. [66] showed that at service (50 percent) and ultimate (90 percent) loads, the FRP-reinforced concrete beams developed deflections three times higher than those of the steel-reinforced beams. Nawy and Newerth [67] reached the same conclusion.

Larralde and Zerva [80] found that theoretical deflection predictions underestimated test deflections at loads above 50 percent of ultimate. However, theoretical and measured deflections agreed for loads below 30 percent of ultimate capacity.

A study by Faza and GangaRao [69] proposed the following expression to compute the modified moment of inertia to be used in deflection calculations by the moment-area method:

$$I_m = \frac{23 I_{cr} I_e}{8 I_{cr} + 15 I_e}$$

where $I_m$ is the modified moment of inertia and the other terms are as defined before.

This equation was developed for a bending member subjected to four-point loading, assuming the central portion of the beam to be fully cracked and the ends to be uncracked.

A study by Engel et al. [81] proposed the use of the following modified ACI 318 equation to compute the deflection of concrete beams reinforced with FRP grids:

$$I_e = I_{cr} + \left(\frac{M_{cr}}{M_a}\right)^3 \left(\beta I_g - I_{cr}\right)$$

where,

$$M_{cr} = \frac{0.622\sqrt{f_c'} I_g}{h - c}$$

$$\beta = \alpha\left(\frac{E_r}{E_s} + 1\right)$$

$$I_{cr} = \frac{bc^3}{3} + \frac{E_r}{E_c} A_r (d - c)^2$$

$M_{cr}$     = cracking moment *(N·mm)*

$h$     = height of beam *(mm)*

$c$     = distance from top of the beam to neutral axis *(mm)*

$f_c'$     = concrete compressive strength *(N/mm²)*

$I_g$     = gross moment of inertia *(mm⁴)*

$E_s$, $E_r$, and $E_c$ = elastic moduli of steel, FRP reinforcement, and concrete, respectively *(N/mm²)*

$\alpha$     = bond-dependent coefficient

$$E_c \quad = 4730\,(f_c')^{1/2}\ (N/mm^2)$$

$d \qquad$ = distance from top of the beam to bottom of the reinforcement *(mm)*

$A_r \qquad$ = cross-sectional area of the reinforcement *(mm$^2$)*

$M_a \qquad$ = maximum moment in the member at stage deflection is computed

The researchers found that beam deflections prior to the occurrence of the first crack are concrete dominated [81]. They tested beams with different grid configurations. Grids with fibers that cross the grid intersections and grids with fibers turned at right angle to the grid intersections were tested. After cracking, the flexural stiffness indicated that beams reinforced with grids that have a portion of the fibers turned at the joints tend to be more compliant than beams reinforced with grids that have all fibers passing straight through the joint. For all grid joint designs, the modified ACI code design predictions are in good agreement with the actual deflection response for the midpoint deflection of FRP grid-reinforced concrete beams. The stiffness of the grids can be calculated from a grid section in a stand-alone tension test.

Harik et al. [82] tested FRP-reinforced concrete deck panels. The design of FRP decks was based on the AASHTO 1998-LRFD specifications. The investigation included measurement of deflections, observation of the response of panels under cyclic loading, and development of a factor of safety against failure. The results indicated that the deck panels met the AASHTO deflection and strength criteria requirements. The authors do not specifically mention the AASHTO criteria.

Braimah et al. [83] conducted tests on concrete beams prestressed with carbon-fiber-reinforced polymer (CFRP) strands and steel strands. The investigators recorded the ratio of the long-term deflection measured at 402 days to initial deflection. For an uncracked beam with CFRP tendons and initial prestress of 70 percent of ultimate strength of the tendons, the ratio of long-term to instantaneous deflection was 1.47. For a beam with CFRP tendons and an initial prestress of 55 percent of ultimate, the deflection ratio was 1.15. A beam prestressed to 50 percent of the ultimate strength of steel strands showed a deflection ratio of 1.26. Overall, the CFRP prestressed beams showed a

comparable performance to that of steel beams. The ratio of the long-term deflection to short-term deflection of CFRP prestressed beams depends on the level of prestress, with the ratio increasing as the prestress level increases. It was also found that the strains in the prestressing tendons of the cracked beams decreased with time, while the strains of the tendons in the uncracked beam showed a small increase with time.

Joh et al. [84] tested 17 beams reinforced with 9 types of FRP bars. The bars used were made of GFRP, AFRP, CFRP, and steel. The authors made the following observations:

**Long-Term Deflection:** The deflection of FRP-reinforced concrete beams increased with time for all beam specimens.

**Influence of Type of Fiber Used in the Bar:** The ratio of long-term deflection measured at 9.5 months to short-term deflection was 1.88 for beams with GFRP bars, 2.88 for beams with AFRP bars, and 2.10 for beams with CFRP bars, on average.

**Effect of Bar Configuration:** The rate of deflection increase for beams reinforced with braided bars was 10 percent smaller than that of beams with spiral bars, while the rate of deflection increase for beams with ribbed bars was 10 percent larger than that of beams with spiral bars.

**Effect of Elastic Modulus of the Bar:** No direct relationship between elastic modulus of the bar and the rate of increase of deflection has been reported.

**Effect of Reinforcement Ratio:** The authors suggested that there is not a significant influence of the reinforcement ratio on the long-term deflection of concrete beams.

Toutanji and Saafi [73] tested concrete beams reinforced with GFRP bars. The beams were 180 mm wide by 300 mm high by 3 meters long. The GFRP bars contained approximately 65 percent E-glass fibers and 35 percent resin by weight. All bars were 12.7 mm in diameter and had a tensile strength and elastic modulus of 695 MPa and 40 GPa, respectively. Steel stirrups 9.5 mm (0.375 in.) in diameter were used for shear reinforcement. The authors found that the deflections predicted using the ACI equation were lower than the measured deflections. As a result of the findings, the researchers

proposed the following equation to estimate the deflection of concrete beams reinforced with FRP bars [73]:

For $\dfrac{E_{FRP}}{E_s}\rho_{FRP} < 0.3$

$$I_e = I_g \left(\frac{M_{cr}}{M_a}\right)^{\left(6-\frac{10E_{FRP}}{E_s}\rho_{FRP}\right)} + I_{cr}\left[1-\left(\frac{M_{cr}}{M_a}\right)^{\left(6-\frac{10E_{FRP}}{E_s}\rho_{FRP}\right)}\right] \leq I_g$$

For $\dfrac{E_{FRP}}{E_s}\rho_{FRP} \geq 0.3$

$$I_e = I_g \left(\frac{M_{cr}}{M_a}\right)^3 + I_{cr}\left[1-\left(\frac{M_{cr}}{M_a}\right)^3\right] \leq I_g$$

where all the terms are as defined before, except as noted:

$E_{FRP}$   = longitudinal modulus of elasticity of FRP reinforcement

$E_s$     = modulus of elasticity of steel reinforcement

$\rho_{FRP}$   = FRP longitudinal reinforcement ratio in percentage


      Summarizing, some authors report that the use of the ACI 318 equation $I_e = I_g\left(\frac{M_{cr}}{M_a}\right)^3 + I_{cr}\left[1-\left(\frac{M_{cr}}{M_a}\right)^3\right] \leq I_g$ for the computation deflections of FRP-reinforced concrete members is conservative, while other researchers report the opposite. Expressions for the computation of the deflections using the moment-curvature diagram seem to give good results. The long-term deflections of CFRP prestressed beams depend on the level of prestress with the ratio increasing as the prestress level increases. Beams with GFRP bars have the least long-term deflections among FRP-reinforced concrete beams, followed by CFRP bars, and then AFRP bars. Braided bars had the least rate of increase of long-term deflection, followed by spiral bars, and finally ribbed bars. The elastic modulus of the bar and the reinforcement ratio have no effect on the rate of increase of deflection.

## FATIGUE PERFORMANCE

The fatigue performance of FRP-reinforced concrete beams is described in this section.

Iwamoto et al. [21] conducted tests on concrete beams with dimensions 150 x 150 x 2100 mm. Two types of prestressing tendons were used to reinforce the beams. One set of tendons was made with braided aramid fiber bars 6 mm and 8 mm in diameter. The other tendons were made of 7 mm diameter steel wire. The strength of concrete was between 59 and 64 MPa. Three levels of initial tension of the tendon were selected: 40, 60, and 70 percent of the tensile strength of the FRP bar. A sinusoidal load was applied to the specimen. The higher amplitude load varied from 45 to 80 percent of the static ultimate strength of the beam. The lower amplitude was 4.9 kN. The frequency of the sinusoidal load was 4 Hz. The failure modes of the beams with aramid tendons included tendon rupture, development of bond cracks, and shear compression failure. The fatigue strength at 2 million cycles was not less than 65 percent of the static ultimate strength of the beams. Bond between aramid tendons and concrete deteriorated more than that of the specimens containing prestressing wire. Rubbing between aramid fibers and concrete deteriorated bonding. Therefore, the fatigue strength of beams with aramid fiber tendons cannot be predicted by fatigue tests on isolated aramid fiber bars. The rigidity of the beam did not decrease much under cyclic loading.

Benmokrane et al. [72] tested concrete slabs 3.2 meters long, 1 meter wide, and 260 mm thick, reinforced with NEFMAC® CFRP girds. The beams were subjected to four million cycles of loading, with load amplitude of 10 to 100 kN. The first 2 million cycles were applied at a frequency of 2 Hz and the remaining cycles at 3 Hz. After 4 million cycles, the maximum deflection was 12 mm (span/250). The same slab had a defection of 8 mm under 100 kN load applied statically before the fatigue test.

Summarizing, fatigue deteriorates the bonding between the concrete and the FRP tendons more than it deteriorates the bonding of steel wires. Four million cycles of loading increased the static deflections of slabs with CFRP grids by 50 percent.

## SHEAR STRENGTH

This section describes the results of experimental investigations on the shear strength of FRP-reinforced concrete members.

Shear capacity of FRP-reinforced concrete members is generally lower than that for steel-reinforced members [17]. This difference is due to larger crack widths and reductions in compressive stress blocks. Most of the test data available is for sections where shear is not a critical parameter [17]. Test data indicate that FRP stirrups will fail at the bend at a lower load than predicted. The low modulus of elasticity of FRP stirrups results in larger cracks. This cracking hampers the participation of several components of the concrete that contribute to the shear strength of concrete sections.

A typical construction problem of GFRP-reinforcing bars is the fact that bends must be prefabricated at the factory. In general, FRP bars made from thermosetting resins cannot be bent in the field or at anytime after fabrication.

Beams under flexure impose tensile and shear stresses on FRP tendons at the location of shear cracks. A model by Park and Naaman [85] based on a beam on elastic foundation model and the Tsai-Hill failure criterion predicted the behavior and failure of FRP tendons as they are stressed in the unsupported length of a crack. The same model determined that the ultimate dowel shear stress ratio decreased elliptically as the tensile stress ratio increased, and the ultimate dowel displacements decreased linearly as the tensile force decreased.

Interesting investigations on the interaction of shear and tensile stresses in FRP bars were accomplished by Ueda et al. [32]. Specimens with 1 mm crack widths failed in shear, and specimens with 3 and 4.2 mm crack widths failed in tension.

Ghandour et al. [86] carried out tests on flat slabs reinforced with FRP bars. The authors found problems of bond slip and crack localization over the main flexural bars. As a result, the slabs failed at loads lower than their expected flexural and punching shear capacities. According to the authors' observations, the ACI 318-95 equation for punching shear capacity ignores the influence of tension flexural reinforcement when calculating the concrete shear resistance, which is heavily dependant on the concrete strength. The ACI expression is:

$$P = 1.33\sqrt{f_c'}(c+d) \cdot d$$

where,

$P$      = punching shear force capacity

$f_c'$      = concrete compressive strength *(MPa)*

$c$      = side dimension of the column *(mm)*

$d$      = effective depth *(mm)*

For slabs reinforced with steel bars with a high modulus of elasticity, concrete in compression will be the dominant factor affecting the concrete shear resistance, since the neutral axis location does not vary much with typical steel reinforcement ratios [86]. Thus, the ACI equation above can provide good predictions. But, when using FRP reinforcement with low modulus of elasticity values, the concrete shear resistance becomes more sensitive to the reinforcement stiffness, since the neutral axis depth reduces significantly with low reinforcement ratios. For this case, the authors estimated that the ACI equation is not conservative and proposed to use the following equation as an alternative:

$$P = \left[ 1.33\sqrt{f_c'}\,(c+d)\cdot d \right] \cdot \left( \frac{E_{FRP}}{E_{steel}} \right)^{0.33}$$

where,

$E_{FRP}$   = modulus of elasticity of FRP reinforcement *(MPa)*

$E_{steel}$   = modulus of elasticity of steel reinforcement *(MPa)*

Bank and Ozel [87] tested concrete beams reinforced with FRP grids fabricated with small pultruded I-profiles. Failure of beams of intermediate length occurred in shear due to stress concentrations at the junctions of the grid elements. The beams appeared to show a somewhat more "ductile" failure mode when they were overreinforced, and the grid failed by shear rupture of the vertical bars, rather than rupture of the longitudinal bars.

Shehata et al. [58] pointed out that stirrups used for shear reinforcement are normally located as an outer reinforcement with respect to the flexural reinforcement and therefore they are more susceptible to severe environmental effects due to the reduced concrete cover provided. The effect of bend radius, the crack angle, the stirrup anchorage, the stirrup spacing, and the material type of flexural reinforcement were evaluated in tests on 52 panel specimens. The following conclusions were drawn:

(a) The bend effect is more critical than the kink effect on the strength capacity of FRP stirrups.

(b) The following limitations were proposed for detailing FRP stirrups to achieve a capacity of at least 50 percent of the guaranteed strength parallel to the fibers:

- The bend radius should not be less than 50 mm or four times the effective bar diameter, whichever is greater.

- The tail length should not be less than 70 mm, or six times the effective bar diameter, whichever is greater.

(c) The effective capacity of FRP stirrups in beam action might be as low as 50 percent of the guaranteed strength parallel to the fibers, provided that the failure occurs due to rupture of FRP stirrups.

(d) Beams reinforced with CFRP strands for flexure showed less concrete contribution to shear strength than did beams reinforced with steel strands. This observation is attributed to the wide cracks, the small depth of the compression zone, and poor dowel action associated with the use of FRP as longitudinal reinforcement.

(e) Shear deformations are not only affected by the elastic modulus of the stirrup material, but also by other factors, such as the bond characteristics of the stirrups. Beams with GFRP stirrups showed better performance than those with CFRP stirrups.

(f) The relatively inexpensive GFRP stirrups could be a good alternative for shear reinforcement in concrete structures.

Razaqpur and Mostofinejad [88] tested four continuous beams with two 6.5 m long spans. The beams were reinforced with FRP grids as shear reinforcement. The beams did not collapse and retained nearly 80 percent of their strength when they reached their load capacity in the negative moment regions. These results are another example of semiductile behavior of overreinforced beams. CFRP stirrups experienced strains of 4000 $\mu$ ($1\mu$ = 1 microstrain = $10^{-6}$ in./in.) without rupture, which is well above the limit of 2000 $\mu$ set by the Canadian Highway Bridge Design Code (CHBDC) [89]. Thus, the authors believe the limit of the CHBDC should be modified. The same tendency was observed in the behavior of beams reinforced with CFRP stirrups and beams reinforced with steel stirrups. The use of CFRP for longitudinal reinforcement reduced the shear strength of the beams due to a lower contribution of aggregate interlock to shear resistance. Low shear force was carried out by the bars in dowel action due to the relatively poor strength and stiffness of FRP bars in the transverse direction. Hence, it may be assumed that most of the shear was carried out by the stirrups. After failure, the concrete was removed from some of the beams to inspect the CFRP grid stirrups. It was observed that even in the most distressed parts of the beam, no CFRP stirrup had actually ruptured.

Deitz et al. [90] tested 12 concrete deck panels reinforced with three reinforcing schemes. One scheme used FRP reinforcement at the top and bottom of the deck. Another

scheme used all epoxy-coated steel reinforcement (ECSR), and the third scheme used FRP bars at the top and ECSR at the bottom. Two modes of failure were observed: the specimens reinforced with ECSR failed in flexure, while the specimens with the other two reinforcement schemes failed in diagonal tension. These modes provided adequate warning of failure even though large crack widths and displacements developed. Deitz et al. [90] estimated that it would take approximately 4.1 years to build up a chloride ion concentration high enough to begin corrosion at the level of the top mat, and 23.3 years to begin corrosion at the bottom mat. Michaluk et al. [91] proposed the use of the following ACI equations for shear strength of concrete members reinforced with FRP reinforcement:

$$V_c = \left(\frac{E_{GFRP}}{E_{steel}}\right)\left(\sqrt{\frac{f_c'}{6}}\right)b_w d$$

$$V_c = \left(\frac{E_{GFRP}}{E_{steel}}\right)\left(f_c' + 120\rho_w \frac{V_u d}{M_u}\right)\frac{b_w d}{7} \le 0.3\sqrt{f_c'}b_w d$$

where,

$V_c$       = nominal shear strength provided by the concrete

$V_u$       = factored shear force at section considered

$M_u$       = factored moment occurring simultaneously with $V_u$ at the section considered

$E_{GFRP}$  = longitudinal elastic modulus of GFRP reinforcing bars

$E_{steel}$    = elastic modulus of steel reinforcement

$f_c'$       = specified concrete compressive strength

$b_w$       = member web width

$d$        = distance from extreme compression fiber to centroid of tensile reinforcement

$\rho_w$       = reinforcement ratio

The authors reported no units.

According to Dietz et al. [90], the above equations yield a ratio of experimental to predicted shear capacities of 3. Based on their test results, Dietz et al. [90] recommended the use of the following equations:

$$V_c = 3 \cdot \left( \frac{E_{GFRP}}{E_{steel}} \right) \cdot \left( \sqrt{\frac{f_c'}{6}} \right) \cdot b_w d$$

$$V_c = 3 \cdot \left( \frac{E_{GFRP}}{E_{steel}} \right) \cdot \left( f_c' + 120\rho_w \frac{V_u d}{M_u} \right) \frac{b_w d}{7} \leq 0.9 \cdot \left( \frac{E_{GFRP}}{E_{steel}} \right) \sqrt{f_c'} b_w d$$

where all the terms are as defined before.

The authors obtained ratios of experimental to predicted shear capacities of 1.04 to 1.17 using their proposed equations.

In summary, the low elastic modulus of FRP reinforcement leads to a lower contribution of the concrete to the shear strength, which leads to a reduction in the overall shear strength of FRP-reinforced concrete members. FRP stirrups can fail at loads as low as 50 percent of the tensile strength of the stirrups due to stress concentrations at the bends. Beams reinforced with FRP stirrups have good flexural performance, can redistribute moments, and the stirrups can reach strains twice as high as the permissible strains of the CHBDC. The ACI equation for the computation of punching shear capacity of slabs seems to be unconservative for FRP-reinforced concrete slabs, and a modification is proposed. The ACI equations for the estimation of the shear strength of beams with FRP stirrups seem to be unconservative, and modified equations are proposed.

## BOND AND DEVELOPMENT LENGTH

For reinforced concrete structures, the bond strength between the reinforcement and the concrete is critical to the performance of the structure. Due to the various reinforcing types (surface deformation, materials, and textures), the constant changing of products by manufacturers, and the lack of industry standards, bond characteristics vary significantly for different FRP products. The ribs (or lugs) on ribbed FRP reinforcement

are mostly resin. Resin has a low-shear modulus and thus may contribute little to the improvement of bond. Also, because FRP reinforcement has a lower modulus of elasticity value, the apparent "slip" (often directly associated with lack of bond) may indeed just be a larger strain in the bar or the ribs. Because of this, results from conventional bond strength tests must be viewed with caution.

Even so, the allowable bond stress value for steel-reinforcing bars is defined as the stress associated with the slip of 0.25 mm at a loaded end of a test sample and 0.05 mm at the free end. These criteria were motivated principally by the need to limit crack width and reinforcement corrosion. These limits may not necessarily be applicable to FRP reinforcement. Bond stress-slip curves for specimens with a bond length of 10 $d_b$ are illustrated in Figure 41. Specimens C1 through C4 are CFRP bars with a wound spiral on the surface, sand-coated surface, twisted strand configuration, and a braided structure, respectively. Specimens A1 through A3 are AFRP bars with a wound spiral on the surface, braided structure with sand-coated surface, and a braided structure without sand-coated surface. Specimen G1 is a GFRP bar with a wound spiral on the surface, and specimen V1 is a Vinylon® FRP bar with a wound spiral on the surface.
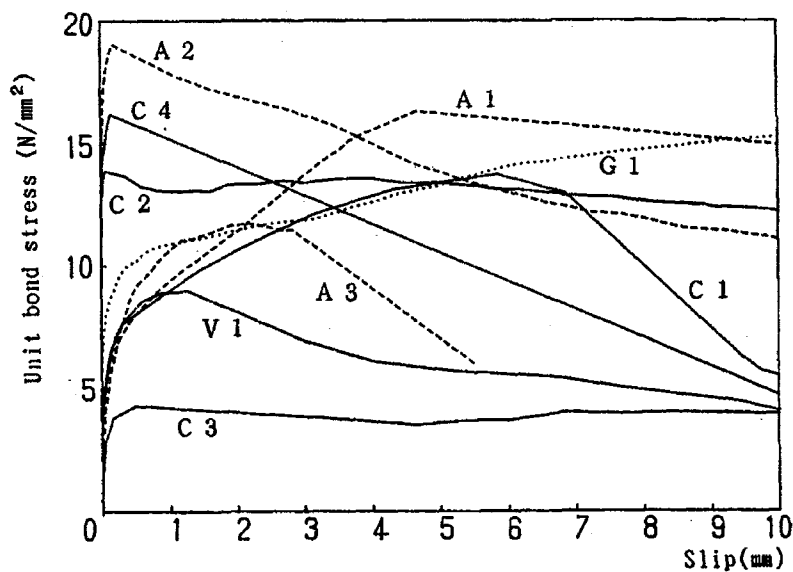


**Figure 41. Typical Bond Stress-Slip Curves of FRP Bars Embedded in Concrete [92].**

94

Large variations in the characteristics of commercially available FRP products make it difficult to develop general development length recommendations. Some of the factors affecting the bond strength of FRP bars are [17]:

(a) size and type of reinforcement (e.g., wires or strands),

(b) surface conditions (e.g., smooth, deformed, or sand-coated),

(c) poisson's ratio,

(d) concrete strength,

(e) concrete confinement (e.g., helix or stirrups),

(f) type of loading (e.g., static, cyclic, or impact),

(g) environmental effects,

(h) amount of concrete cover,

(i) type and volume fractions of fiber and matrix,

(j) matrix material type, and

(k) temperature.

According to a study by Karlsson [93] there are three primary bond failure mechanisms for C-Bar reinforcement bar.

(a) For low $f_c'$ (< 30 MPa), there is rupture of the surrounding concrete.

(b) At intermediate $f_c'$ (38 to 40 MPa), results in damage to the surface of the bar and to the concrete.

(c) At high $f_c'$ (55 to 60 MPa), damage is concentrated on the ribs of C-Bar reinforcement bars, accompanied by low concrete damage.

Cosenza et al. [94] carried out tests on 12.7 mm diameter bars from C-Bar and found a development length of 10 $d_b$ (bar diameters). C-Bar reinforcing bars have a ribbed surface formed with resin and fillers. The resin has low-shear strength as compared to concrete. Therefore, the bars will tend to fail by shearing of the ribs during pull-out tests, for the concrete strengths mentioned before.

95

Shield et al. [95] tested inverted concrete beam specimens 305 mm (12 in.) wide by 457 mm (18 in.) deep by 1.22 m (48 in.) long. No stirrups were used in the beams in order to simulate the lack of confinement present in bars of bridge decks. Bars from two manufacturers were tested:

(a) Hughes Brothers 19.1 mm diameter bar

Bar constituents: 76 percent by weight E-glass Owens-Corning Type 30-366-133 fibers in a 24 percent blended vinyl ester resin. A typical glass roving yields 113 yards per pound, thus, the authors believe the reported fiber type should be Type 30-366-133. Helical wrap with 25.4 mm (1 in.) pitch and 30 ° angle rib.

The average tensile failure stress was 636 MPa (92.4 ksi), with a COV of 0.037. The development length was between 42 $d_b$ and 63 $d_b$. Nonuniformly spaced cracks perpendicular to the bar developed.


(b) C-Bar 15.9 mm diameter bar

Bar constituents: 70 percent E-glass embedded in 10 percent recycled polyester resin. The rib angle was greater than 40 °. The deformations contain 3.5 percent ceramic fibers embedded in 15 percent urethane modified vinyl ester matrix with 1.5 percent corrosion inhibitor. Deformations were spaced at 9.5 mm (3/8 in.). The average tensile failure stress was 438 MPa (63.6 ksi), with a COV of 0.089. The development length was 24 $d_b$ and uniformly spaced cracks developed perpendicular to the bar.


The concrete used had an $f_c'$ of 44.4 MPa (6450 psi) and had 6 percent entrained air. Results indicated that some bars failed in tension at stresses more than $2\sigma$ below the average tensile strength. Two different covers were studied, 2 $d_b$ and 3 $d_b$.


Katz et al. [96] studied the bond behavior of five rebar types at room and high temperatures. One bar had lugs on the surface to provide the desired bond to concrete. Three other bar types had an extra layer of resin on the surface and a coat of sand. Also, a steel bar was included in the study for comparison purposes. The bars were tested at room temperature (RT = 20 °C), at 130 °C, and at 250 °C. Two main bond failure mechanisms

were observed. At room temperature, portions of the concrete surface in contact with the FRP bars pulled out in some specimens, as evidenced by portions of concrete attached to the surface of the FRP bar. At high temperatures, however, all the slip took place at the surface of the FRP bar, since the shear properties of the resin on the surface of the FRP bar deteriorated.

At 250 °C all FRP bars lost 80 percent or more of their RT bond strength, while the steel bars lost only 40 percent of their RT bond strength [96]. The bond strength of all FRP bars decreases with increase in temperature, and it appears to level off at a temperature of approximately 200 °C. The authors agree with a model proposed by Greszczuk [97] that assumes that the controlling parameters for bond strength are the shear modulus and the thickness of the outer layer of resin of the FRP rebar. The "bond stiffness" (initial slope of the bond-slip curve at the loaded end) decreases with increasing temperature. Residues of concrete were found between the deformations of steel bars for all the tested temperatures. FRP bars with helical fiber wrapping and sand coating tended to exhibit better bond behavior than was seen in bars that relied on lugs of polymer for bond strength. The FRP bars with lugs of resin showed abrupt drops in the bond-slip curves after the peak load was reached. The bond strengths of two FRP bar types were lower than the bond strength of steel bars. The other two FRP bar types exhibited higher bond strength when compared with steel bars.

Malvar [98] performed tension and bond pull-out tests on four reinforcing bar types. All bars had a diameter of 19 mm and were composed of E-glass fibers with a fiber volume fraction of 45 percent, embedded in a vinyl ester or polyester resin. Some test procedures and the test results are described next:

**Tension Tests:** The tension tests were carried out following the standard ASTM D 3916-84. The author reported problems with the gripping system and designed four aluminum blocks bolted together to grip the bars. The secant modulus from tension tests was used because it was expected that a working stress approach would be used in design. The rebar strengths varied from 448 MPa (65 ksi) to 709 MPa (103 ksi) and the moduli of

elasticity ranged from 28 GPa ($4.1x10^6$ psi) to 47 MPa ($6.9x10^6$ psi). Bar failure initiated at the kinks produced by helical wrapped fibers.

**Bond Tests:** FRP bars were embedded in a 76 mm (3 in.) diameter by 102 mm (4 in.) long concrete cylinder. The outer concrete surface was surrounded by a split, threaded steel pipe, which carried the pull-out force through shear stresses. The specimens were tested in pull-out tension while confining pressure was applied around the steel pipe through a cut ring stressed with a jack. Prior to each test, the concrete cylinder was pre-cracked by applying 3.45 MPa (500 psi) confining pressure around it while pulling on the bar, until longitudinal splitting of the concrete cylinder occurred. Then, the desired confining pressure was applied followed by tension. Five different confining pressure levels were studied: 3.45 (500), 10.3 (1500), 17.2 (2500), 24.1 (3500), and 31 MPa (4500 psi). Measured adhesion (bond stress at zero average slip) was between 0.69 MPa (100 psi) and 2.1 MPa (300 psi). Beyond this adhesion, the slope of the bond-slip curve appears to increase with higher confinement. During the bond test, lateral deformations of the confining ring were monitored. Records revealed that the specimen experiences a moderate lateral expansion up to the point of maximum bond stress. Thereafter, the lateral displacement increases noticeably, although the bond stresses are decreasing. For an identical amount of confinement, bond strength for a steel bar is, on average, 1.2 to 1.5 times higher than that for a FRP bar. Large variations in indentation depths of the bars resulted in a large variation of bond strength. Bond strength can be increased threefold by increasing confining pressure by a factor of 7.

Cosenza et al. [99] reviewed the current knowledge of bond performance of FRP bars embedded in concrete. Their findings are divided into several sections as follows: **Mechanics of Stress Transfer from FRP Bars to Concrete:** Bond is controlled by several factors: chemical bond, friction due to surface roughness of FRP bars, mechanical interlock of FRP bars against the concrete, hydrostatic pressure against the FRP bars due to shrinkage of hardened concrete, and swelling of FRP bars due to temperature change and moisture absorption. During initial pull-out, adhesion, or chemical bond, is the main resisting mechanism; after adhesion is lost, once slip begins, friction and mechanical

interlock become the primary means of stress transfer. Kanakubo [100] classifies bond mechanisms as friction-resistant types or bearing-resistant types.

**Bond of Straight FRP Bars:** Friction is the main bond-resisting mechanism for straight bars. There is no contribution of mechanical interlock. Bond strength of straight bars is independent of concrete strength and depends primarily on the quality of the resin. Sand-coated bars show large values of bond strength as compared to smooth bars; however, when the peak bond stress is reached, the bar pulls out in a brittle manner. Makitani et al. [92] found that adhesion can contribute an important fraction of the bond strength.

**Bond of Deformed FRP Bars:** In this case, mechanical interlock is the main bond-resisting mechanism, although there are contributions from adhesion and friction as well. It was found that the longitudinal shear modulus of the FRP bar is an important parameter. Hattori et al. [101] found that the concrete surface is not crushed significantly, whereas there is strong damage to the outer bar surface. Coating the surface of bars with sand enhances the bond strength and bond stiffness but leads to more brittle bond behavior. Bars with a surface coated with sand have excellent bond strength ($\tau_m > 10$ MPa), even higher than steel bars. The bond strength of smooth FRP bars is poor ($\tau_m < 2.37$ MPa). The bond strength of spiral-glued bars has values slightly higher than those of smooth bars ($\tau_m = 4.50$ MPa).

**Effect of Confinement Pressure:** Confining pressure increases the bond strength of FRP bars.

**Effect of Bar Diameter:** Bond strength increases as the bar diameter increases.

**Top-Bar Effect:** The researchers found that for their test conditions, the bond strength of the top bar has 66 percent of the bond strength of the bottom bar. Benmokrane and Masmoudi [102] proposed modification factors (ratio of the pull-out strength of the bottom bars to the pull-out strength of the top bars) of 1.23 and 1.18 for different bar types.

**Effect of Embedment Length:** Specimens with shorter embedment length develop higher bond strengths.

**Effect of Temperature Change:** Al-Zaharani [103] found more reduction in bond strength at temperatures lower than the curing temperature than reductions found at temperatures higher than the curing temperature. Honma and Maruyama [104] found that

bond strength decreases at increasing temperatures; due to a reduction of the resin stiffness. The resin exhibits a reduction of strength as well.

**Effect of Environmental Conditions:** Mashima and Iwamoto [105] found that specimens under freeze-thaw cycles did not evidence an appreciable reduction in bond strength. Al-Dulaijan et al. [106] detected considerable reduction in bond strength of bars immersed in a high pH solution for 28 days. This reduction seems to be a result of degradation of the resin.

**Analytical Models for Bond-Slip Behavior:** Cosenza et al. [99] present four models: Malvar model, BPE model, modified BPE model, and CMR model.

GangaRao and Faza [107] tested 20 specimens with different reinforcement sizes and surface types (ribbed and sand-coated). The researchers suggested the following design equation to compute the development length of GFRP bars:

$$l_d = K_1 \frac{f_u A_b}{\sqrt{f_c'}}$$

where,

$l_d$ = development length *(in.)*

$A_b$ = cross-sectional area of bar *(in.$^2$)*

$f_u$ = tensile strength of bar *(psi)*

$f_c'$ = concrete compressive strength *(psi)*

$K_1$ = 1/16

Pleiman [108] carried out more than 70 pull-out tests on GFRP-reinforcing bars (E-glass fibers), 49 tests on Kevlar (AFRP) bars, and some steel bars. Tests were performed on 6.4 mm, 9.5 mm, and 12.7 mm GFRP bars, and on 12.7 mm AFRP bars. Results suggested that GFRP and AFRP had similar behaviors and that both had lower bond strengths than steel bars. The author proposed to use the equation developed by GangaRao and Faza, using $K_1 = 1/20$ for GFRP and $K_1 = 1/18$ for AFRP, respectively.

Based on pull-out tests on GFRP bars (E-glass fibers and polyester resin, with a sand-coated surface) Chaallal et al. [109] recommended a design development length of 20 $d_b$.

Daniali [110] tested GFRP bars (E-glass and vinyl ester resin) in 30 concrete beam specimens. He concluded that the development length for 12.7 mm diameter bars was 16 $d_b$ and 23 $d_b$ for 19.1 mm diameter bars, provided that shear reinforcement was provided along the entire length of the beam.

A study of the development length of 102 GFRP bars, some straight and some with a 90-degree hook, led to a proposed allowable slip limit of 0.0025 in. for the free end and 0.015 in. for the loaded end of FRP bars tested in pull-out [111]. Also recommended was the basic development length equation suggested by GangaRao cited above, using $K_1 = 21.3$. To account for the influence of concrete cover, a factor of 1.0 can be used with concrete cover of not less than two times the bar diameter. A factor of 1.5 can be used with concrete cover of one bar diameter or less. The development length $l_d$, obtained as the product of the basic development length and the confinement modification factors, should not be less than:

$$l_d = 0.00035 d_b f_u$$

where,

$l_d$    = development length *(in.)*

$d_b$    = bar diameter *(in.)*

$f_u$    = ultimate tensile strength of the FRP bar *(psi)*

A factor of 1.25 can be used for top reinforcing bar. The development length of top bars modified with this factor should not be less than 380 mm (15 in.).

The ACI state-of-the-art report [17] stated that for hooked GFRP reinforcing bars with a tensile strength of 517 MPa (75,000 psi), the basic development length, $L_{hb}$, should be computed by:

$$L_{hb} = 1820 \frac{d_b}{\sqrt{f_c'}}$$

where $L_{hb}$ is the basic development length (in.) of a hooked bar, and $d_b$ and $f_c'$ are as defined before.

The ACI report [17] suggested that for reinforcing bars with tensile strengths other than 517 MPa (75,000 psi), a modification factor $f_u/75,000$ should be used. When side cover and cover on bar extensions are not less than 64 mm (2.5 in.) and 51 mm (2 in.), respectively, a modification factor of 0.7 should be used. To prevent pull-out failure, the development length $L_{dh}$, obtained as the product of the basic development length of a hooked bar times the modification factor, should not be less than 152 mm or 8 times the bar diameter.

An alternative method for testing the bond strength was proposed by Porter et al. [31]. The researchers tested over 100 cantilever beams and obtained the following expression to compute the minimum embedment length, $L_d$, of 8 mm (0.325 in.) and 12.7 mm (0.5 in.) diameter bars for zero end slip tolerance:

$$L_d = \frac{0.59 f_u A_b}{c_b^2 \sqrt{f_c'}}$$

where,

$f_u$  = ultimate tensile strength of the reinforcement *(psi)*

$A_b$  = area of the bar *(in.²)*

$c_b$  = circumference of the bar *(in.)*

$f_c^{'}$ = compressive strength of concrete *(psi)*

If 2.5 mm (0.10 in.) slip is allowed at the end of the embedment, the above equation becomes:

$$L_d = \frac{0.42 f_u A_b}{c_b^2 \sqrt{f_c^{'}}}$$

where all the terms are as defined before.

Cosenza et al. [94] tested bond specimens in pull-out for 12.7 mm diameter Grade B E-Glass C-Bar reinforcement bars and made the following observations:

(a) Three different modes of failure were noted: 1) pull-out failure in specimens with embedment lengths of 5 $d_b$; 2) combined pull-out and tension failure in specimens with embedment lengths of 10 $d_b$; and 3) tensile failure of the bar in specimens with embedment lengths from 20 $d_b$ to 30 $d_b$.

(b) Since bars with an embedment length of 10 $d_b$ failed in tension accompanied by initial pull-out failure, the authors concluded that the development length of the bar was 10 $d_b$.

(c) In the case of pull-out failure, damage throughout the concrete was observed and the ribs of the bar were superficially sheared off. This work validated other work that found that bond strength depends on the strength of the concrete as well as on the strength of the ribs. The strength of the concrete was 37 MPa and 40 MPa in the specimens that failed in pull-out. The concrete compressive strength was determined from 150 mm cubic specimens.

(d) Slips measured at the loaded end and at the free end were not the same, thus invalidating the assumption of uniform slip used in the authors' bond-slip constitutive relationship described next.

For s =< 0.25 mm

$$\tau_b(s) = 20.5 s^{\frac{1}{4}}$$

For s > 0.25 mm

$$\tau_b(s) = 14.6 - 7.4s$$

where $s$ is the slip of the bar and $\tau_b(s)$ is the bond stress.

Wang et al. [112] carried out pull-out tests to determine the bond of CFRP, GFRP, and AFRP rebars with different surface finishes. The following observations resulted:

**Influence of the Type of Fiber Used in the Bar:** CFRP bars had the highest bond strength among all of the bars with the same type of surface configuration. The bond of GFRP bars appeared to be as strong as that of CFRP bars. The bond of AFRP bars was the lowest.

**Influence of Bar Configuration:** Bond of FRP bars is greatly affected by the bar configuration. Strand bars had the lowest bond strength, approximately 50 percent of the bond strength of deformed bars. The bond strength of indented bars was also far lower than that of the deformed bars. All deformed bars had about the same bond strength.

**Influence of Elastic Modulus:** The authors suggest that except for the strand bars and indented bars, the bars with a larger elastic modulus appeared to have higher bond strength. However, the experimental data presented by the authors does not show a consistent influence, if any, of the elastic modulus.

**Influence of Embedment Length:** The maximum bond stress of FRP bars decreases with embedment length of the bar in concrete.

Wang et al. [112] proposed the following equation to model the bond strength between FRP bars and concrete:

$$\tau_{bu} = K\sqrt{f_c'}$$

where,

$\tau_{bu}$   = bond strength of the bar

$f_c^{'}$   = concrete compressive strength

$K$   = represents the effects of the type of fiber material, elastic modulus, and configuration of the bar and is evaluated as follows:

$$K = K_m K_s K_l K_o$$

where,

$K_m$   = coefficient for the type of fiber material (equal to 1.0 for steel)

$K_s$   = coefficient for the surface shape of the bar (equal to 1.0 for steel)

$K_l$   = coefficient for the embedment length of the bar in concrete (equal to 1.0 for standard specimens with an embedment length of 60 mm)

$K_o$   = coefficient that includes the effects of other factors such as size of the bar and stress conditions. From the experimental results $K_o = 3.0$.

The authors suggest the values listed in Tables 4, 5, and 6, for the $K_m$, $K_s$, and $K_l$, respectively.

### Table 4. Suggested Values of $K_m$.

| Material Type of Bar | Glass Fiber | Aramid Fiber | Carbon Fiber | Steel |
|---|---|---|---|---|
| $K_m$ | 0.95 | 0.80 | 1.05 | 1.0 |

### Table 5. Suggested Values of $K_s$.

| Configuration of Bar | Spirally Patterned | Braided | Ribbed | Compound Patterned | Indented | Strand | Deformed Steel bar |
|---|---|---|---|---|---|---|---|
| $K_s$ | 0.95 | 1.0 | 0.95 | 0.90 | 0.55 | 0.45* | 1.0 |

*The coefficient is suitable for the strand bar with 19.1 mm (¾ in.) diameter.

### Table 6. Suggested Values of $K_l$.

| Embedment Length (mm) | 60 | 100 | 160 |
|---|---|---|---|
| $K_l$ | 1.0 | 1.0 | 0.90 |

105

Sakai et al. [113] investigated the bond-splitting behavior of continuous fiber-reinforced concrete members. The authors designed a test to determine the bond-splitting strength of concrete with FRP bars. FRP bars were cast in a small rectangular concrete slab, providing an embedment length of four times the diameter of the bar. The results showed that the bond-splitting strength is not influenced by the longitudinal modulus of elasticity of the bar, and that it is approximately proportional to the thickness of the concrete cover. At long bond lengths, the bond strength is inversely proportional to the embedment length.

Makitani et al. [92] investigated the bond performance of carbon, aramid, glass, and Vinylon FRP bars in concrete. The authors fabricated beam-type specimens, where the bond length of the specimens was lap spliced in a region confined by stirrups. The samples had concrete cover of 50 mm. The authors reported that for the 9.5 mm diameter bars, a splice length of 40 $d_b$ was sufficient to develop the strength of all bar types. The bond strength of the FRP bars increased up to 40 $d_b$ and decreased for longer development lengths as depicted in Figure 42.
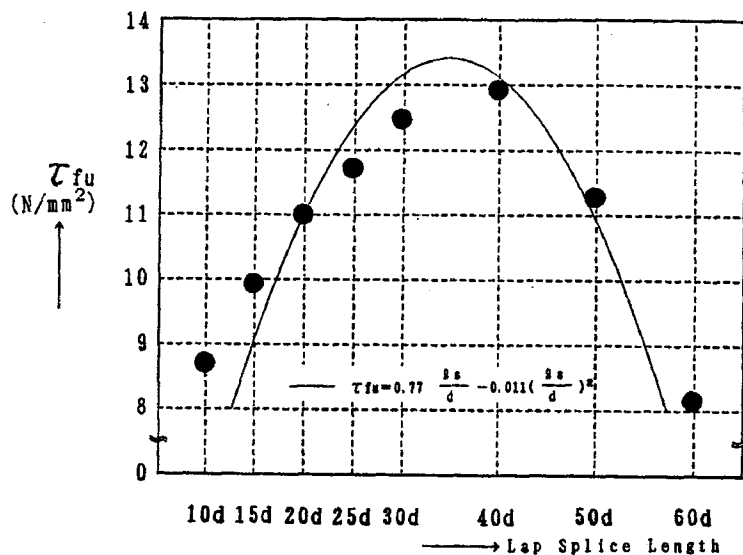


**Figure 42. Relationship Between Bond Stress
and Lapped Splice Length. [92].**

106

Summarizing, bond strength is affected by the size and type of reinforcement, surface condition of the bar, concrete strength, concrete confinement, matrix material type, bar/concrete interface, and temperature. Bond strength of FRP bars deteriorates at high temperatures. Sand-coated bars have better bond performance than smooth bars. Bond strength increases with bar diameter and decreases with bar embedment length. Freeze-thaw cycles apparently have no effects on the bond strength of FRP bars. There is a reduction in the bond strength of FRP bars in high pH solutions. This reduction is believed to be the result of degradation of the resin on the surface of the bar. Some FRP bars have higher bond strength than steel bars, but some others have lower bond strength. Top bars have lower bond strength than bottom bars. Bond strength of CFRP and GFRP bars appears to be higher than the bond strength of AFRP bars. Bond strength is not influenced by the longitudinal modulus of elasticity of the FRP bars. Adhesion and friction are the two main bond strength mechanisms between FRP bars and concrete.

## THERMAL EFFECTS

Gentry and Husain [20] performed thermoelastic analyses of plain and spirally wrapped composite bars embedded in concrete and subjected to a uniform temperature increase. Commercially produced composite bars possess a transverse CTE three to five times the CTE of concrete. It was found that spiral wrapping restrains the thermal expansion of FRP bars in the transverse direction, in addition to increasing the bonding of the bar to concrete. Analysis and anecdotal information agree that thermal stresses can cause cracking of the concrete. Cracking decreases with a decreasing bar diameter and increasing confining pressure of the concrete. Mechanical tensile strain in the longitudinal direction of the bars will tend to alleviate the thermal swelling of the reinforcement. Assuming that the reinforcement is operating at approximately 40 percent of its tensile capacity–around 600 MPa for the glass vinyl ester bar studied–the thermal swelling potential at a temperature increase of 40 °C is offset by the transverse shrinkage due to axial tensile strain.

In summary, the large difference between the transverse coefficient of thermal expansion of FRP bars and that of the concrete may lead to crack initiation or crack propagation on the surface of concrete elements reinforced with FRP bars.

# VII. APPLICATIONS AND DEVELOPMENT OF FRP REINFORCEMENT

## CANADA

In 1998, the Canadian Society for Civil Engineering created a technical committee that studied the use of advanced composite materials in bridges and structures [114]. Shortly after the technical committee was developed, committee members made a number of trips to Europe and Japan and published two state-of-the-art books on the subject.

Benmokrane et al. [72] implemented a research program to use CFRP for reinforcement in a concrete deck on the Joffre Bridge located over the Francois River in Sherbrooke, Quebec, Canada. Over 180 instruments were installed on the bridge to monitor its performance. From static and dynamic load tests, it was concluded that the bridge superstructure deflections and FRP reinforcement stresses were well within their allowable limits.

Eight precast concrete girders on the Centre Street/Beddington Trail Bridge were installed in February 1993 in Calgary, Alberta [115]. The bridge is a two-span 23.83 and 19.23 m continuous skew bridge. The bridge used CFRP bars and Carbon Fiber Composite Cable (CFCC®) reinforcement; both carbon fiber FRP products were produced in Japan. The bridge also used NEFMAC, a Japanese product made of glass or carbon fibers wound to form a grid with intersecting layers.

Construction of a bridge located over the Assiniboine River, Parish of Headingley, Winnipeg, Manitoba, Canada, was planned using FRP reinforcement [116]. The bridge consists of five spans, 32.5 meters each, with a total length of 165.1 m. The bridge girders had an AASHTO I-section, spaced at 1.8 m in the transverse direction and supporting a slab 187 mm thick. The girders were pretensioned with 40 strands. Two

types of carbon fiber composites were used as prestressing reinforcement, CFCC and Leadline®, both produced in Japan.

**Design of FRP-Reinforced Concrete Structures in Canada**

Some brief design criteria, results from the initial trips made by the Canadian committee to Europe and Japan, can be found in a document published by the Canadian Society for Civil Engineering [53]. The Canadian Highway Bridge Design Code, published in 1994, was the first Canadian code to incorporate provisions for the design of concrete structures using FRP products [114]. A synthesis of the design provisions of the CHBDC can be found in a paper by Bakht et al. [19]. Two general documents for designing FRP-reinforced concrete structures in Canada are *S06-97-Design and Construction of Building Components with Fibre Reinforced Plastics* [117], and *Section 16 – Fibre Reinforced Structures & Commentary to Section 16* [118].

**FRP Production in Canada**

In 1993 the only Canadian company that commercially produced GFRP bars was Pultrall Incorporated located in Thedford Mines, Quebec.

**EUROPE**

In the 1970s, a researcher at the University of Stuttgart conducted extensive research and pointed out that glass fiber bars were ideally suited for prestressed concrete structures [119]. Further application was limited at that time by the lack of reliable anchorage systems. Since then, many structures have been built in Europe using FRP reinforcement.

In 1986, in Dusseldorf, the Ulenbergstrasse Bridge was opened to traffic [53]. It was the first highway bridge prestressed with cables consisting of glass fiber bars and instrumented with fiber-optic sensors as well as copper wire sensors. The optical fiber

sensors allow for the monitoring of the full length of the prestressing cables, while the copper wire sensors detect when a bar or tendon ruptures and the location of the rupture. The bridge is a two-span continuous structure with 21.3 and 25.6 m. A total of 59 tendons, each composed of 19 bars 7.5 mm in diameter, were used to provide forces of 600 kN per unit [119].

Glass fiber tendons were used to rehabilitate the Marie d'Ivry subway station in Paris, France [119]. As a result of excavations on the side of the old subway structure, considerable cracking occurred in the concrete vault over a length of nearly 110 m. Thirty-six glass fiber prestressing cables were installed to strengthen the vault. The service load per tendon was 650 kN.

Piers were anchored with masonry bolts to the masonry walls to rehabilitate the Monastery of Heydau in Altmorschen [119]. Concerns regarding the durability of steel anchors made FRP anchors a viable option. Thus, glass fiber anchors grouted with resin were used.

Two 7 m long pedestrian bridges were built in Tring, Hertfordshire, U. K. [120]. These were the first prestressed brick box girder decks built with FRP cables. The bridges had a 75 mm camber. After letting the masonry cure for two weeks, the bridges were prestressed with Parafil® tendons. The tendons were stressed at 200 kN each, for a total prestressing force in the deck of 800 kN. Each bridge was instrumented with 22 vibrating string wires and a number of foil strain gages to monitor its performance over time.

**Design of FRP-Reinforced Concrete Structures in Europe**

The Federation International du Beton (*fib*) Task Group 9.3 is the main European group developing guidelines for the design of concrete structures with FRP products. The following guidelines are currently being developed: *Kunststof Wapeningselementen in Beton – Preadvies* [121], *Modifications to NS3473 When Using Fibre Reinforced Plastic*

*(FRP) Reinforcement* [122], and *Interim Guidance on the Design of Reinforced Concrete Structures Using Fibre Composite Reinforcement* [123].

**FRP Production in Europe**

The following FRP products are manufactured in Europe [119].

(1) The Polystal® bar consists of 68 percent of glass fibers by volume and 32 percent of resin (modified unsaturated polyester). The bars have a diameter of 7.5 mm and are protected by a polyimide coating.

(2) In 1983, AKZO and HBG began fabricating Twaron® aramid FRP tendons under the name Arapree® (*ara*mid *pre*stressing *e*lement). Arapree consists of bundles of Twaron fibers embedded in an epoxy resin. The tendon composition is 35 to 45 percent of Twaron fibers and 65 to 55 percent of resin.

(3) Parafil ropes, developed by the Imperial Chemical Industries (ICI) Company, and now produced by Linear Composites, Ltd., have a core of parallel filaments of yarn with a thermoplastic sheath. Different core yarns can be used. The anchorage of the Parafil system consists of an internal spike that grips the fibers against an external conical barrel. Threads are used at the ends of the barrel to prestress the ropes at typical values of 60 percent of the rope capacity.

**JAPAN**

Research and development of FRP concrete structures began in Japan in the 1980s [2, 124]. In 1988, a comprehensive five-year national research project for the use of new materials in the construction field was launched and sponsored by the Ministry of Construction. The selected Japanese team decided that concrete structures prestressed by FRP tendons were more promising than structures without prestressing, and prestressed FRP structures would be effective under extraordinary environmental conditions such as chemical attack, deicing salts, and the corrosive action of seawater. This work resulted in significant developments in the field of FRP reinforcement.

The Japanese FRP research project is outlined in Table 7.

**Table 7. Outline of Japanese National FRP Research Plan [124].**

| Content of Tentative Guideline | Research Items |
|---|---|
| 1.0 General<br>1.1 Scope<br>1.2 Nomenclature<br>1.3 Symbol<br>2.0 Design Method<br>2.1 Design Philosophy<br>2.2 Safety Factors and Design<br>3.0 Material<br>3.1 General<br>3.2 Material, Kind, Quality, and Coefficients of<br>      Mechanical Properties of Concrete | |
| 3.3 Quality, Configuration, Dimensions, and Coefficients<br>      of Mechanical Properties of FRPR | • Test of Tensile Strength<br>• Bond Strength by Simple Pull-Out Test<br>• Chemical Resistance<br>• Creep under Tension<br>• Compressive Strength and Behavior under Tension and<br>   Compression Reversals and Cyclic Tension<br>• Tensile Strength at High and Low Temperature |
| 3.4 Other Materials<br>4.0 Loads and Their Combinations<br>4.1 Loads<br>4.2 Combination of Loads<br>5.0 Stress and Deformation<br>5.1 Fundamental Analysis of Stress and Strain<br>5.2 Analysis of Stress and Deformation of Frames<br>5.3 Analysis of Stress and Deformation of Slabs and<br>      Beams | |

113

## Table 7. Outline of Japanese National FRP Research Plan Continued...[124].

| Content of Tentative Guideline | Research Items |
|---|---|
| 6.0 Ultimate State Design<br>6.1 General<br>6.2 Examination of Members under Ultimate State | |
| (1) Ultimate Strength for Axial Force | • Compressive Strength and Behavior under Tension and Compression Reversals and Cyclic Tension<br>• Effect of Confinement by Lateral Reinforcement |
| (2) Ultimate Flexural Strength | • Flexural Behavior of Simple Beams<br>• Flexural Behavior Beams Subjected to Antisymmetrical and Cyclic Loading<br>• Evaluation of Crack Width<br>• Tension Stiffening Effect |
| (3) Ultimate Shearing Strength | • Shear Behavior of Beams Subjected to Antisymmetrical Loading<br>• Tensile Strength of Bent Corner<br>• Behavior of Bars under Tension Combined Shear |
| (4) Ultimate Bond-Splitting Strength | • Bond-Splitting Behavior by Simplified Method<br>• Bond-Splitting Behavior by Cantilever Method<br>• Bond-Splitting Behavior of Beams Subjected to Antisymmetrical and Cyclic Loading |
| (5) Ultimate Torsional Strength | |
| 6.3 Examination of Frames under Ultimate State | • Structural Behavior of Frame |
| 6.4 Examination of Floor Slabs and Beams under Ultimate State | • Flexural Behavior of Simple Beams<br>• Flexural Behavior Beams Subjected to Antisymmetrical and Cyclic Loading<br>• Shear Behavior of Beams Subjected to Antisymmetrical Loading<br>• Tensile Strength of Bent Corner |
| 7.0 Serviceability State Design<br>7.1 General | |
| 7.2 Examination of Crack | • Evaluation of Crack Width<br>• Flexural Behavior of Simple Beams |
| 7.3 Examination of Deflection | • Behavior of RC and PC Beams Subjected to Long-Term Loading |
| 7.4 Examination of Vibration | • Flexural Behavior of Simple Beams |
| 8.0 Structural Detail | |
| **Appendix** | |
| 1. Standard Test Method | • Examination of Testing Method of Tensile Strength |
| 2. Example of Structural Design | • Structural Behavior of Frame |
| 3. Evaluation Standard of Durability | • Heat Cycle at Dry and Wet State by Bond Test<br>• Chemical Resistance<br>• Behavior of RC and PC Beams Subjected to Long-Term Loading |
| 4. Evaluation Standard of Fire Resistance | • Tensile Strength at High Temperature<br>• Flexural Behavior of Beams under Heating<br>• Flexural Behavior of Beams after Heating |

Many structures have been built in Japan using FRP products. Some interesting projects are described next.

A prestressed concrete floating bridge was built over a pond on a golf course in Japan [124]. The bridge has a length of 56.37 m, a width of 4 m, and consists of six prestressed concrete beams. The beams have a core of styrofoam, 8 pieces of FiBRA-K192 (FRP) tendons, continuous CLATEC ROD® (FRP) spiral stirrups, and FiBRA-K64 (aramid FRP) in a mesh shape for both the deck board and walls. CLATEC ROD is made with 60 percent of a high-tenacity Vinylon or high-tenacity polyvinyl alcohol (PVA) fiber and an epoxy resin. FiBRA is a continuous fiber rod formed by braiding high-strength fibers impregnated with an epoxy resin.

CLATEC ROD 10D was used in an open-hearth electric furnace of an iron mill to provide protection from high-voltage currents and heat buildup in concrete slabs [125]. Precast panels of 13 $m^2$ were used.

A bridge in the Soto-Noto of Ishikihawa Prefecture, Japan, was badly corroded due to the presence of salt and moisture [126]. To replace the bridge, the first concrete bridge prestressed with carbon fiber tendons was designed and constructed. The bridge has a span of 6.1 m and a width of 7 m. The cables used in the bridge were of the type CFCC.

A prestressed concrete bridge was built using Technora bars in the Oyama factory of Sumiken Concrete Industry Corporation in the Prefecture of Togichi, Japan [127]. One traffic lane was built with a pretensioned system and the other with a post-tensioned system. The pretensioned bridge was 12.5 m long, while the post-tensioned bridge was 25 m long. Technora spirally wound bars 6 mm in diameter were used in all tendons. A bundle of 3 Technora bars 6 mm in diameter were used in the main cables of the pretensioned bridge. The same type of cable was used for the prestressing of the cross-

beams and slabs. The cables used in the post-tensioned bridge consisted of a bundle of 19 Technora 6 mm diameter bars.

**Two-Dimensional FRP-Reinforcement Systems in Japan**

Japanese researchers and corporations have introduced a two-dimensional reinforcement system made of grids manufactured by setting layers of resin-soaked fibers at right angles. A sketch of 2-D reinforcement is shown in Figure 43.
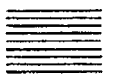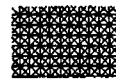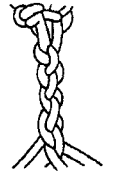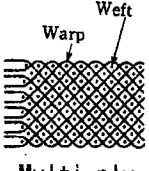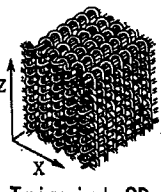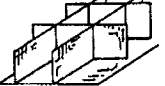
| Dimension \ Axis | 1 Mono-axial | 2 Biaxial | 3 Triaxial | 4~ Multi-axial | | |
|---|---|---|---|---|---|---|
| 1D | Pultrusion rod | — | — | — | | |
| 2D | Pre-impregnation sheet | Plane weave | Triaxial weave | Multi-axial weave | | |
| 3D — Linear element | 3D braid | Multi-ply weave | Triaxial 3D weave | 4-axial / 5-axial / 6-axial Multi-axial weave | | |
| 3D — Plane element | Laminate type | H or I beam | Honey-comb type | — | | |

**Figure 43. Fiber Configurations for Composite Materials [128].**

By March 1992, a total of 1,150,000 $m^2$ of NEFMAC had been used for concrete reinforcement [129]. NEFMAC has been successfully used to reinforce shotcreted tunnel linings using the New Austrian Tunneling Method (NATM). It was used to reinforce shotcrete in the repair of a railway tunnel. Its nonconductive properties were decisive to prevent electric shock. The use of NEFMAC reduced the reinforcement installation time by nearly 70 percent.

NEFMAC was used in the construction of the control building in the Antarctic base of Japan [129]. The building had to be constructed by the members of the expedition without construction training in a short time. The product was also used to reinforce the concrete foundation of an earth magnetism observatory in which no metals could be used and for the construction of a light-weight curtain wall in a building, with the approval of the Japanese Minister of Construction.

## Three-Dimensional FRP-Reinforcement Systems in Japan

The Japanese researchers and corporations also developed three-dimensional reinforcement systems manufactured by weaving FRP threads in three-dimensional configurations. A sketch of the 3-D reinforcement is shown in Figure 43.

Some important advantages of composite materials such as three-dimensional fabric reinforcement are labor savings and reduction of construction time [128]. Three-dimensional fiber-reinforced-concrete (FRC) panels were used in a chlorine gas storeroom at the Higashi-Murayama purification plant in Japan. This use was the first commercial application of the panels in a structure. The original design required the wall between a chlorine gas storeroom and an adjacent room to be made of precast concrete panels reinforced with stainless steel bars. Nevertheless, leakage of chlorine gas was possible and due to the need of a durable material, 3D-FRC panels were used. The fabric was made of PAN-type carbon fibers and the matrix was VRFC with 1 percent of Vinylon short fibers. The weight of a standard panel is approximately 250 kg.

In addition a 3-D FRC was used as parapet panels in the Suidobashi Building of Tokyo Dental College [128]. The rovings used for the fabrics were aramid fibers for the X- and Y-axes, and carbon fibers for the Z-axis. The fiber arrangement was selected to avoid radio wave interference. VRFC was used for the matrix. The weight of a standard panel is approximately one ton. The panels were tested for wind resistance under 5 kN/$m^2$ leeward and 3.3 kN/$m^2$ windward pressure. The panels showed adequate strength and stiffness.

The 3-D FRC was first applied on a large scale on the 23-story Sea Fort Square building in the sea front area of Shinagawa, Tokyo. A total of 1500 $m^2$ was applied. FRP materials were chosen because of the light-weight of the panels and because of concerns of salt-induced aluminum corrosion. Sixty-minute fire resistance tests were successfully conducted following JIS A 1304 standards. Maximum temperature of the unexposed surface was 103 °C when heated from the exterior face and 110 °C when heated from the interior face. Both temperatures were well below the 260 °C maximum allowable by JIS A 1304 specifications. No deformation, fractures, or cracks that could hamper the fire resistance of the panels were observed after the fire test.

**Design of FRP-Reinforced Concrete Structures in Japan**

Recent Japanese design guides for concrete members reinforced with FRP products are readily available in Japan. Currently, seven design guides have been published. These include:

(a) AIJ, *Evaluation Items and Evaluation Methods for New Reinforcement Materials and New Reinforced Concrete* (in Japanese), Report, Task Committee on Continuous Fibre Composite Materials, Architectural Institute of Japan, Tokyo, Japan, 1991.

(b) JSCE, *Application of Continuous Fiber Reinforcement Materials to Concrete Structures* (in Japanese), Concrete Library No. 72, Japanese Society for Civil Engineering, Tokyo, Japan, 1992.

(c) JSCE, *State-of-the-Art Report on Continuous Fibre Reinforcing Materials,* Concrete Engineering Series 3, Japanese Society for Civil Engineering, Tokyo, Japan, 1993.

(d) BRI, *Design Guidelines of FRP Reinforced Concrete Building Structures* (in Japanese), Building Research Institute, Japanese Ministry of Construction, Tokyo, Japan, 1993.

(e) Sonobe et al., *Design Guidelines of FRP Reinforced Concrete Building Structures,* **Journal of Composites for Construction,** Vol. 1, No. 3, August 1997, ASCE, USA, pp. 90–115, August 1997.

(f) BRI, *Design Guidelines for FRP Prestressed Concrete Members* (in Japanese), Building Research Institute, Japanese Ministry of Construction, Tokyo, Japan, 1995.

(g) JSCE, *Recommendation for Design and Construction of Concrete Structures Using Continuous Fiber Reinforcing Materials,* Concrete Engineering Series 23, Ed. A. Machida, Research Committee on Continuous Fibre Reinforcing Materials, Japan Society of Civil Engineers, Japan, 1997.

(h) JCI, *Technical Report on Continuous Fibre Reinforced Concrete,* Technical Committee on Continuous Fibre Reinforced Concrete (JCI TC952), Japan Concrete Institute, Japan, 1998.

**FRP Production in Japan**

In 1993 there were 15 commercially available FRP products for concrete reinforcement produced in Japan. They are presented in Table 8.

**Table 8. Continuous Fiber Reinforcement Manufactured in Japan [124].**

| | Developer and Maker (*) | Fiber Type | Binder | Configuration |
|---|---|---|---|---|
| 1 | Obayashi-Gumi (G.C.)<br>Mitsubishi-Kasei (F.M.) | Carbon (Pitch) | Epoxy | Round,<br>Deformed |
| 2 | Kajima (G.C.)<br>Arisawa (B.M.)<br>Akzo (B.M. and F.M.) | Carbon (Pan, Pitch),<br>Aramid, Vinylon | Epoxy | 3 Dimension |
| | | Aramid | Epoxy | Plate |
| 3 | Shimizu (G.C.)<br>Dainihon-Glass (B.M.) | Glass (E),<br>Carbon (Pan) | Vinyl-ester | 2 and 3 Dimension<br>Grid (NEFMAC) |
| 4 | Kumagai-Gumi (G.C.)<br>Arisawa (B.M.) | Carbon (Pan),<br>Glass (E) | Epoxy, PPS | Deformed,<br>Spirally wound |
| 5 | Taisei (G.C.)<br>Toyo-Rayon (F.M.) | Carbon (Pan) | Special Cement and<br>Silica Fume | Plate, Shell Plate,<br>Rod |
| 6 | Mitsui (G.C.)<br>Dupon, Tore Kepler (F.M.) | Aramid,<br>Carbon (Pan) | Epoxy | Braided (FiBRA) |
| 7 | Tokyo-Seiko (B.M.)<br>Toyo-Rayon (F.M.) | Carbon (Pan) | Epoxy,<br>Bismareimid | Twist (CFCC) |
| 8 | Sumitomo (G.C.)<br>Teijin (F.M.) | Aramid | Vinyl-ester | Deformed |
| 9 | Mitsubishi-Rayon (F.M., B.M.) | Carbon (Pan) | Epoxy | Round, Deformed |
| 10 | Tore (F.M., B.M.) | Carbon (Pan) | Epoxy | Twilled |
| 11 | New Nippon Steel (S.M.)<br>Kanebo (F.M., B.M.) | Carbon (Pitch),<br>Aramid | Epoxy | Mesh |
| | | Carbon | Epoxy | Twist |
| 12 | Kurare (F.M., B.M.) | Vinylon | Epoxy | Twilled, Braided |
| 13 | Okumura-Gumi (G.C.)<br>Showa-Kohbunshi (F.M., B.M.) | Carbon (Pitch),<br>Aramid, Glass (E) | Vinyl-ester | Spirally wound |
| 14 | Takenaka-Komuten (G.C.) | Carbon (Pitch, Pan),<br>Aramid | Epoxy | 3 Dimension |
| 15 | Osaka-Gas (F.M.) | Carbon (Pitch) | Epoxy | Braided, Round,<br>Mesh |

* G.C.: general contractor, F.M.: fiber maker, B.M.: bar maker, S.M.: steel maker

## UNITED STATES

The ASCE's Civil Engineering Research Foundationprogram funded approximately $4,000,000 for the investigation and use of FRP-reinforcing bars through 2002 and is anticipated to involve the development of second-generation reinforcing bar systems. ACI Committee 440 has completed its state-of-the-art report on this subject and is writing a manual of design and construction practice. In addition, the American Society for Testing and Materials (ASTM) is developing new standards and test methods for the use of FRP reinforcement. The ACI committee 440 has recently received TAC approval to publish the *Guide for the Design and Construction of Concrete with FRP Bars.*

In a joint research effort among US Army Corp of Engineers (USACE), the West Virginia University, and the West Virginia Department of Transportation, a bridge deck

120

was constructed using FRP-composite reinforcing bar in August 1996 [130]. A draft report has been issued that describes the design methodologies necessary for using FRP-reinforcing bars as concrete reinforcement and required construction technologies used on the actual bridge deck.

The University of Kentucky and the Kentucky Department of Transportation led a joint project to construct a FRP-reinforced concrete bridge deck in 1997. Currently, a research team is monitoring the structural behavior of the system, including deflection, crack formation, and strain measurement. The FRP-reinforced portion of the deck is limited to a 2.75 m (9 ft) by 4.75 m (15 ft) section of the top mat near the center of the deck.

A transversely post-tensioned bridge deck was installed on the access route to a factory near Rapid City, South Dakota [55]. The bridge was designed, manufactured, and installed by the South Dakota School of Mines and Technology in 1991. The bridge has a 200 mm (8 in.) concrete deck supported on steel stringers. The bridge spans 9.1 m (30 ft) and is 6.1 m (20 ft) wide. The entire structure was prefabricated at the university and shipped to the site. Glass, carbon, and steel tendons were used as prestressing reinforcement, each on a 10-foot section of the bridge. The cables were prestressed to 55 percent of their ultimate strength.

A group of concrete piles prestressed with glass and carbon FRP tendons were fabricated and driven in a sandy soil by the Florida Southern University and the Florida Department of Transportation [55]. All the piles were driven successfully; however, after driving all the piles, an additional driving force was applied to the piles. During the overdriving, the glass fiber spirals of the GFRP-reinforced concrete piles fractured. The glass fiber spirals were designed for the same driving force as the piles with steel reinforcement, but failed at lower loads.

Other bridges have been constructed using FRP reinforcement. These structures include:

(a) Rouge River Bridge completed in 1997, in Southfield, Michigan.

(b) A small bridge was built by researchers at the University of New Hampshire and opened to traffic in the spring of 1993 [55].

**Design of FRP-Reinforced Concrete Structures in the United States**

In the United States, design guidelines for concrete members reinforced with FRP products are given in reference [17].

**FRP Production in the United States**

The following FRP products are currently manufactured in the U.S.:

(1) Hughes Brothers produces glass-reinforced FRP bars with filament-wound fibers wrapped around the bars [131]. They produce bars in diameters of 6.4 mm (0.25 in.), 9.5 mm (0.375 in.), 12.7 mm (0.5 in.), 15.9 mm (0.625 in.), 19.1 mm (0.75 in.), 22.2 mm (0.875 in.), 25.4 mm (1.125 in.), and 32.3 mm (1.25 in.) The bars have a nominal 75 percent glass fiber content by weight. Hughes Brothers can also manufacture FRP bars with limited angle and radius bends.

(2) Marshall Industries produces C-Bar reinforcing bar with a glass fiber volume fraction of 60 percent in the core of the bar and urethane modified vinyl ester resin [29, 132]. Ceramic fibers used to reinforce the bars' surface deformations are present in a volume fraction of 3 percent [132]. Currently C-Bar reinforcing bars are available in 9.5 mm (0.375 in.), 12.7 mm (0.5 in.), 15.9 mm (0.625 in.), and 19.1 mm (0.75 in.) diameters [29]. C-Bar bars are also manufactured with bends and stirrups.

(3) TILLCO Company is another producer of FRP bars. TILLCO produces glass FRP bars with a fiber weight fraction of approximately 70 percent of the composite. The resin types being used are vinyl ester and isophtalic [133].

# VIII. CONCLUSIONS AND RECOMMENDATIONS

It is clear that there are a number of factors that need to be resolved regarding the use of FRP-reinforcing bars in concrete structures. Some important factors are related to durability, including moisture absorption and alkali degradation of glass fibers. Another factor is that GPRP bar manufacturers use glass fibers and resins from different producers, thus resulting in the production of materials with different mechanical and durability characteristics.

Cracking and deflection of FRP-reinforced concrete members are more likely to control the design of FRP-reinforced concrete members than in the case of steel-reinforced concrete members. As mentioned in the report, crack widths should not only be limited for durability and aesthetic reasons, but also for structural reasons in FRP-reinforced concrete flexural members. Further research is needed.

Bond of FRP-reinforcing bars to concrete is one of the areas that needs more research efforts. Bond of FRP-reinforcing bars depends highly on the surface characteristics of the bars. Therefore, bond of FRP bars to concrete needs to be investigated for each bar size and type. As noted in the report, the fatigue strength of FRP-reinforced concrete members depends upon the bond of the FRP bars to concrete.

It needs to be investigated whether high temperatures can cause FRP-reinforced concrete members to crack. The higher temperatures in Texas require further testing.

The shear strength of FRP bars is one of the areas where less research has been performed, and, therefore, one of the areas where there is less confidence. Similarly, little confidence exists in the modeling of creep behavior of FRP composites. Further research work is needed.

Finally, it is imperative to determine the mechanical properties of FRP bars used in reinforced concrete elements. Currently, this information is needed to carry out a more reliable design.

# IX. REFERENCES

[1] Bakis, C., *FRP Reinforcement: Materials and Manufacturing*, in **Fiber-Reinforced-Plastic (FRP) Reinforcement for Concrete Structures: Properties and Applications**, Nanni, A., ed., The Netherlands: Elsevier Science Publication, pp. 13–58, 1993.

[2] Nanni, A., **Fiber-Reinforced-Plastic (FRP) Reinforcement for Concrete Structures: Properties and Applications**, The Netherlands: Elsevier Science Publication, pp. 3–12, 1993.

[3] Agarwal, B., and Broutman, L., **Analysis and Performance of Fiber Composites**, 2$^{nd}$ Ed., U.S.A.: John Wiley and Sons, 1990.

[4] Sawyer, L., and Grubb, D., **Polymer Microscopy**, Great Britain: Chapman and Hall, 1996.

[5] Chung, D., **Carbon Fiber Composites**, Boston: Butterworth-Heinemann, 1994.

[6] Watt, W., and Perov, B., **Strong Fibers**, Handbook of Composites, Amsterdam; New York: North-Holland, Elsevier Science Publication Corporation, 1985.

[7] Miller, E., **Introduction to Plastics and Composites**, New York: Marcel Decker, 1996.

[8] Strong, A., **Plastics, Materials and Processing**, U.S.A.: Second Edition, Prentice Hall, 2000.

[9] Rosen, S., **Fundamental Principles of Polymeric Materials for Practicing Engineers**, New York: Barnes and Noble, Inc., 1971.

[10] Nielsen, L., and Landel, R., **Mechanical Properties of Polymers and Composites**, Second Edition, New York: Marcel Decker, 1994.

[11] Haward, R., **The Physics of Glassy Polymers**, Great Britain: John Wiley and Sons, 1973.

[12] Chanda, M., and Roy, S., **Plastics Technology Handbook**, New York: Marcel Dekker, Inc., 1987.

[13] Encyclopaedia Britannica Online, http://www.eb.com, 2000.

[14] Rosato, D., DiMattia, D., and Rosato, D., **Designing with Plastics and Composites**, U.S.A.: Van Nostrand Reinhold, 1991.

[15] Broutman, L., **Composite Materials, Volume 5, Fracture and Fatigue**, U.S.A.: Academic Press, 1974.

[16] Japan Society of Civil Engineers, *Recommendation for Design and Construction of Concrete Structures Using Continuous Fiber Reinforcing Materials*, Concrete Engineering Series 23, Ed. A. Machida, Research Committee on Continuous Fibre Reinforcing Materials, Japan Society of Civil Engineers, Japan, 1997.

[17] ACI Committee 440, **State-of-the-Art Report on Fiber Reinforced Plastic Reinforcement for Concrete Structures**, Detroit: American Concrete Institute, 1996.

[18] Mutsuyoshi, H., and Machida, M., *Mechanical Properties and Flexural Strength of PC Beams Using FRP as External Cables*, Proceedings of Japan Society of Civil Engineers, Vol. 16, No. 442, pp. 153–159, 1992.

[19] Bakht, B., Al-Bazi, G., Banthia, N., Cheung, M., Erki, M., Faoro, M., Machida, A., Mufti, A., Neale, K., and Tadros, G., *Canadian Bridge Design Code Provisions for*

*Fiber-Reinforced Structures*, Journal of Composites for Construction, pp. 3–15, February 2000.

[20] Gentry, R., and Husain, M., *Thermal Compatibility of Concrete and Composite Reinforcements*, **Journal of Composites for Construction**, New York: pp. 82–86, May 1999.

[21] Iwamoto, K., Uchita, Y., Takagi, N., and Kojima, T., *Flexural Fatigue Behavior of Prestressed Concrete Beams Using Aramid-Fiber Tendons*, Proceedings, ACI International Symposium, Fiber-Reinforced-Plastic Reinforcement for Reinforced Concrete Structures, Detroit: American Concrete Institute, pp. 509–523, 1993.

[22] Yamasaki, Y., Masuda, Y., Tanano, H., and Shimizu, A., *Fundamental Properties of Continuous Fiber Bars*, Proceedings, ACI International Symposium, Fiber-Reinforced-Plastic Reinforcement for Reinforced Concrete Structures, Detroit: American Concrete Institute, pp. 715–730, 1993.

[23] Hoffman, P., McClure, R., and West, H., *Temperature Problem in a Prestressed Box-Girder Bridge*, Transportation Research Record 982, **Bridges and Foundations**, Washington, D.C.: TRB, pp. 42–50, 1984.

[24] Shiu, K., *Seasonal and Diurnal Behavior of Concrete Box-Girder Bridges*, Transportation Research Record 982, **Bridges and Foundations**, Washington, D.C.: TRB, pp. 50–56, 1984.

[25] Deitz, D., *GFRP Reinforced Concrete Bridge Decks*, Ph.D. Dissertation, University of Kentucky, 1998.

[26] Faza, S., and GangaRao, H., *Glass FRP Reinforcing Bars for Concrete*, in **Fiber-Reinforced-Plastic (FRP) Reinforcement for Concrete Structures: Properties and**

**Applications**, Nanni, A., ed., The Netherlands: Elsevier Science Publication, pp. 167–188, 1993.

[27] Tamuzs, V., and Tepfers, R., *Ductility of Non-Metallic Hybrid Fiber Composite Reinforcement for Concrete*, Non-Metallic (FRP) Reinforcement for Concrete structures, Proceedings of the Second International RILEM Symposium (FRPRCS-2), Great Britain: E and FN SPON, pp. 18–25, 1995.

[28] Uomoto, T., and Hodhod, H., *Properties of Fiber Reinforced Plastic Rods for Prestressing Tendons*, Proceedings, ACI International Symposium, Fiber-Reinforced-Plastic Reinforcement for Reinforced Concrete Structures, Detroit: American Concrete Institute, Detroit: American Concrete Institute, pp. 101–115, 1993.

[29] Marshall Industries Composites, Inc., *Design Manual*, U.S.A.: Marshall Industries Composites, Inc., 1999.

[30] Wu, W., *Thermomechanical Properties of Fiber Reinforced Plastic (FRP) Bars*, Ph.D. Dissertation, West Virginia University, Morgantown, 40 pp., 1991.

[31] Porter, M., Hughes, B., Barnes, B., and Viswanath, K., *Non Corrosive Tie Reinforcing and Dowel Bars for Highway Pavement Slabs*, Department of Civil and Construction Engineering, Engineering Research Institute, Iowa State University, Ames, 1993.

[32] Ueda, T., Sato, Y., Kakuta, Y., Imamura, A., and Kanematsu, H., *Failure Criteria for FRP Rods Subjected to a Combination of Tensile and Shear Loads*, Non-Metallic (FRP) Reinforcement for Concrete Structures, Proceedings of the Second International RILEM Symposium (FRPRCS-2), Great Britain: E and FN SPON, pp. 26–33, 1995.

[33] Budelmann, H., and Rostasy, F., *Creep Rupture Behavior of FRP Elements for Prestressed Concrete – Phenomenon, Results and Forecast Models*, Proceedings, ACI

International Symposium, Fiber-Reinforced-Plastic Reinforcement for Reinforced Concrete Structures, Detroit: American Concrete Institute, pp. 87–100, 1993.

[34] Schwarz, M., **Composite Materials Handbook**, U.S.A.: McGraw Hill, 1992.

[35] Rahman, A., Taylor, D., and Kingsley, C., *Evaluation of FRP as Reinforcement for Concrete Bridges*, Proceedings, ACI International Symposium, Fiber-Reinforced-Plastic Reinforcement for Reinforced Concrete Structures, Detroit: American Concrete Institute, pp. 87–100, 1993.

[36] Gorty, S., *Mechanical Properties of Composite Cables*, MS thesis, South Dakota School of Mines & Technology, Rapid City, pp. 21–33, 1994.

[37] Kaski, G., and Dolan, W., *Creep Rupture of Fiber Reinforced Polymer Prestressing Tendons Under Curvature*, ACI Fourth International Symposium Fiber Reinforced Polymer Reinforcement for Reinforced Concrete Structures, U.S.A.: American Concrete institute, pp. 23–32, 1999.

[38] Tannous, F., and Saadatmanesh, H., *Durability of AR Glass Fiber Reinforced Plastic Bars*, **Journal of Composites for Construction**, pp. 12–19, February 1999.

[39] Schnabel, W., **Polymer Degradation Principles and Practical Applications**, United Kingdom: Macmillan Publishing Co., Inc., 1981.

[40] Okamoto, T., Matsubara, S., Tanigaki, M., and Hasuo, K., *Practical Application and Performance of PPC Beams Reinforced with Braided FRP Bars*, Proceedings, ACI International Symposium, Fiber-Reinforced-Plastic Reinforcement for Reinforced Concrete Structures, Detroit: American Concrete Institute, pp. 875–894, 1993.

[41] Sen, R., Mariscal, D., and Shahawy, M., *Investigation of S-2 Glass/Epoxy Strands in Concrete*, Proceedings, ACI International Symposium, Fiber-Reinforced-Plastic

Reinforcement for Reinforced Concrete Structures, Detroit: American Concrete Institute, pp. 15–33, 1993.

[42] Uomoto, T., and Nishimura, T., *Deterioration of Aramid, Glass, and Carbon Fibers Due to Alkali, Acid, and Water in Different Temperatures*, ACI Fourth International Symposium Fiber Reinforced Polymer Reinforcement for Reinforced Concrete Structures, U.S.A.: American Concrete institute, pp. 515–522, 1999.

[43] Vijay, P., and GangaRao, V., *Accelerated and Natural Weathering of Glass Fiber Reinforced Plastic Bars*, ACI Fourth International Symposium Fiber Reinforced Polymer Reinforcement for Reinforced Concrete Structures, U.S.A.: American Concrete institute, pp. 605–614, 1999.

[44] Katsuki, F., and Uomoto, T., *Prediction of Deterioration of FRP Rods Due to Alkali Attack*, Non-Metallic (FRP) Reinforcement for Concrete structures, Proceedings of the Second International RILEM Symposium (FRPRCS-2), Great Britain: E and FN SPON, pp. 82–89, 1995.

[45] Sekijima, K., Otsuka, Y., and Konno, T., *Durability of Fiber Reinforced Polymer Reinforcement Embedded in Concrete*, ACI Fourth International Symposium Fiber Reinforced Polymer Reinforcement for Reinforced Concrete Structures, U.S.A.: American Concrete institute, pp. 501–513, 1999.

[46] ASTM D 3916 - 94, *Standard Test Method for Tensile Properties of Pultruded Glass-Fiber-Reinforced Plastic Rod*, Annual Book of ASTM Standards, Section 8 Plastics, Edmonson, M.D.: American Society for Testing and Materials, Vol. 08.02, pp. 500–503, 1999.

[47] ASTM D 4476 - 97, *Standard Test Method for Flexural Properties of Fiber Reinforced Pultruded Plastic Rods*, Annual Book of ASTM Standards, Section 8 Plastics,

Edmonson, M.D.: American Society for Testing and Materials, Vol. 08.03, pp. 68–72, 1999.

[48] ASTM D 4475 - 96, *Standard Test Method for Apparent Horizontal Shear Strength of Pultruded Reinforced Plastic Rods by the Short-Beam Method*, Annual Book of ASTM Standards, Section 8 Plastics, Edmonson, M.D.: American Society for Testing and Materials,Vol. 08.03, pp. 65–67, 1999.

[49] ASTM D 3914 - 96, *Standard Test Method for In-Plane Shear Strength of Pultruded Glass-Reinforced Plastic Rod*, Annual Book of ASTM Standards, Section 8 Plastics, Edmonson, M.D.: American Society for Testing and Materials, Vol. 08.02, pp. 490–495, 1999.

[50] Chen, H., Sami, Z., and GangaRao, H., *Acoustic Emission Characteristics of FRP Bars and FRP Reinforced Concrete Beams*, Fourth International Symposium on Acoustic Emission from Composite Materials, Seattle, AECM-4: ASNT, pp. 147–156, July 1992.

[51] Chen, H., Sami, Z., and GangaRao, H., **Identifying Damages in Stressed Aramid FRP Bars Using Acoustic Emission**, Dynamic Characterization of Advanced Materials, P. Raju and R. Gibson, ed., NCA-Vol. 16, 172, American Society of Mechanical Engineers, pp. 171–178, November 1993.

[52] Belarbi, A., Chandrashekhara, K., and Watkins, S., *Performance Evaluation of Fiber Reinforced Polymer Reinforcing Bar Featuring Ductility and Health Monitoring Capacity*, ACI Fourth International Symposium Fiber Reinforced Polymer Reinforcement for Reinforced Concrete Structures, U.S.A.: American Concrete institute, pp. 1–12, 1999.

[53] The Canadian Society for Civil Engineering, **Advanced Composite Materials with Application to Bridges**, Montreal: Canadian Society for Civil Engineering, 1993.

[54] Tanano, H., Masuda, Y., and Tomosawa, F., *Characteristics and Performance Evaluation Methods of Continuous Fiber Bars State-of-the-Art Studies on Fire Properties and Durability of Continuous Fiber Reinforced Concrete in Japan*, ACI Fourth International Symposium Fiber Reinforced Polymer Reinforcement for Reinforced Concrete Structures, U.S.A.: American Concrete institute, pp. 523–533, 1999.

[55] Dolan, C., *FRP Development in the United States*, in **Fiber-Reinforced-Plastic (FRP) Reinforcement for Concrete Structures: Properties and Applications**, Nanni, A., ed., The Netherlands: Elsevier Science Publication, pp. 129–163, 1993.

[56] Nilson, A., and Winter, G., **Design of Concrete Structures**, 11th Ed., U.S.A.: McGraw Hill, 1991.

[57] White, R., Gergely, P., and Sexsmith, R., **Structural Engineering**, Vol. 3, Behavior of Members and Systems, U.S.A.: John Wiley and Sons, 1974.

[58] Shehata, E., Morphy, R., and Rizcalla, S., *Fiber Reinforced Polymer Reinforcement for Concrete Structures*, ACI Fourth International Symposium Fiber Reinforced Polymer Reinforcement for Reinforced Concrete Structures, U.S.A.: American Concrete institute, pp. 157–167, 1999.

[59] Faza, S., and GangaRao, H., *Theoretical and Experimental Behavior of Concrete Beams Reinforced with Fiber Reinforced Plastic Rebars*, Proceedings, ACI International Symposium, Fiber-Reinforced-Plastic Reinforcement for Reinforced Concrete Structures, Detroit: American Concrete Institute, pp. 599–614, 1993.

[60] Seely, F., and Smith, J., **Resistance of Materials**, Fourth Edition, U.S.A.: John Wiley and Sons, 1947.

[61] Beer, F., and Johnston, R., **Mechanics of Materials**, Second Edition, U.S.A.: McGraw Hill, 1992.

[62] Nadai, A., **Plasticity, A Mechanics of the Plastic State of Matter**, McGraw Hill, 1931.

[63] Naaman, A., and Jeong, S., *Structural Ductility of Concrete Beams Prestressed with FRP Tendons*, Non-Metallic (FRP) Reinforcement for Concrete Structures, Proceedings of the Second International RILEM Symposium (FRPRCS-2), Great Britain: E and FN SPON, pp. 379–386, 1995.

[64] American Concrete Institute, **Building Code Requirements for Structural Concrete (ACI 318-05) and Commentary (ACI 318-95)**, U.S.A., American Concrete Institute, 1995.

[65] Nakano, K., Matsuzaki, Y., Fukuyama, H., and Teshigawara, M., *Flexural Performance of Concrete Beams Reinforced with Continuous Fiber Bars*, Proceedings, ACI International Symposium, Fiber-Reinforced-Plastic Reinforcement for Reinforced Concrete Structures, Detroit: American Concrete Institute, pp. 743–766, 1993.

[66] Benmokrane, B., Theriault, M., Masmoudi, R., and Rizkalla, S., *Effect of Reinforcement Ratio on Concrete Members Reinforced with FRP Bars*, 42nd International SAMPE Symposium, Covina, California: Society for the Advancement of Materials and Process Engineering, pp. 87–98, May 1997.

[67] Nawy, E., and Newerth, G., *Behavior of Fiberglass Reinforced Concrete Beams*, **Journal of the Structural Division**, U.S.A.: American Society of Civil Engineers, pp. 203–215, September, 1971.

[68] Bank, L., Xi, Z., and Munley, E., *Tests of Full-Size Pultruded FRP Grating Reinforced Concrete Bridge Decks*, Materials Performance and Prevention of

Deficiencies and Failures, Proceedings of the Materials Engineering Congress, Atlanta, pp. 618–631, August 1992.

[69] Faza, S., and GangaRao, H., *Bending and Bond Behavior of Concrete Beams Reinforced with Fiber Reinforced Plastic Rebars*, WVDOH-RP-83 Phase I Report, West Virginia University, Morgantown, pp.128–173, 1992.

[70] Nanni, A., *Flexural Behavoiour and Design of RC Members Using FRP Reinforcement*, U.S.A.: **Journal of Structural Engineering**, American Society of Civil Engineer, Vol. 119, No. 11, pp. 3344–3359, 1993.

[71] Faza, S., and GangaRao, H., *Pre- and Post-Cracking Deflection Behaviour of Concrete Beams Reinforced with Fibre-Reinforced Plastic Rebars*, Neale, K., and Labossiere, P., eds., 1st International Conference on Advanced Composite Materials in Bridges and Structures, Montreal: Canadian Society for Civil Engineering, pp. 151–160, 1992.

[72] Benmokrane, B., Masmoudi, R., Chekired, M, Rahman, H., Debbache, Z., and Tadros, G., *Design, Construction, and Monitoring of Fiber Reinforced Polymer Reinforced Concrete Bridge Deck*, ACI Fourth International Symposium Fiber Reinforced Polymer Reinforcement for Reinforced Concrete Structures, U.S.A.: American Concrete institute, pp. 87–101, 1999.

[73] Toutanji, H., and Saafi, M., *Deflection and Crack Width Predictions of Concrete Beams Reinforced with Fiber Reinforced Polymer Bars*, ACI Fourth International Symposium Fiber Reinforced Polymer Reinforcement for Reinforced Concrete Structures, U.S.A.: American Concrete institute, pp. 1023–1034, 1999.

[74] Sonobe, Y., Fukuyama, H., Okamoto, T., Kani, N., Kimura, K., Kobayashi, K., Masuda, Y., Matsuzaki, Y., Mochizuki, S., Nagasaka, T., Shimizu, A., Tanano, H.,

Tanigaki, M., and Teshigawara, M., *Design Guidelines of FRP Reinforced Concrete Building Structures*, **Journal of Composites for Construction**, U.S.A.: American Society of Civil Engineers, pp. 90–115, August 1997.

[75] Makizumi, T., Sakamoto, Y., and Okada, S., *Control of Cracking by Use of Carbon Fiber Net as Reinforcement for Concrete*, Proceedings, ACI International Symposium, Fiber-Reinforced-Plastic Reinforcement for Reinforced Concrete Structures, Detroit: American Concrete Institute, pp. 287–299, 1993.

[76] Park, R., and Paulay, T., **Reinforced Concrete Structures**, U.S.A.: John Wiley and Sons, 1975.

[77] Taerwe, L., and Matthys, S., *Structural Behaviour of Concrete Slabs Prestressed with AFRP Bars*, Non-Metallic (FRP) Reinforcement for Concrete Structures, Proceedings of the Second International RILEM Symposium (FRPRCS-2), Great Britain: E and FN SPON, pp. 421–429, 1995.

[78] Benmokrane, B., Chaallal, O., and Masmoudi, R., *Flexural Response of Concrete Beams Reinforced with FRP Reinforcing Bars*, **ACI Structural Journal**, U.S.A.: American Concrete Institute, Vol. 93, No. 1, pp. 46–55, 1996.

[79] Razaqpur, A.G., Svecova, D., and Cheung, M.S., *Rational Method for Calculating Deflection of Fiber-Reinforced Polymer Reinforced Beams*, **ACI Structural Journal**, Technical Paper, U.S.A.: American Concrete Institute, pp. 175–184, January-February 2000.

[80] Larralde, J., and Zerva, A., *Load-Deflection Performance of FRP Grating-Concrete Composites*, Advanced Composite Materials in Civil Engineering Structures, Proceedings of the Specialty Conference, Las Vegas, pp. 271–277, February 1992.

[81] Engel, R., Croyle, M., Bakis, C., and Nanni, A., *Deflection of Reinforced Concrete Beams Reinforced by Fiber Reinforced Polymer Grids with Various Joint Designs*, ACI Fourth International Symposium Fiber Reinforced Polymer Reinforcement for Reinforced Concrete Structures, U.S.A.: American Concrete institute, pp. 75–85, 1999.

[82] Harik, I., Alagusundaramoorthy, P., Siddiqui, R., Lopez-Anido, R., Morton, S., Dutta, P., and Shahrooz, B., *Testing of Concrete/FRP Composite Deck Panels*, Proceedings of ASCE 5th Material Congress, U.S.A.: American Society of Civil Engineers, pp. 351–358, 1999.

[83] Braimah, A., Green, M., Soudki, K., and Clapp, F., *Long-Term Behavior of Concrete Beams Prestressed with Carbon Fiber Tendons*, ACI Fourth International Symposium Fiber Reinforced Polymer Reinforcement for Reinforced Concrete Structures, U.S.A.: American Concrete institute, pp. 547–557, 1999.

[84] Joh, O., Wang, Z., and Goto, Y., *Long-Term Deflection of Fiber Reinforced Polymer Concrete Beams*, ACI Fourth International Symposium Fiber Reinforced Polymer Reinforcement for Reinforced Concrete Structures, U.S.A.: American Concrete institute, pp. 577–590, 1999.

[85] Park, S., and Naaman, A., *Mathematical Model for Fiber Reinforced Polymer Dowels Subjected to Tensile and Shear Forces*, ACI Fourth International Symposium Fiber Reinforced Polymer Reinforcement for Reinforced Concrete Structures, U.S.A.: American Concrete institute, pp. 55–63, 1999.

[86] Ghandour, A., Pilakoutas, K., and Waldron, P., *New Approach of Punching Shear Capacity Prediction of Fiber Reinforced Polymer Reinforced Concrete Flat Slabs*, ACI Fourth International Symposium Fiber Reinforced Polymer Reinforcement for Reinforced Concrete Structures, U.S.A.: American Concrete institute, pp. 135–144, 1999.

[87] Bank, L., and Ozel, M., *Shear Failure of Concrete Beams Reinforced with 3-D Fiber Reinforced Plastic Grids*, ACI Fourth International Symposium Fiber Reinforced Polymer Reinforcement for Reinforced Concrete Structures, U.S.A.: American Concrete institute, pp. 145–156, 1999.

[88] Razaqpur, A., and Mostofinejad, D., *Experimental Study of Shear Behavior of Continuous Beams Reinforced with Carbon Fiber Reinforced Polymer*, ACI Fourth International Symposium Fiber Reinforced Polymer Reinforcement for Reinforced Concrete Structures, U.S.A.: American Concrete institute, pp. 169–178, 1999.

[89] Canadian Highway Bridge Design, **Fiber Reinforced Concrete**, Section 16, Final Draft, Canadian Highway Bridge Design Code Committee on Fiber Reinforced Concrete, Canada: Canadian Society for Civil Engineering, December 1996.

[90] Deitz, D., Harik, I., and Gesund, H., *One-Way Slabs Reinforced with Glass Fiber Reinforced Polymer Reinforcing Bars*, ACI Fourth International Symposium Fiber Reinforced Polymer Reinforcement for Reinforced Concrete Structures, U.S.A.: American Concrete institute, pp. 279–286, 1999.

[91] Michaluk, C., Rizcalla, S., Tadros, S., and Benmokrane, B., *Flexural Behavior of One-Way Concrete Slabs Reinforced by Fiber Reinforced Plastic Reinforcements*, **ACI Structural Journal**, U.S.A.: American Concrete Institute, Vol. 95, No. 3, pp. 353–364, 1998.

[92] Makitani, E., Irisawa, I., and Nishimura, N., *Investigation of Bond in Concrete Member with Fiber Reinforced Plastic Bars*, Proceedings, ACI International Symposium, Fiber Reinforced Plastic Reinforcement for Reinforced Concrete Structures, Detroit: American Concrete Institute, pp. 315–331, 1993.

[93] Karlsson, M., *Bond Between C-Bar FRP Reinforcement and Concrete*, Chalmers University of Technology. Pub. No. 98:3, Work No. 22, Graduation Thesis: E-91:1, Gotenborg, Sweden, 1997.

[94] Cosenza, E., Manfredi, G., Pecce, M., and Realfonzo, R., *Bond Between Glass Fiber Reinforced Plastic Reinforcing Bars and Concrete – Experimental Analysis*, ACI Fourth International Symposium Fiber Reinforced Polymer Reinforcement for Reinforced Concrete Structures, U.S.A.: American Concrete institute, pp. 347–358, 1999.

[95] Shield, C., French, C., and Hanus, J., *Bond of Glass Fiber Reinforced Plastic Reinforcing Bar for Consideration in Bridge Decks*, ACI Fourth International Symposium Fiber Reinforced Polymer Reinforcement for Reinforced Concrete Structures, U.S.A.: American Concrete Institute, pp. 393–406, 1999.

[96] Katz, A., Berman, N., and Bank, L.C., *Effect of High Temperature on Bond Strength of FRP Rebars*, **Journal of Composites for Construction**, U.S.A.: American Society of Civil Engineers, pp. 73–81, May 1999.

[97] Greszczuk, L., *Theoretical Studies on the Mechanics of the Fiber-Matrix Interface in Composites*, **Interfaces in Composites**, ASTM STP 452, West Conshohocken, Pa.: American Society for Testing and Materials, 42–58, 1969.

[98] Malvar, J., *Tensile and Bond Properties of GFRP Reinforcing Bars*, **ACI Materials Journal**, U.S.A.: American Concrete Institute, pp. 276–285, May-June 1995.

[99] Cosenza, E., Manfredi, G., and Realfonzo, R., *Behavior and Modeling of Bond of FRP Rebars to Concrete*, **Journal of Composites for Construction**, U.S.A.: American Society of Civil Engineers, pp. 40–51, May 1997.

[100] Kanakubo, T., Yonemaru, K., Fukuyama, H., Fujisawa, M., and Sonobe, Y., *Bond Performance of Concrete Members Reinforced with FRP Bars*, Proceedings, ACI

International Symposium, Fiber-Reinforced-Plastic Reinforcement for Reinforced Concrete Structures, Detroit: American Concrete Institute, pp. 767–788, 1993.

[101] Hattori, A., Inoue, S., Miyagawa, T., and Fujii, M., *A Study on Bond Creep Behavior of FRP Rebars Embedded in Concrete*, Non-Metallic (FRP) Reinforcement for Concrete Structures, Proceedings of the Second International RILEM Symposium (FRPRCS-2), Great Britain: E and FN SPON, pp. 172–179, 1995.

[102] Benmokrane, B., and Masmoudi, R., *FRP C-Bar as Reinforcing Rod for Concrete Structures*, Proceedings 2nd International Conference on Advanced Composite Materials in Bridge Structures, M. El-Bardy, ed., Montréal: Canadian Society for Civil Engineering, 1996.

[103] Al-Zaharani, M., *Bond Behaviour of Fiber Reinforced Plastic (FRP) Reinforcements With Concrete*, Ph.D. Thesis, Pennsylvania State University, University Park, Pa., 1995.

[104] Honma, M., and Maruyama T., *Bond Properties of Carbon Fiber Reinforced Plastic Rods at Elevated Temperatures*, Proceedings, Architectural Institute of Japan Convention, Vol. C (in Japanese), Japan: Architectural Institute of Japan, 1989.

[105] Mashima, M., and Iwamoto, K., *Bond Characteristics of FRP Rod and Concrete after Freezing and Thawing Deterioration*, Proceedings, ACI International Symposium, Fiber-Reinforced-Plastic Reinforcement for Reinforced Concrete Structures, Detroit: American Concrete Institute, pp. 51–69, 1993.

[106] Al-Dulaijan, S., Nanni, A., Al-Zaharani, M., Bakis, C., and Boothby, T., *Bond Evaluation of Environmentally Conditioned GFRP/Concrete Systems*, Proceedings, 2nd Conference on Advanced Composite Materials in Bridge Structures, M. El-Badry, ed., Montréal: Canadian Society for Civil Engineering, 1996.

139

[107] GangaRao, V., and Faza, S., *Bending and Bond Behavior and Design of Concrete Beams Reinforced with Reinforced Plastic Rebars*, Technical Report, Construction Facilities Center, West Virginia University, Morgantown, pp. 47–154, 1991.

[108] Pleimann, L., *Strength, Modulus of Elasticity, and Bond of Deformed FRP Rods*, Advanced Composite Materials in Civil Engineering Structures, Proceedings of the Specialty Conference, Las Vegas: American Society of Civil Engineers, pp. 99–110, February 1992.

[109] Chaallal, O., Benmokrane, B., and Masmoudi, R., *An Innovative Glass-Fiber Composite Rebars for Concrete Structure*, Advanced Composite Materials in Bridges and Structures, Proceedings of the 1st Inernational Conference, Sherbrooke: Canadian Society for Civil Engineering, pp. 169–177, 1992.

[110] Daniali, S., *Development Length for Fiber Reinforced Plastic Bars*, Advanced Composite Materials in Bridges and Structures, Proceedings of the 1st International Conference, Sherbrooke: Canadian Society for Civil Engineering, pp. 179–188, 1992.

[111] Tao, S., *Bond of Glass Fiber Reinforced Plastic Reinforcing Bars to Concrete*, Ph.D. dissertation, Department of Civil Engineering, University of Arizona, Tucson, 197 pp., 1994.

[112] Wang, Z., Goto, Y., and Joh, O., *Bond Strength of Various Types of Fiber Reinforced Plastic Rods*, ACI Fourth International Symposium Fiber Reinforced Polymer Reinforcement for Reinforced Concrete Structures, U.S.A.: American Concrete Institute, pp. 1117–1130, 1999.

[113] Sakai, T., Kanakubo, T., Yonemaru, K., and Fukuyama, H., *Bond Splitting Behavior of Continuous Fiber Reinforced Concrete Members*, ACI Fourth International

Symposium Fiber Reinforced Polymer Reinforcement for Reinforced Concrete Structures, U.S.A.: American Concrete Institute, pp. 1131–1144, 1999.

[114] Erki, M., and Rizkalla, S., *A Canadian Perspective on R&D, Design/Codes and Technical Committees*, in **Fiber-Reinforced-Plastic (FRP) Reinforcement for Concrete Structures: Properties and Applications**, Nanni, A., ed., The Netherlands: Elsevier Science Publication, pp. 89–97, 1993.

[115] Grant, L., Tadros, G., and Rizcalla, S., *Toward Development of Bridges in the Next Century*, Non-Metallic (FRP) Reinforcement for Concrete Structures, Proceedings of the Second International RILEM Symposium (FRPRCS-2), Great Britain: E and FN SPON, pp. 654–662, 1995.

[116] Fam, A., Abdelrahman, A., Rizcalla, S., and Saltzberg, W., *FRP Flexural and Shear Reinforcements for Highway Bridges in Manitoba, Canada*, Non-Metallic (FRP) Reinforcement for Concrete Structures, Proceedings of the Second International RILEM Symposium (FRPRCS-2), Great Britain: E and FN SPON, pp. 395–402, 1995.

[117] Canadian Standards Association, *S806-97 - Design and Construction of Building Components with Fibre Reinforced Plastics*, (Draft 2), Draft issue of CSA S806, CSA Technical Committee on FRP Components and Reinforcing Materials for Buildings, Canadian Standards Association, Canada, June 1996.

[118] Canadian Highway Bridge Design Code, *Section 16 - Fibre Reinforced Structures and Commentary to Section 16*, (Final Draft), Canadian Highway Bridge Design Code, Ministry of Transportation, Canada, 26 pp. and 22 pp., July 1996.

[119] Taerwe, L., *FRP Developments and Applications in Europe*, in **Fiber-Reinforced-Plastic (FRP) Reinforcement for Concrete Structures: Properties and Applications**, Nanni, A., ed., The Netherlands: Elsevier Science Publication, pp. 99–114, 1993.

[120] Shaw, H., Caine, J., Southcombe, C., and Easterbrook, D., *Design, Construction and Instrumentation of Prestressed Masonry Box Girder Pedestrian Footbridges*, Non-Metallic (FRP) Reinforcement for Concrete Structures, Proceedings of the Second International RILEM Symposium (FRPRCS-2), Great Britain: E and FN SPON, pp. 672–679, 1995.

[121] CUR, *Kunststof Wapeningselementen in Beton - Preadvies*, CUR report 96-9 (in Dutch), CUR preliminary advisory Committee PC 97, Centre of Civil Engineering Research and Codes (CUR), The Netherlands, 66 pp., September 1996.

[122] SINTEF, *Modifications to NS3473 When Using Fibre Reinforced Plastic (FRP) Reinforcement*, SINTEF Report STF22A98741, Norway: Sintef Structures and Concrete, 40 pp., April 1998.

[123] IStructE, *Interim Guidance on the Design of Reinforced Concrete Structures Using Fibre Composite Reinforcement*, United Kingdom: Institution of Structural Engineers, 116 pp., August 1999.

[124] Sonobe, Y., *An Overview of R&D in Japan*, in **Fiber-Reinforced-Plastic (FRP) Reinforcement for Concrete Structures: Properties and Applications**, Nanni, A., ed., The Netherlands: Elsevier Science Publication, pp. 115–128, 1993.

[125] Okasaki, M., *Properties and Applications of Vinylon FRP Rod (CLATEC ROD)*, in **Fiber-Reinforced-Plastic (FRP) Reinforcement for Concrete Structures: Properties and Applications**, Nanni, A., ed., The Netherlands: Elsevier Science Publication, pp. 189–222, 1993.

[126] Santoh, N., *CFCC (Carbon Fiber Composite Cable)*, in **Fiber-Reinforced-Plastic (FRP) Reinforcement for Concrete Structures: Properties and Applications**, Nanni, A., ed., The Netherlands: Elsevier Science Publication, pp. 223–247, 1993.

[127] Noritake, K., Kakihara, R., Kumagai, S., and Mizutani, J., *Technora, an Aramid FRP Rod*, in **Fiber-Reinforced-Plastic (FRP) Reinforcement for Concrete Structures: Properties and Applications**, Nanni, A., ed., The Netherlands: Elsevier Science Publication, pp. 267–290, 1993.

[128] Nakagawa, H., Kobayashi, M., Suenaga, T., Ouchi, T., Watanabe, S., and Satoyama, K., *Three-Dimensional Fabric Reinforcement*, in **Fiber-Reinforced-Plastic (FRP) Reinforcement for Concrete Structures: Properties and Applications**, Nanni, A., ed., The Netherlands: Elsevier Science Publication, pp. 387–404, 1993.

[129] Sugita, M., *NEFMAC-Grid Type Reinforcement*, in **Fiber-Reinforced-Plastic (FRP) Reinforcement for Concrete Structures: Properties and Applications**, Nanni, A., ed., The Netherlands: Elsevier Science Publication, pp. 355–385, 1993.

[130] GangaRao, H., Thippeswamy, H., and Kumar, S., *Analysis and Design of McKinleville Bridge*, Report to WVDOT-DOH, U.S.A.: West Virginia Department of Transportation, 1995.

[131] Hughes Brothers, Inc., *Hughes Brothers Glass Fiber Reinforced Polymer Rebar*, Brochure, U.S.A.: Hughes Brothers, Inc., 1998.

[132] Bradberry, T. E., *FRP Reinforcing Bars for Concrete Bridge Decks*, Proceedings, Texas Section ASCE, Spring Meeting, Austin, Texas: American Society of Civil Engineers, pp. 1-13, April 5-8, 2000.

[133] TILLCO, *Fiberglass Reinforced Plastic Rebar*, http://www.tillco.com, 2000.